No. SE-7
No. 58

SILICON WEB PROCESS DEVELOPMENT

ANNUAL REPORT

JPL NO. 9950-378

C. S. Duncan, R. G. Seidensticker, J. P. McHugh,
F. E. Hill, M. E. Skutch, J. M. Driggers and
R. H. Hopkins

DOE/JPL-954654/80/11

Contract No. 954654

June 30, 1980

The JPL Low-Cost Silicon Solar Array Project is sponsored by the U. S. Department of Energy and forms part of the Solar Photovoltaic Conversion Program to initiate a major effort toward the development of low-cost solar arrays. This work was performed for the Jet Propulsion Laboratory, California Institute of Technology by agreement between NASA and DOE.

Westinghouse R&D Center
1310 Beulah Road
Pittsburgh, Pennsylvania 15235

DRD No. SE-7
DRL No. 58

SILICON WEB PROCESS DEVELOPMENT

ANNUAL REPORT

APR - 1979 APR - 1980

C. S. Duncan, R. G. Seidensticker, J. P. McHugh,
F. E. Hill, M. E. Skutch, J. M. Driggers and
R. H. Hopkins

DOE/JPL-954654/80/11

Contract No. 954654

June 30, 1980

The JPL Low-Cost Silicon Solar Array Project is sponsored by the U. S. Department of Energy and forms part of the Solar Photovoltaic Conversion Program to initiate a major effort toward the development of low-cost solar arrays. This work was performed for the Jet Propulsion Laboratory, California Institute of Technology by agreement between NASA and DOE.

Westinghouse R&D Center
1310 Beulah Road
Pittsburgh, Pennsylvania 15235

TABLE OF CONTENTS

TABLE OF CONTENTS (Cont.)

LIST OF ILLUSTRATIONS

LIST OF ILLUSTRATIONS (Cont.)

LIST OF TABLES

1. SUMMARY

During this reporting period significant milestones have been met. A new barrier crucible design which consistently maintains melt stability over long periods of time has been successfully tested and used in long growth runs. The pellet feeder for melt replenishment was operated continuously for growth runs of up to 17 hours (a one day growth cycle). The liquid level sensor comprising a laser/sensor system was operated, performed well, and meets the requirements for maintaining liquid level height during growth and melt replenishment. An automated feedback loop connecting the feed mechanism and the liquid level sensing system was designed and constructed and, during the preparation of this report, operated successfully for 3 1/2 hours demonstrating the feasibility of semi-automated dendritic web growth.

The web throughput task has resulted in a demonstration of wider good quality web as well as a demonstration of higher throughput rates. A summary of the accomplishments during the report period is listed below.

	Start of Phase III	Present Status
Throughput	23.6cm^2/min	27.2cm^2/min
Width	4.2cm	4.7cm
Cell Efficiency	15.5%	15.5%
Continuous Feeding	0.8 hours	17 hours
Liquid Level Sensor	Bench Tested	Installed and Operating
Semi-automated Growth	Conception	Functionally-demonstrated for 3 1/2 hours

The economic analysis of the dendritic web process was updated. The sensitivity of the cost of sheet to variations in capital equipment cost and recycling dendrites was calculated; and it was shown that these factors have relatively little impact on sheet cost. An important finding was that dendrites from web which had gone all the way through the solar cell fabrication process, when melted and grown into web, produce crystals which show no degradation in cell efficiency.

Material quality remains high and cells made from web grown at the start, during, and the end of a run from a replenished melt show comparable efficiencies.

2. INTRODUCTION

Silicon dendritic web is a single crystal silicon ribbon material which provides substantial advantages for low cost manufacture of solar cells. A significant feature of the process is the growth from a melt of silicon without constraining dies resulting in an oriented single crystal ribbon having excellent surface features. In common with other more classical processes, such as Czochralski growth, impurity rejection into the melt permits the use of less pure "solar grade" starting material without significantly affecting cell performance. A unique property of the dendritic web process is the growth of long ribbons of controllable thickness which not only facilitates automation of subsequent processing into solar cells, but also results in high material utilization since cutting and polishing is not required.

At the conclusion of Phase II of this program, all the individual elements required for low cost production were demonstrated. An output rate of 23.6cm^2/minute was demonstrated. Solar cell efficiencies over 15% AM1 with an average efficiency of all cells 13% AM1. The feasibility of concurrent feeding of silicon into the melt during crystal growth was established and cells made from this material were demonstrated to have the same efficiency as those grown from unreplenished silicon. Economic analyses show that the JPL cost allocation for ribbon can be met and surpassed. Finally, identification of the factors critical to meeting price objectives were identified.

At the start of this program the requirements for liquid level control in order to meet the technical and economic objectives of the sheet task were established. This report describes the accomplishments during the last year in automated growth of dendritic web. We describe the progress in melt replenishment, melt level sensing, throughput of web, equipment development, and semi-automated growth. The appendices

include the summary of the individual web runs made during the period as well as solar cell data. Scientific reports generated during this period are also appended and include an analysis of the fundamental limitations on the growth of dendritic web.

3. PROGRESS IN WEB TECHNOLOGY DEVELOPMENT

3.1 Melt Replenishment

3.1.1 Background

The economic requirements for melt replenishment in sheet technology are well established. Substantial economics are realized by increasing the productivity of the equipment and more efficient use of material, labor, and facilities. The dendritic web process further benefits from melt replenishment in that maintaining the solid-liquid interface at a nearly constant position in the furnace provides a consistent thermal environment to the growing web reducing stress in the ribbon and permitting higher output rates. Further the constant melt level simplifies the control system that is required for automated operation of the equipment.

Since a likely outcome of the LSA silicon materials task is solar grade silicon in pellet form, our concept for a melt replenishment system utilizes pellets 2-4mm in diameter. The use of pellets provides several advantages:

(1) The pellets cause only slight temperature perturbations when fed into the melt.

(2) Additional system power requirements are small; in fact, with the thermal modifications used to optimize the replenishment/growth setup, experimental results show lower power requirements.

(3) The pellets are readily metered with simple, inexpensive equipment to replace the silicon consumed in growth.

(4) The approach lends itself to automation.

At the end of the last phase, successful demonstration of the feasibility of this concept was established. A mechanically-activated, inexpensive, programmable pellet feeder was tested and web was grown from the replenished melt. Solar cells made on this material gave good efficiencies verifying that material quality is not adversely affected by melt replenishment. Successful growth while replenishing was demonstrated for approximately one hour. Reasons for the termination of growth were analyzed and attributed to thermal asymmetry and oxide formation resulting in free floating silicon particles, or "ice" which attack to the crystal, terminating growth.

3.1.2 Accomplishments

The development of the melt replenishment system was shifted from the "W" furnace to the RE furnace. The activity during this year has centered on refining the design of the pellet feeder and delivery system, the design, development and demonstration of compartmented crucibles to isolate the replenishment chamber from the growth chamber, the design, development and demonstration of both passive and active thermal shields to provide control of temperature gradients in the system during feeding and growth, and the development of a melt level sensing system. As a result of this activity melt replenishment has progressed considerably. We have made a growth run with 17 hours of manually activated continuous feeding (although not continuous growth), the length of run equivalent to a 1 day growth cycle. Growth of individual crystals with feeding for periods of over 2 hours are common. Continuous concurrent replenishment and growth has been demonstrated for 3 hours 20 minutes. The melt replenishment concept is well established and both the RE and J furnaces are now equipped for feeding, enhancing the rate of progress in combining of melt replenishment with throughput development. The feed rate of pellets has progressed from the experimental rate of 1 pellet/min. to rates which maintain a constant melt level, with the thermal geometry capable of handling even higher feed rates as the crystal area growth rate increases.

The following sections describe the activities over the past year.

Mechanically-Activated Pellet Feeder

The feeder which has been used in most of the feed experiments is well described in Reference 1 and can be seen in Figure 1. The feeder is comprised of a rotating disk constructed of polished stainless steel which rotates at the same speed as pellets are fed. The dish is inclined to permit a flow of pellets to the lower side. A hole slightly larger than the pellet can accept only a single pellet which is separated from the pellets in the feeder body. A cam activated spring-loaded gate releases a pellet with every revolution of the dish. The pellet is released to a funnel leading into a delivery tube located over the feed compartment in the crucible. This system has performed well and was essentially duplicated as a feeder for the J furnace. One modification was replacement of the stainless steel separator bowl by a teflon bowl to eliminate the possiblity of the silicon pellets chipping the steel and resulting in possible contamination of the melt. Other refinements include seals improvement and modified pellet chutes.

If the feeders are overfilled, the pellets tend to pack in a tight layer on the bottom of the feeder bowl, inhibiting feeding. In order to accomodate the need for larger numbers of pellets as runs become longer and feed rates are increased, a batch feeder was designed and constructed. With this the furnace operator can refill the pellet feeder without opening the system to air, thus avoiding the risk of back diffusion of oxygen into the furnace. The batch feeder is shown installed on the J furnace in Figure 2. A close up view of the batch feed apparatus as shown on Figure 3. As can be seen from the photograph the batch feeder is essentially a quartz tube enclosing a plunger mechanism. Access to the batch feeder is through a port which permits additional pellets to be placed in the reservoir as required. This component can be isolated while the reloading is taking place. For test purposes this isolation is accomplished with a simple mechanical clamp.

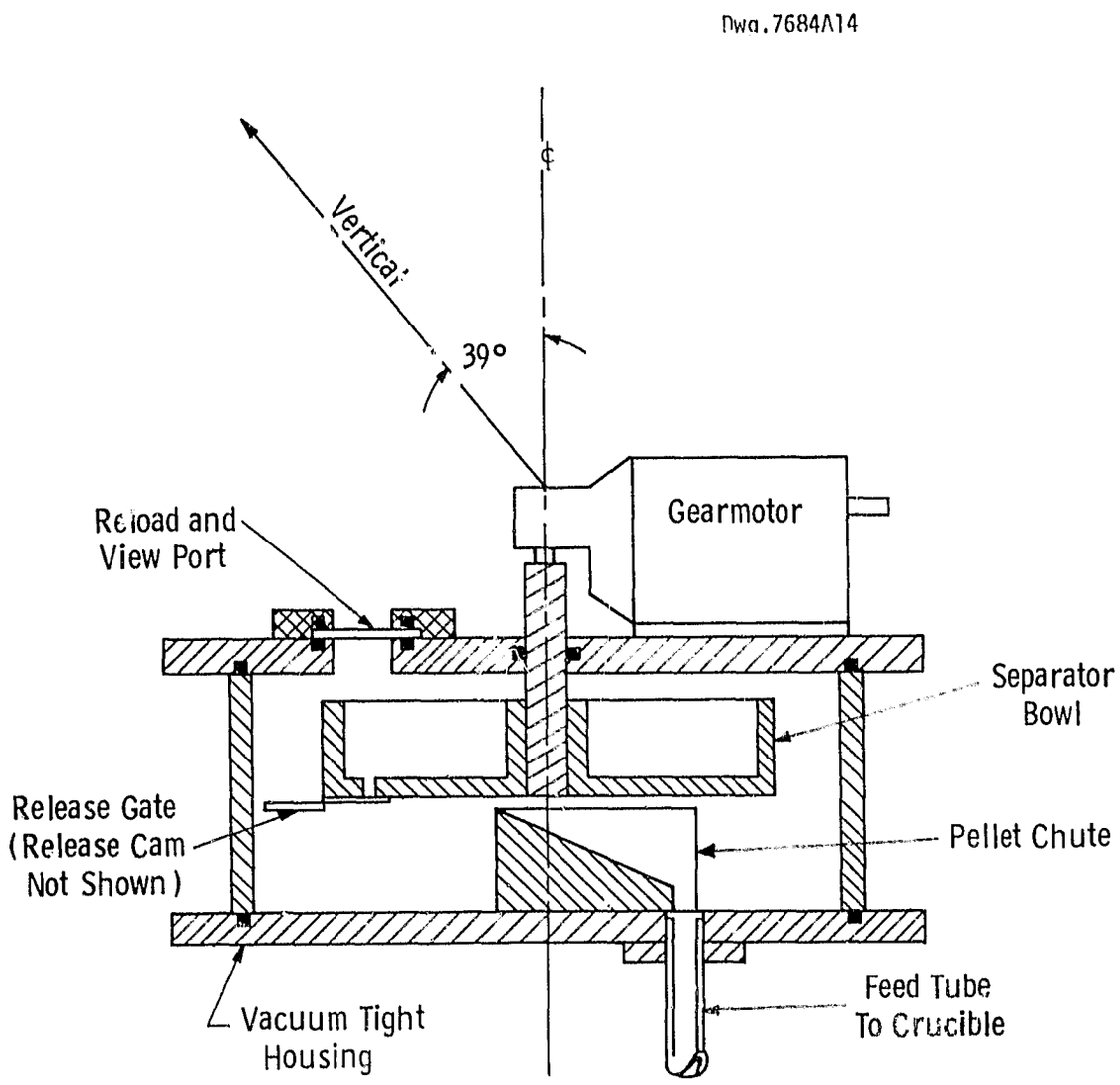

Figure 1 Mechanically-activated pellet reservoir and feeder.

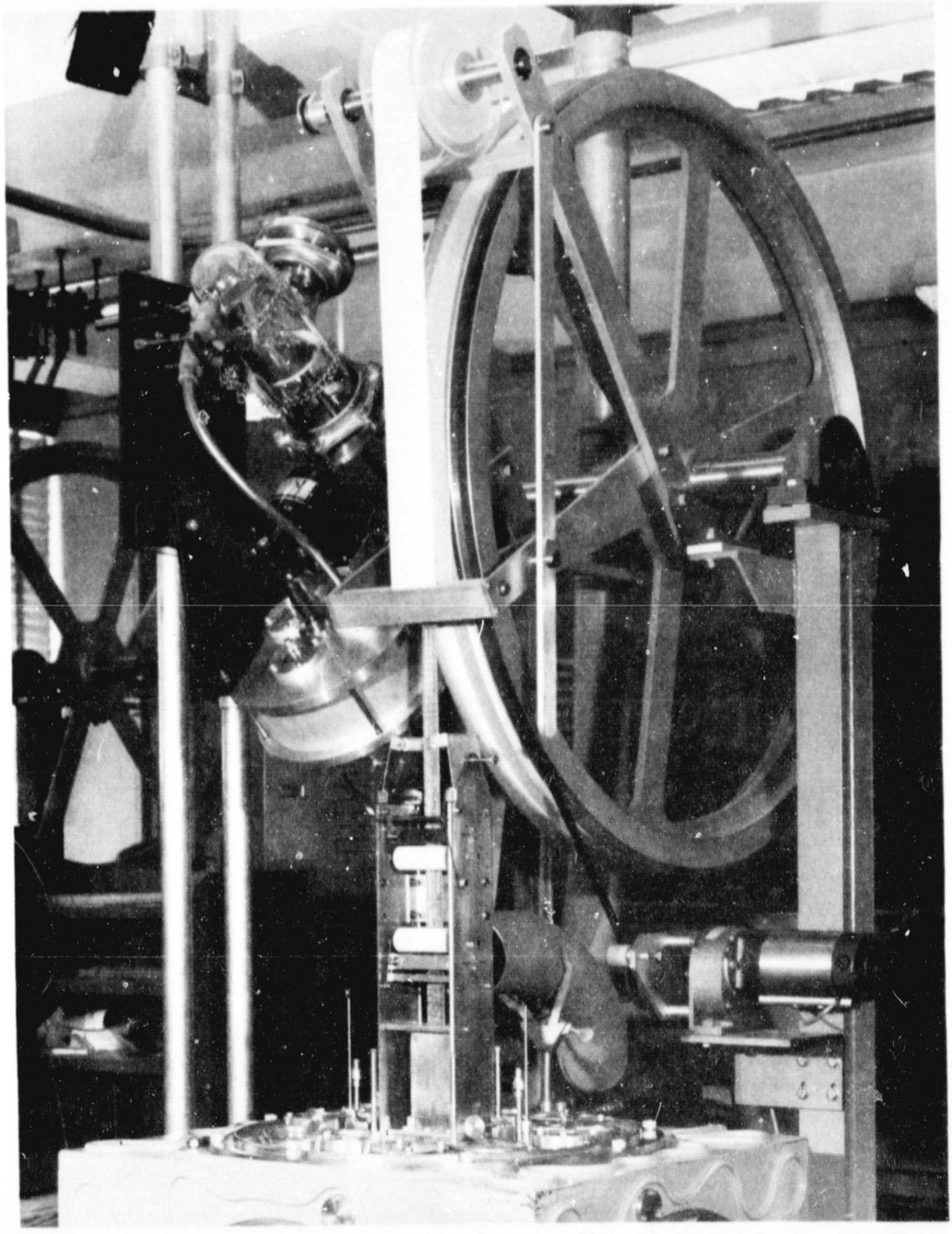

Figure 2 Batch and Pellet Feeder Installed on J-Furnace

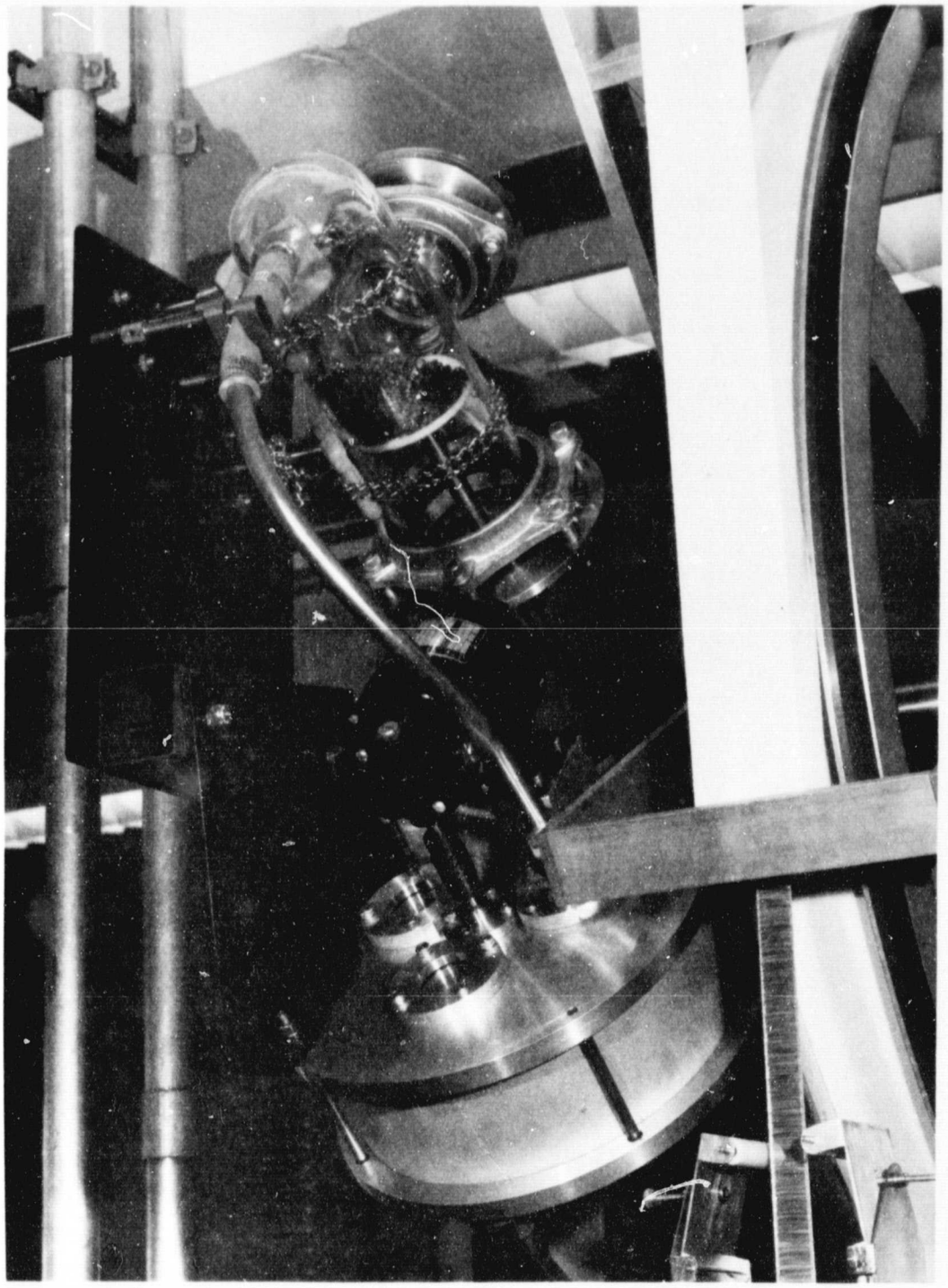

Figure 3 Closeup of Batch and Pellet Feeder

Compartmented Crucible

The introduction of solid pellets into molten silicon has the potential for interfering with the dendritic web growth. Pellets dropping into the melt can perturb the surface, float to the growing crystal, cause variations in the thermal symmetry, and chip off condensed oxide which will nucleate the undercooled melt and cause ice. Therefore, it is necessary to isolate the feed chamber in the crucible from the section in which the crystal is grown. This isolation is accomplished by constructing a barrier in the crucible between the two compartments. An example is shown in Figure 4. The concept requires that the barrier be above the level of the liquid in order to prevent introduction of solids into the growth region. However, communication between the two compartments must be maintained to allow free flow of liquid to maintain melt height, so the barriers must have an opening between the two compartments.

Several modifications were made in the barrier used in the crucible. Three examples of the several barrier configurations that were tried are shown in Figure 5. Barrier configurations A & B are similar except that the opening is located along the walls of the crucible in one case, while with B, the opening is in the center. Several variations of width and height were examined. Although successful feeding runs were performed with both designs, occasional dewetting of the feed compartment occurs resulting in termination of the run. The dewetting is characterized by spontaneous withdrawal of the molten silicon from the feed compartment into the growth compartment. Not only does this perturb growth but it also inhibits the melting of subsequent pellets fed into the growth compartment.

Configuration C in Figure 5 evolved over a series of experimental runs. The performance of this "fence" configuration has been excellent. No dewetting was observed in the feed chamber even when steep temperature gradients have been imposed on the crucible. We hypothosize that the lower strip of the barrier which makes contact with the base of the crucible serves as a mechanism to overcome the

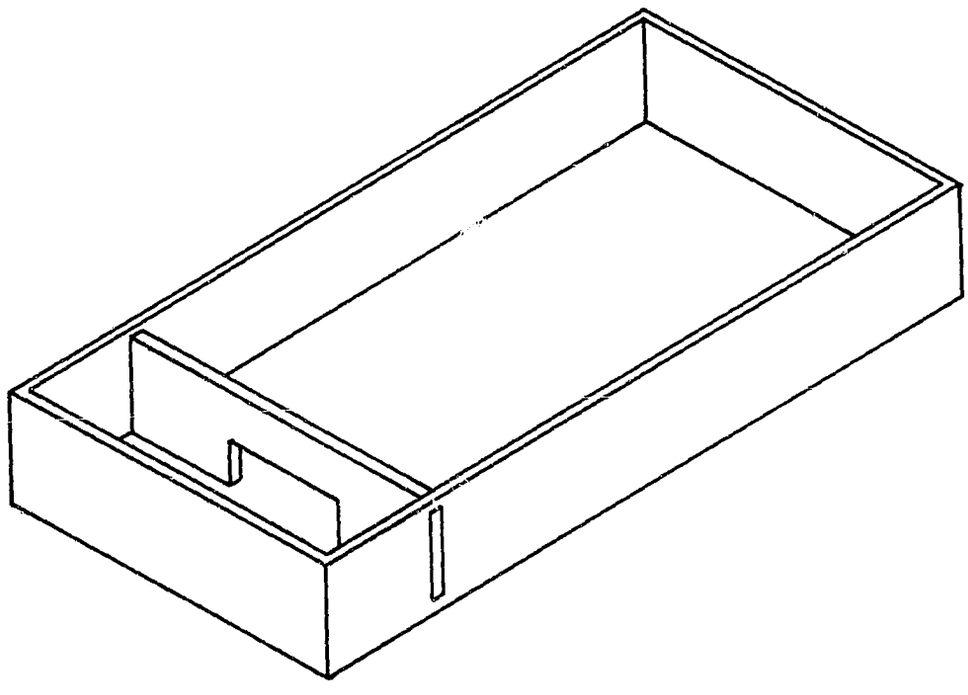

Figure 4 Barrier Type Crucible

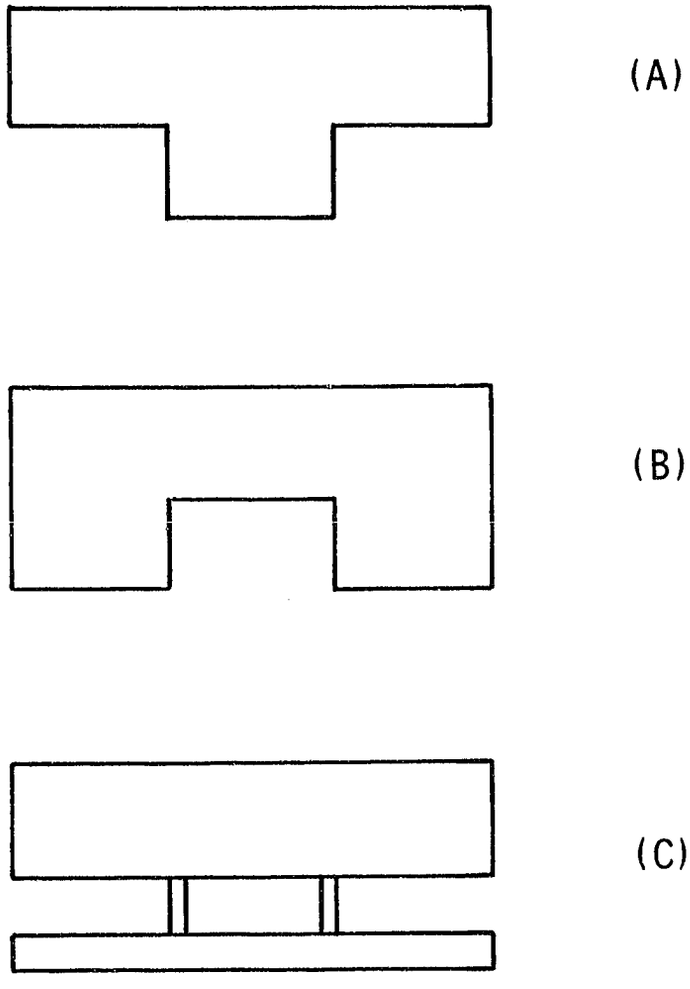

Figure 5 New crucible barrier design (C) used to eliminate melt dewetting observed with hotter end shields. Older designs previously used, A and B.

surface tension force of liquid silicon. When intermittent dewetting of the crucible wall in the feed chamber occurs, the liquid is prevented from flowing out of the feed chamber into the substantially larger growth chamber. The vertical posts may also be helpful in retaining silicon in the feed chamber. However, their prime function is to support the upper portion of the barrier which will sag at operating temperature with time.

Melt Level Sensor

Complementary to the concept of melt replenishment is the necessity to detect variation in the height of the melt. Variations in the height of the liquid influence the long term stability of growth. In addition, although the amount of silicon withdrawn from the melt can be estimated and the silicon melt can be replenished accordingly, the precision with which one can do this is inadequate for long term growth. In order to develop automated equipment a reliable melt level sensor must be developed. After evaluating several types of sensing methods, we chose to use a reflected laser beam with an electro-optical position sensor. This method appeared most suitable in meeting of the following requirements:

- compatible with web growth and the web growth apparatus,
- accurate to within one millimeter or better,
- capable of both measurement and control,
- constant calibration during a growth cycle, and
- reasonable cost.

A schematic view of the laser/detector setup is provided in Figure 6. A 2 milliwatt helium-neon laser is used as the light source, and a commercially available solid state position detector senses the beam.

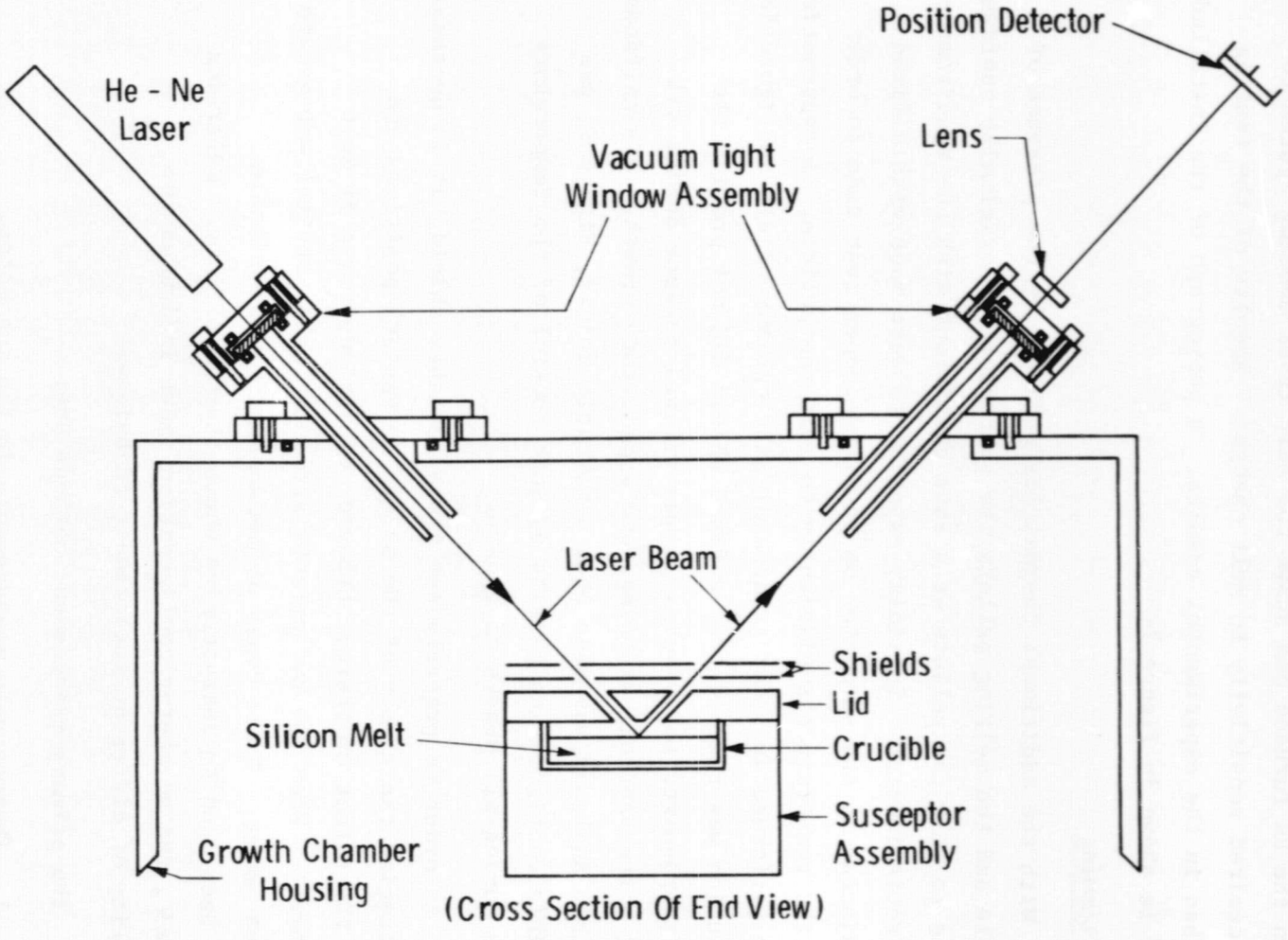

Figure 6 Schematic Depiction of Melt Level Sensor for Web Growth

Initial tests of the setup used mercury as a model liquid in a bench test and proved the system to be functionally satisfactory. Testing in the RE furnace has shown the melt level sensing system to have the desired sensitivity to melt changes. Results of the testing aredescribed in the experimental results. A photograph of the installed apparatus is shown in Figure 7.

Thermal Trimming

With the additional thermal loads caused by the presence of a feed hole and the melting pellets, the susceptor as originally configured was unable to melt the pellets at a rate consistant with the requirements for melt replenishment. Initially experiments were made with a fixed shield adjacent to the susceptor on the feed compartment side in order to raise the temperature sufficiently to melt the pellets. A systematic study was performed in order to determinethe optimum shield configuration. The conclusion was reached that a fixed shield did not provide the flexibility required to assure a proper thermal balance during all phases of a run seeding, widening, and steadystate growth. A significant step in this analysis was made when a moveable shield, Figure 8, was added. This configuration permits dynamic control of the temperature gradients during all phases of growth.

In order to properly use the adjustable shield, it is necessary to characterize the effect of the shield in various positions and evaluate the effect on thermal behavior of various rates of melt replenishment. When the two effects are in balance, optimal web growth conditions exist. Three types of measurements are available and have been used to characterize these thermal effects. Referring to Figure 9, the susceptor configuration shown indicates the availability of different measurement techniques.

The primary measurement methods are:

1. Thermocouple measurements in the susceptor,
2. Dendrite "hold" points measured in the center of the melt, and
3. Infrared pyrometer determination of melt temperature changes.

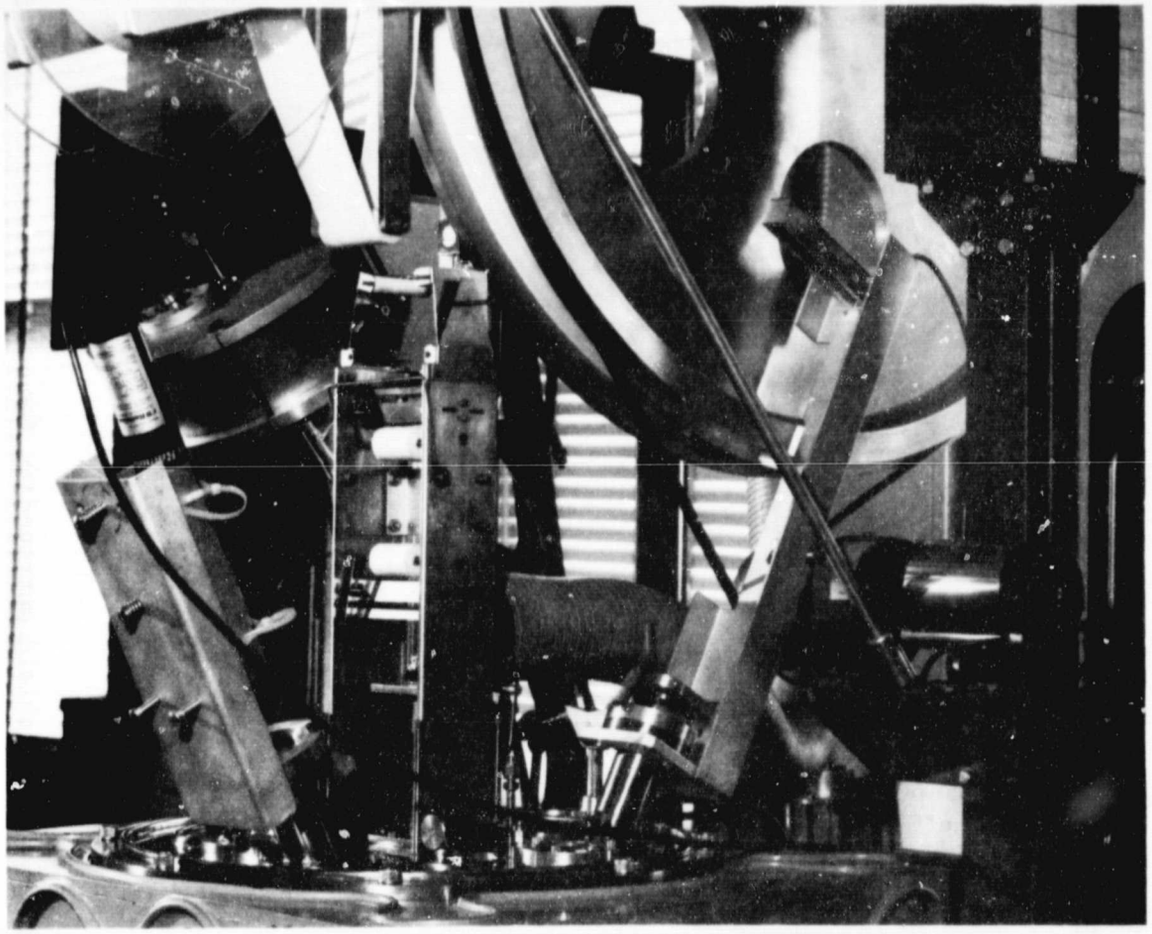

Figure 7 Laser/Sensor Liquid Level System Installed on RE Furnace

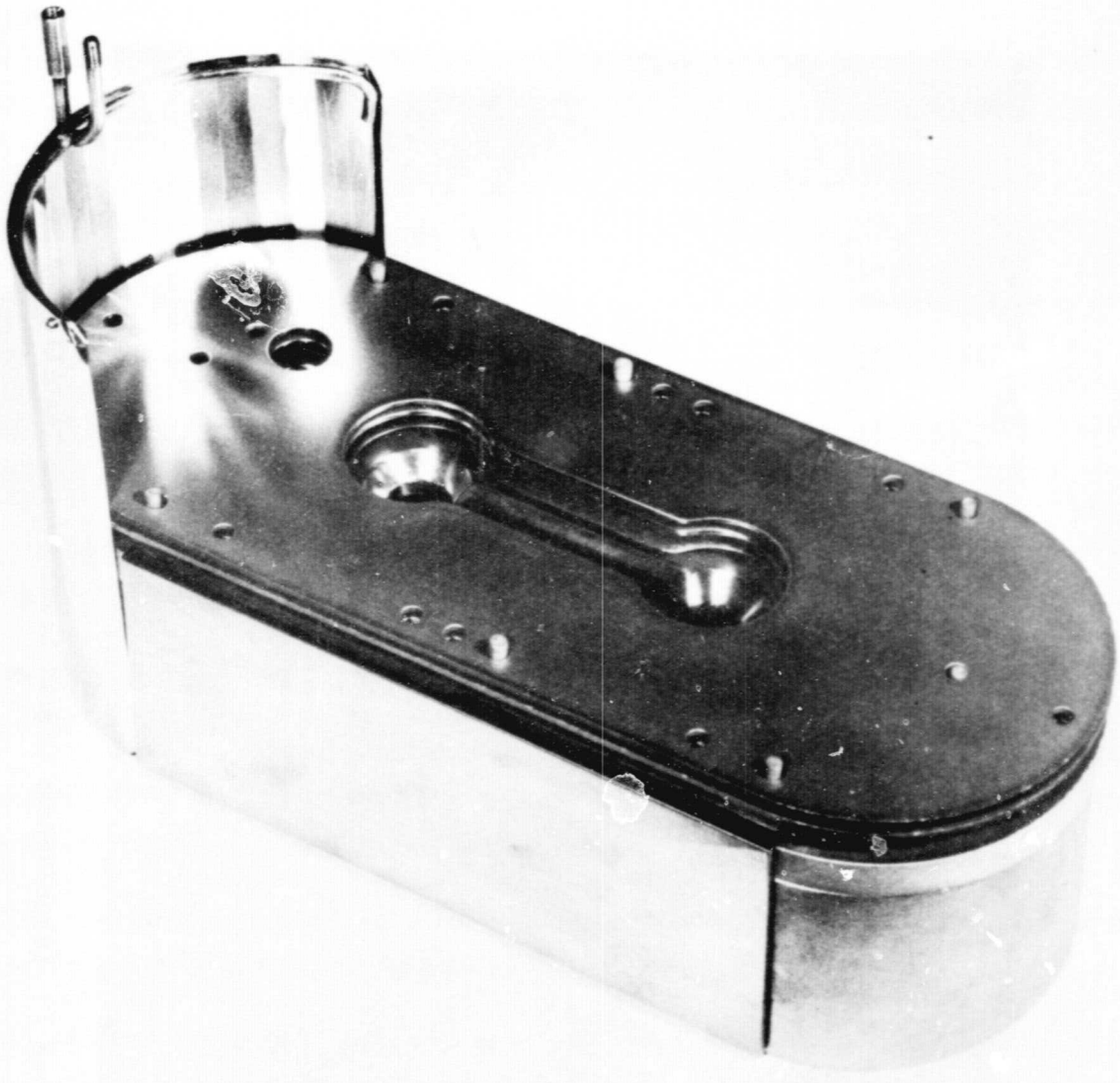

Figure 8 Adjustable thermal shield surrounding feed end of susceptor used for web growth.

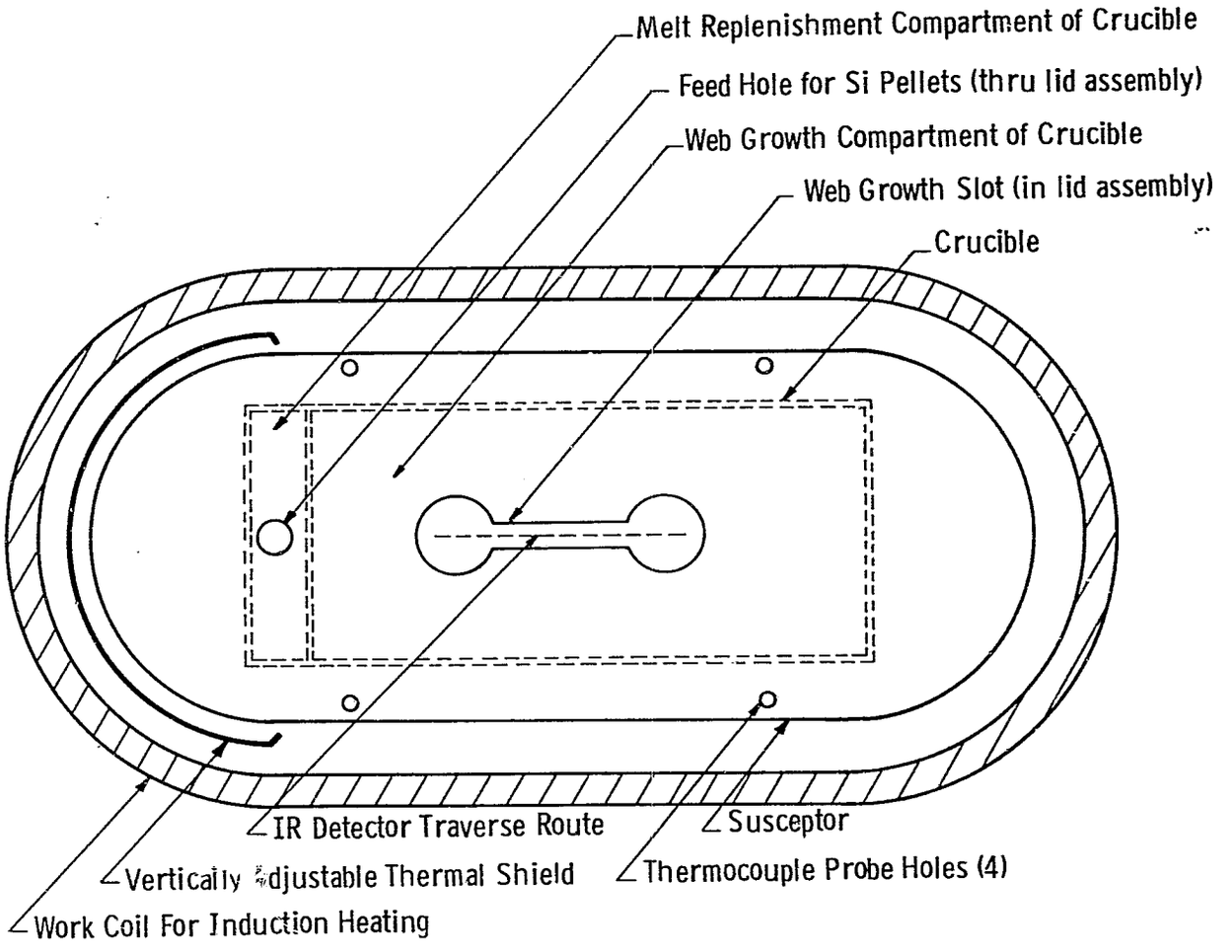

Figure 9 Top view susceptor system showing location of vertically adjustable heat shield, melt temperature profile measurement and thermocouple probe holes.

Two of the thermocouples were located in the back wall of the susceptor, near the bottom, 4 1/8" apart. A third thermocouple was located in the center of the susceptor, below the crucible. The infrared measurements were made by placing the infrared pyrometer either at the center of the dogbone slot, or one inch to either side. For the infrared measurements, the pyrometer was temporarily mounted above the growth chamber.

One set of measurements compared the thermocouple readings as the end shield, was moved with a dendrite "hold" temperature being found at each shield position to maintain a constant melt temperature at the center. These measurements are plotted in Figure 10. As expected, the axial thermocouple held essentially constant, within the accuracy of the "hold point." The changes in temperature determined from the thermocouples in the susceptor wall indicate that the shield shifts the total thermal distribution in the susceptor. With the shield inserted 4cm, for example, a temperature change of over 10° compared to the case with no shielding was achieved.

Since a dendrite could not be inserted while the infrared pyrometer was in position, and since the axial thermocouple essentially followed the "hold" temperature, the thermocouple was used thereafter as the control. The infrared pyrometer readings at the center of the melt held fairly constant, $\pm \sim 2/3°$. Again, as the shield was lowered, the relative changes in melt temperatures (at the points one inch from the center) became large (Figure 11), over 10°C with the shield lowered 4.8cm. Since the measurement points are closer than in Figure 10, this implies the gradient in the liquid is actually larger than in the susceptor wall.

In using the infrared pyrometer, we found that temperature fluctuations of $\pm$ 1/4° at a given point were generally present. This was confirmed to be in the melt rather than an instrument problem by sighting the pyrometer onto the lid and observing no fluctuations. Since the magnitude of the fluctuation was fairly constant, the pyrometer values in Figure 11 are the average of the extremes measured at a given point without error bars. Also, the pyrometer is quite sensitive to the back/front location in the slot. Part of this sensitivity

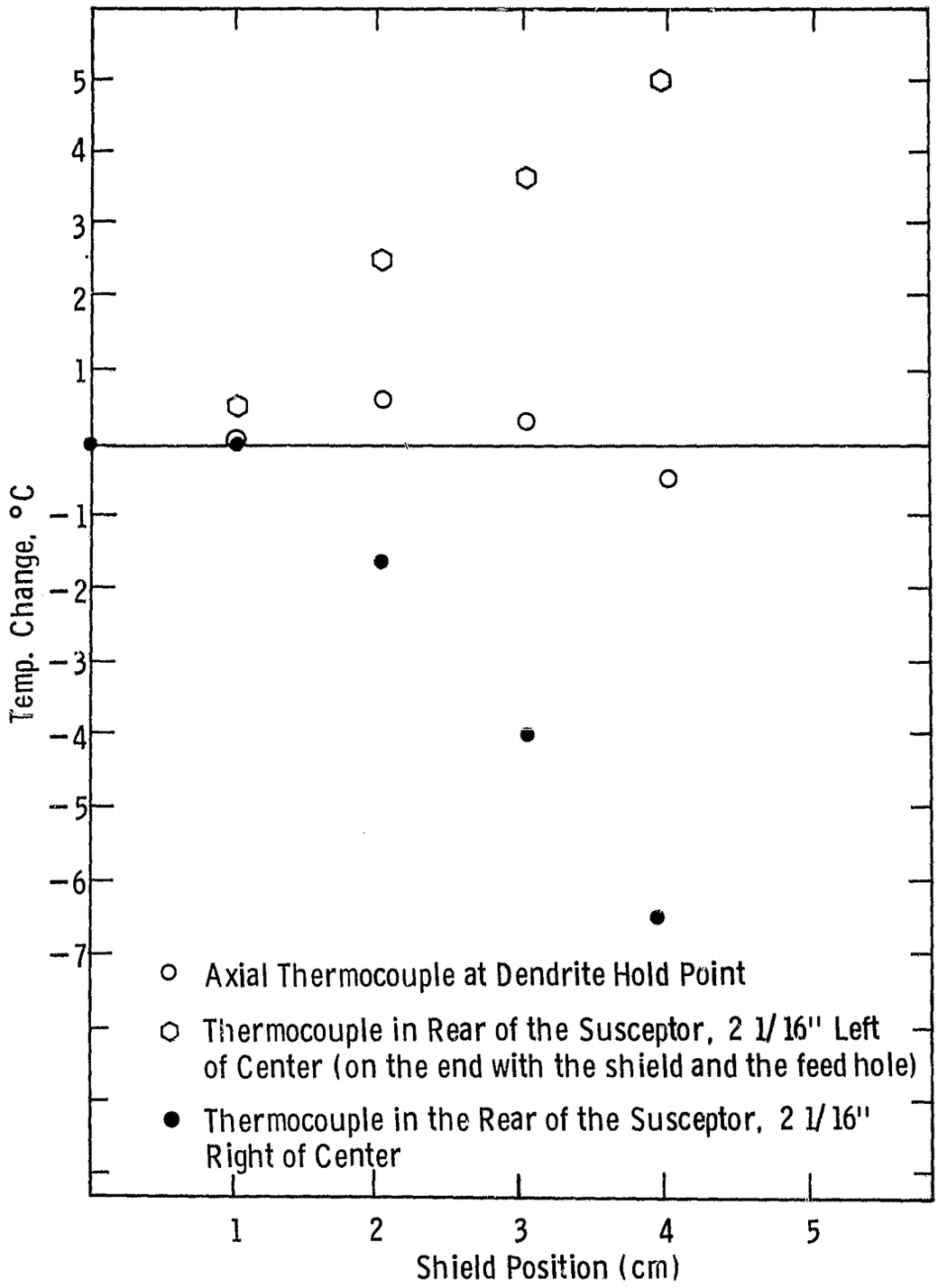

Figure 10 Comparison of temperature changes at various susceptor points vs the end shield position. At 0 cm the shield is not affecting the susceptor; at 1 cm the shield has been lowered, and is shielding the top centimeter of the susceptor.

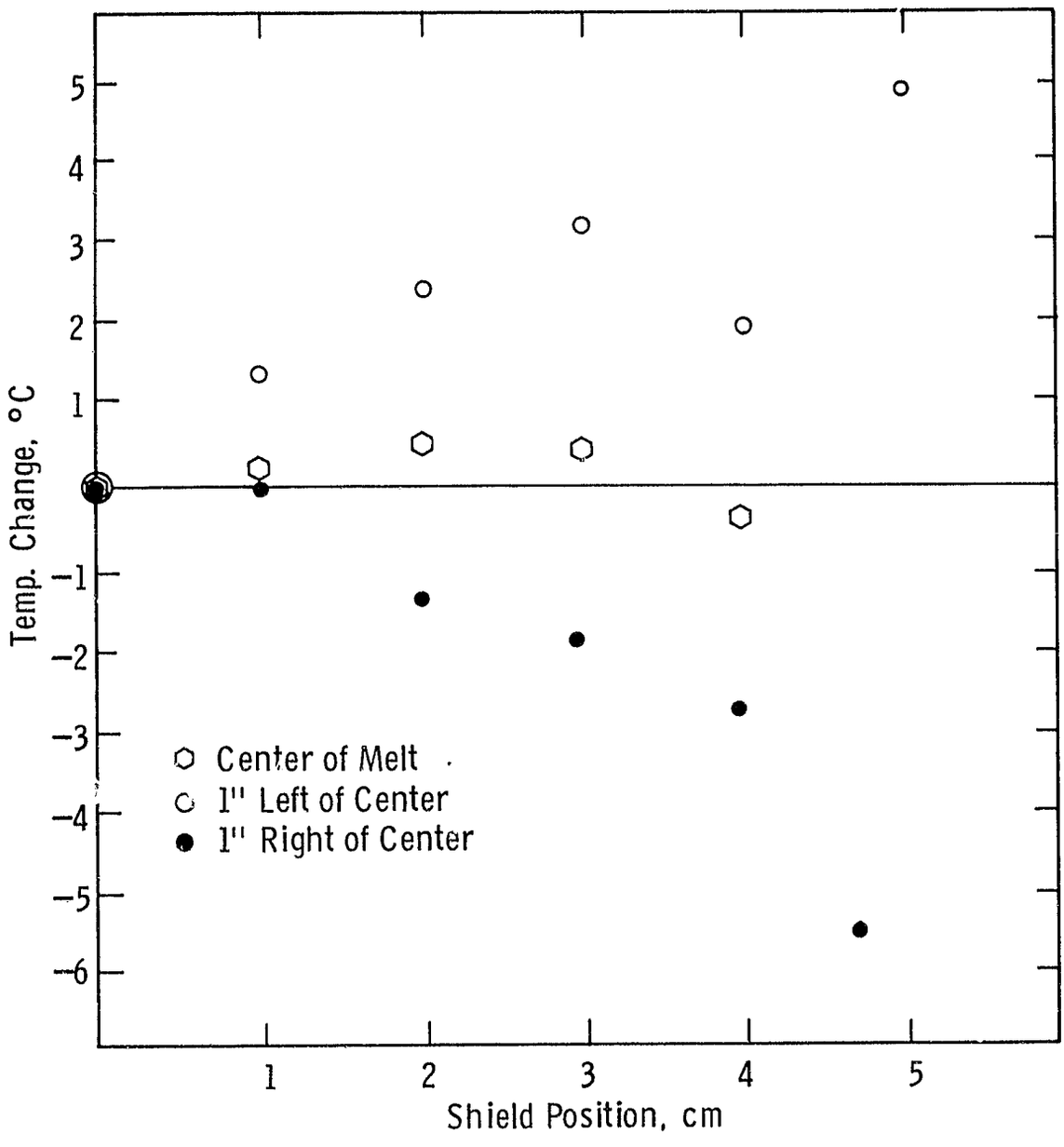

Figure 11 Comparison of temperature changes in the silicon melt at different end shield positions. Points represent average values of pyrometer readings at each location.

is due to "clipping" of the view angle by the chimney through which the pyrometer views the melt surface. Although small dimensional variations in the chimney add to alignment difficulties and make actual temperature measurement along the slot very difficult, relative temperature changes still can be made easily.

In the last set of measurements the infrared pyrometer was mounted one inch from the center on the left or feed side. The results of this set of data, where temperature changes were recorded as the feed rate was changed for various shield positions, can be seen in Figure 12.

Pellet feed rates of 2 per minute introduce a negligible thermal effect; at 10 pellets per minute a depression of about 1°C was observed (at the sensor location one inch to the left at the melt center). The temperature depression in the feed chamber is actually somewhat lower than this as shown in other experiments where freezing occurred with partial shield insertion. By use of the movable shield we have been able to control the temperature distribution for pellet melting during all elements of feeding and web growth.

Experimental Results

Considerable progress was made in melt replenishment task. Despite delays in the delivery of components for the melt level system, the need to develop a reliable compartmented crucible, and the efforts involved in developing a shield system to maintain the required thermal symmetry during feeding, convincing demonstrations of the melt replenishment system have been performed. Among the runs were several of 5 or more hours, one 13 hour run, and one 17 hour run-the equivalent of a one day cycle. Although there were difficulties encountered, none were related to pellet feeding. It is notable that in addition to the length of the runs, feed rates consistent with the rate of withdrawal of the web crystal have been demonstrated.

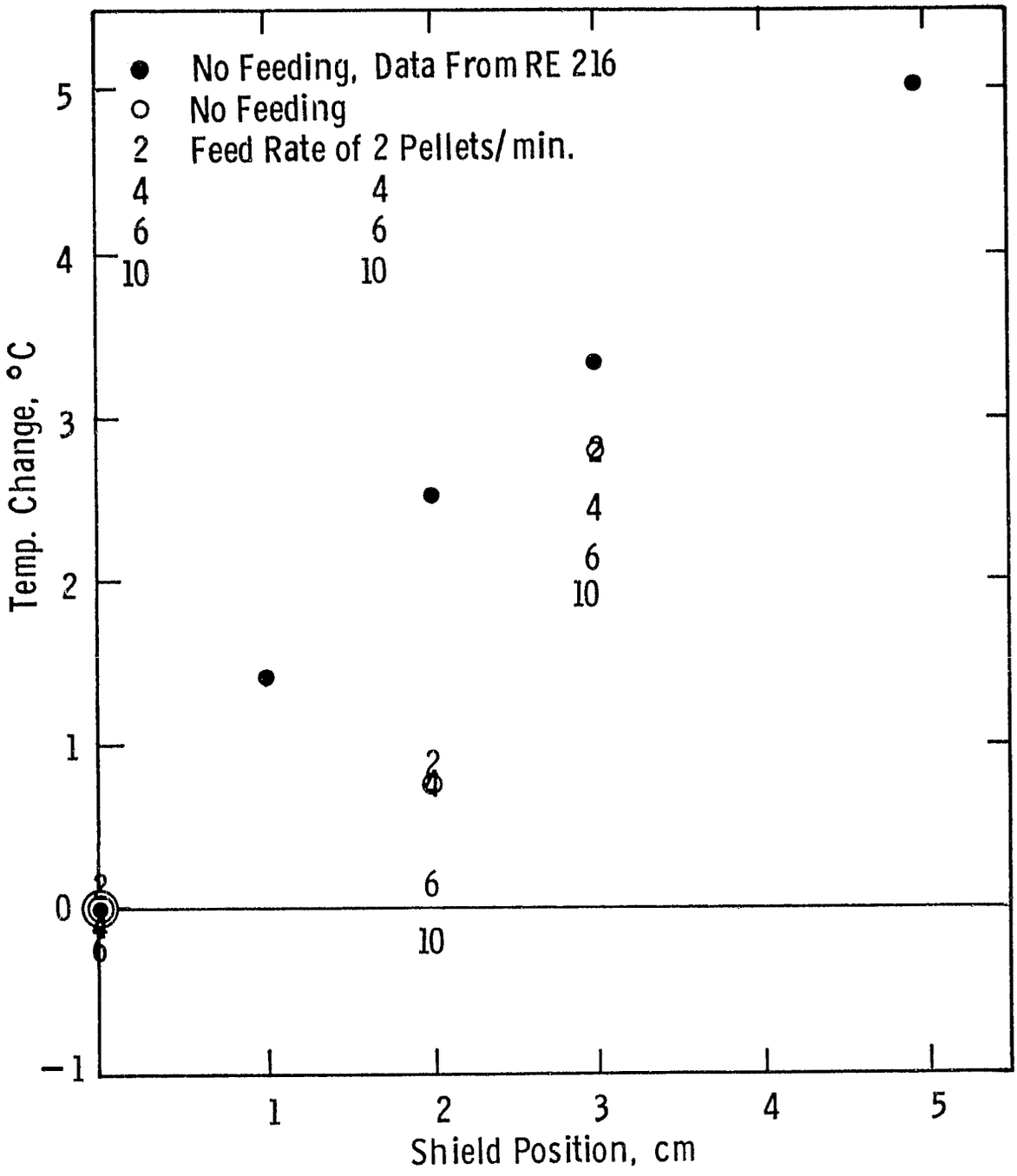

Figure 12 Effects of pellet feeding rate on temperature, compared at various end shield positions.

An evaluation of the sensitivity of the melt level sensing system verified the acceptability of the equipment to meet the requirements for automated growth. In Figure 13 is a reproduction of the tracing on the strip chart recorder of the melt level sensor during web crystal growth. Prior to the start of crystal growth the trace is level indicating no change in liquid level. After the initiation of growth the trace is deflected to the left indicating a lowering of the melt level. A total of 26 grams of silicon was removed by the crystal growth which corresponds to 13 mV. A 1mm change in melt level corresponds to a change of 20 grams of silicon; this is the equivalent to a 10 mV reading on the detector which is readily sensed.

In Figure 14 is an example of the strip chart reading of a run during which pellets were fed concurrent with the growth of the crystal. The pellet feed rate was adjusted independently of the melt level sensor. (Automated Feeding will be discussed in a later section.) The initial feed rate was 8 pellets/minute. The rate was increased to 10 pellets per minute during the run as the sensor indicated a gradual lowering of the melt height. Indications are clear that melt level should be controllable to well below 1mm and satisfactory sensitivity for automated replenishment is available.

Most of the feed runs have been made with the J-181 and J-252 lid and shield configurations. These lids were selected because of their history of reproducible growth of long crystals. Successful five hour runs have been made with both configurations. The 13 hour run was made using J-252. The one day cycle (17 hour run) was made using a modified J-252; i.e. the same lid but modified top shielding over the lid.

The results of these runs are listed on the run summary section in the appendix. However, some comments are appropriate relative to the 17 hour run. The lid/shield configuration used provided stable growth throughout the continuously fed sequence. No ice formation was observed that was attributable to the pellet feed. However, during the run some spalling of oxide accumulated on one of the shields did cause

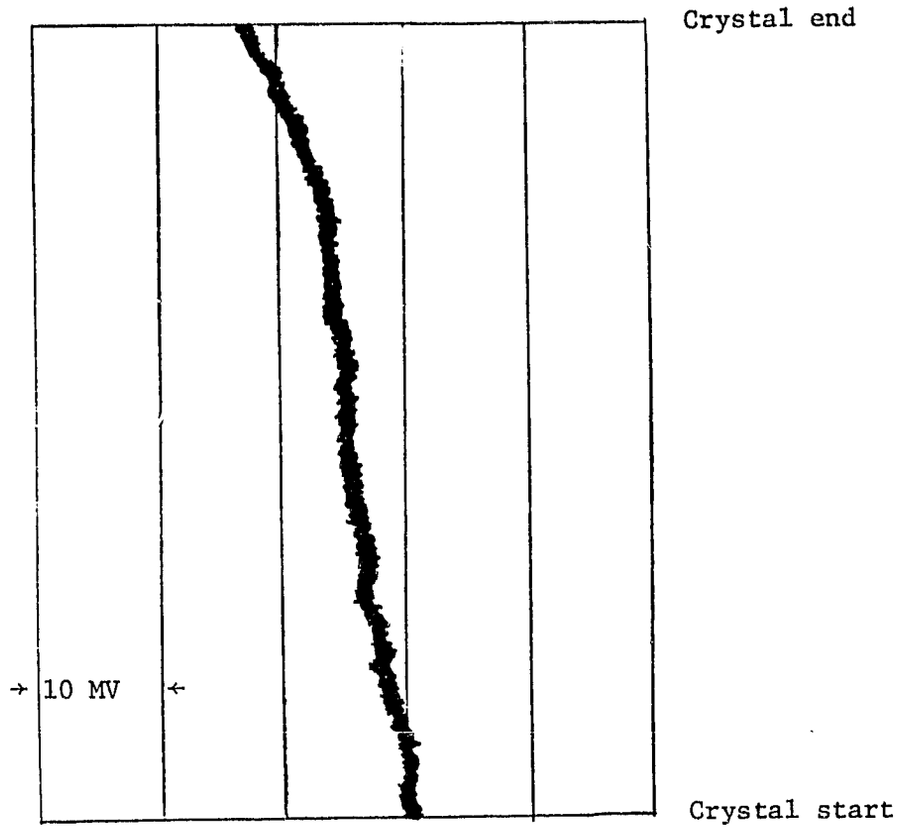

Figure 13 Example output of melt level position detector, taken without melt replenishment

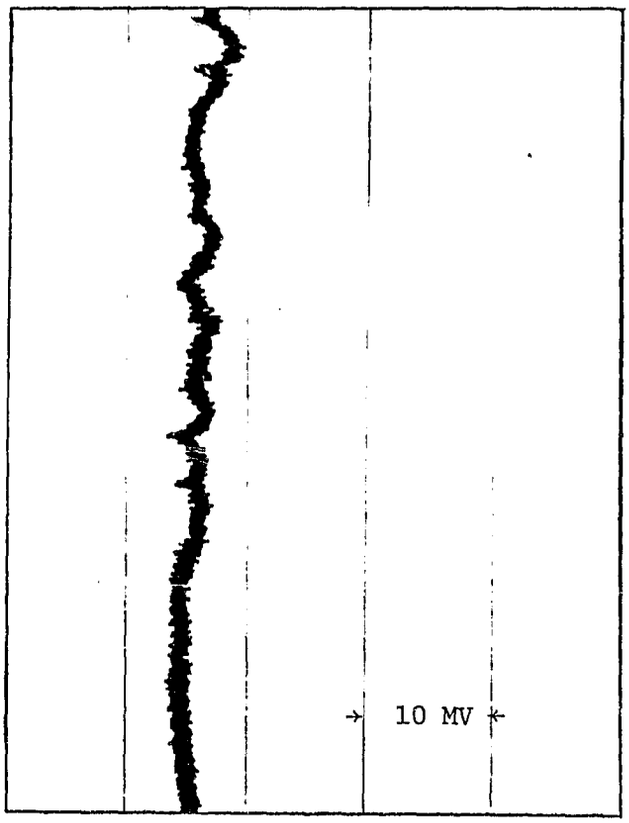

Figure 14 Output of melt level detector during feeding and concurrent growth

termination of crystal growth. As a result although the melt was fed continuously, crystal growth was not continuous. Of the 17 hours of run time 12 hours and forty five minutes was the actual crystal growth time. A further important observation was the solar cell performance of the material grown at different times during the run. Six separate crystals from the start to the end of the run were made into cells. The results are listed below:

Crystal	Uncoated Efficiency	AR-Coated Efficiency
1	9.70	13.9
2	9.43	13.5
3	9.09	13.0
4	9.30	13.3
5	9.72	13.9
6	9.00	12.9

It appears as if the quality of the web remains high with long term melt replenishment.

The run was terminated after seventeen hours because sufficient information had been obtained, not because of operational difficulties. The results do indicate that further shield modifications to minimize oxide accumulation are desirable. Minor tuning of the temperature gradients in the melt is also indicated since dendrite choppiness indicative of convective flow was observed. Clearly, the capability of the system to grow web with melt replenishment is established and the quality of the web crystal is not affected by long term feeding.

3.2 Throughput

3.2.1 Progress

In the past year, system characterization and thermal modeling have provided guidance for the refinement of lid geometries to enhance the throughput of web. The emphasis has been on relatively subtle changes

in temperature distribution in the growing crystal by modification of lid and shield geometry. Experimental highlights of this activity are described followed by a discussion of the complementary work on system characterization and modeling.

At the end of Phase II, the maximum demonstrated web width was 4.2cm and the maximum area throughput was 23.6cm^2/min. Currently, these values are 4.7cm and 27.2cm^2/min respectively. More dramatic than overall width increases has been the increase in width of high quality web crystal before the occurence of stress-induced defomration. A gain of more than - cm as compared to earlier results has been realized through modifications in shield configurations. A sampling of width and thruput results are given in Table 1.

3.2.2 Background

For the dendritic web process, three components are involved in maximizing area throughput: crystal width, growth velocity and affecting both of these, maintaining melt height at the optimum level. Crystal width is limited by the melt temperature profile and stress induced deformation . Growth velocity is limited by the rate at which the heat of fusion is dissipated. For a given configuration, there is an optimum melt level for minimizing stress and maximizing velocity. (See Ref. 1 for detailed discussions of the various thermal aspects of web growth.) In this section, we will discuss the experimental efforts to enhance width (throughput) by reduction of thermal stresses. This effort has had an increasing emphasis on integrating the thermal requirements for width, speed and melt replenishment. This is in contrast to, but a natural progression from, the earlier efforts where each component was studied more or less independently. The purpose here is to ensure that a compatible set of thermal parameters are developed and optimized for future incorporation into an automated growth facility. To this end the J-furnace has been equiped for melt replenishment and work on throughput is being tested under thermal conditions compatible with feeding.

TABLE 1

SOME THROUGHPUT AND WIDTH RESULTS

Run No.	Throughput rate cm^2/min	Width mm	Growth velocity cm/min
J-163	21.7	32.5	6.75
J-164	20.0	34.9	5.74
RE-151	-	43.1	-
RE-156	19.6	39.1	5.0
J-165	-	40.5	-
J-173	22.0	32.8	6.7
J-180	-	40.1	-
J-181	-	42.1	-
J-182	-	44.3	-
J-189	16.6	36.0	4.5
J-192	18.7	36.0	5.2
J-195	21.5	35.8	6.0
J-196	27.1	35.7	7.6
J-200	15.8	47.2	3.3
J-212	16.5	32.9	5.0
J-213	16.6	32.0	5.2

3.2.3 Experimental Configurations for Improved Thruput

The two principal experimental variables which affect web width are the temperature profile in the melt and the temperature distribution in the web in the first few cm above the growth interface. The former determines how wide the crystal can grow. The latter affects the stress in the crystal, which if large will cause degeneration of crystal quality by deformation and force termination of growth at widths smaller than the potential width allowed by the melt profile. These temperature profiles are controlled experimentally by slot geometries and shielding configurations.

During Phases I and II of this program, considerable emphasis was placed on the development of slot geometries which would provide melt temperature profiles conducive to the growth of web crystals 5 to 6 cm wide. During Phase II it became clear that stress in the web width at values below the capabilities of the melt.
profiles, and the stress problem was attacked by a combination of thermal modeling and experiment. During Phase III, stress reduction has been a major objective of the experimental efforts to improve throughput.

The regions in the growing web where the thermal environment (temperature distribution) affect the stress levels in the web are shown in Figure 15. The most critical region falls within the thermal domains of the lid and top shields. Therefore, our approach to minimizing stress has been to test the effects of variations in top shield configurations on growth behavior. Variables include slot geometry, number of shields, spacing between the shields and shield temperatures. A sampling of variations tested is shown in Figure 16. Figure 16A shows a cross section of the base line lid and shield configuration used in earlier experiments[1,2]. The top shielding consists of a thin molybdenum shield which is bent to cover the top edge of the beveled lid slot below it. A 1.5 mm thick shield is placed over both lid and intermediate shield. With this arrangement, argon flow tubes parallel to the slot were needed to prevent silicon monoxide from collecting on the lip of the bent shield. This arrangement consistently produced 3.5 to 3.6cm wide web.

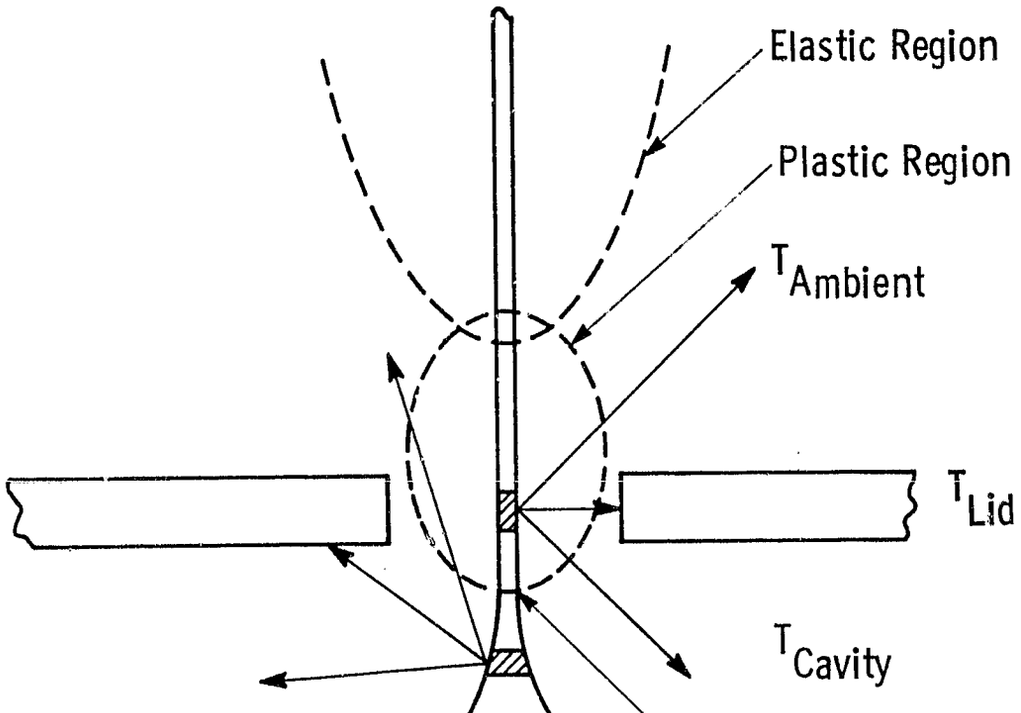

Figure 15 The thermal environment around a growing web crystal. Critical regions for stress generation are noted.

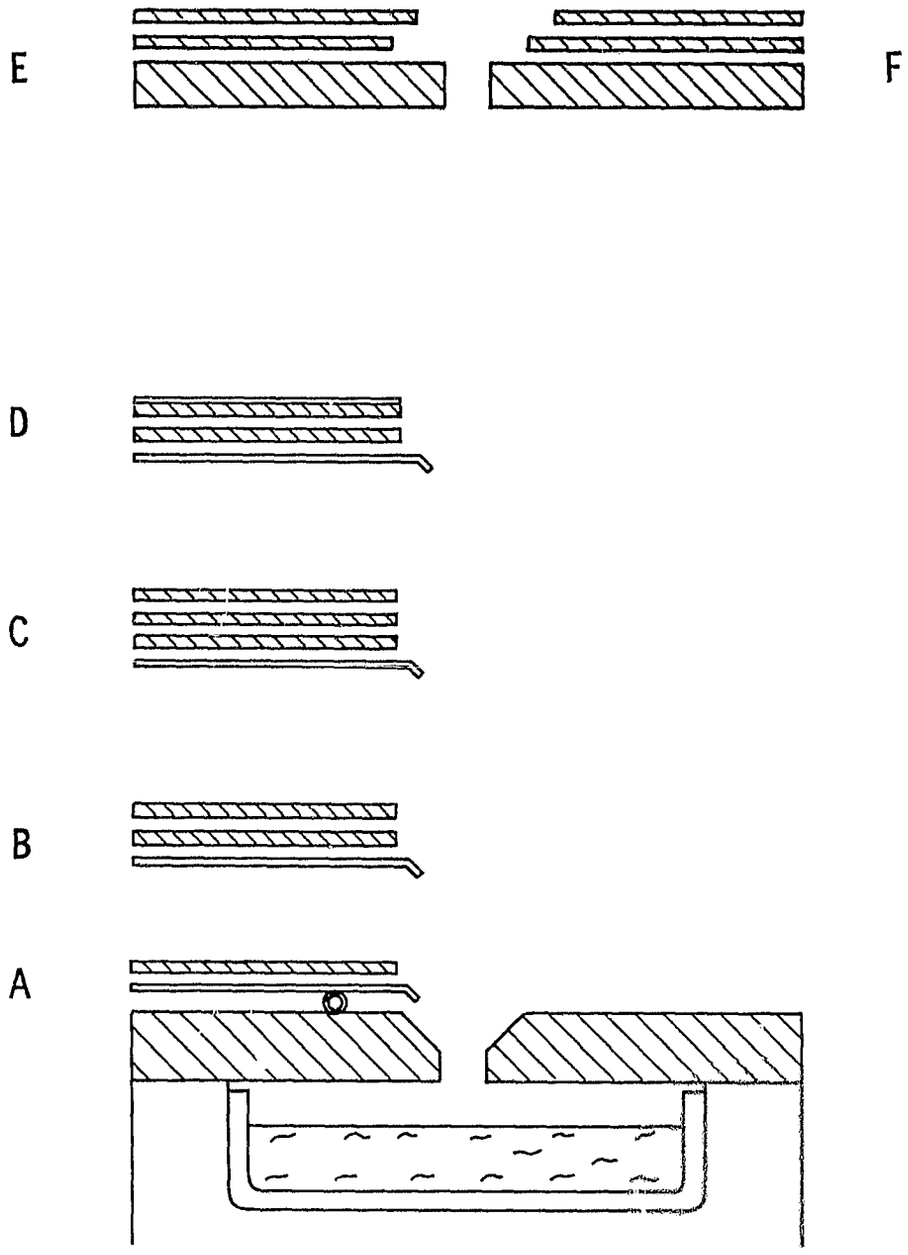

Figure 16 Lid/Shield configurations to control the vertical temperature profile in web crystals.

The first variation to this configuration which we tested was simply the addition of a second 1.5mm thick shield with the same slot shape as the one below, figure 16B. This arrangement immediately yielded increased web width to 4.0-4.2cm in both the J and RE furnaces. Further experience with arrangement yielded wider crystals, to 4.7cm. An additional benefit gained from this configuration is that the formed or bent shield remained oxide-free without the use of the argon flow tubes, thus simplifying the setup.

An obvious extension to this approach was to add a third thick top shield as in Figure 16C. However, this configuration was unsuccessful; free-floating silicon "ice" repeatly formed on the melt. We suspect that the melt at the crucible wall was not quite hot enough to prevent nucleation due to the flattened thermal profile in the liquid.

Another shield variation, shown in Figure 16D, comprised a thin (0.5mm) shield laid atop the second thick shield. The purpose here was to provide a colder view to the web just above the shield stack, which the thermal modeling indicated to be favorable in terms of stress reduction. A crystal width of 4.4cm was attained with this configuration in one run and a thruput of 27.2cm^2/min in another.

A drawback to the thin shield is that the shield became warped with usage. This diminishes the day to day reproducibility for the configuration and its utility in an engineering sense, although the principle of operation for high output rate was demonstrated.

Based on these encouraging results, another approach was taken to provide a colder top most shield. Ordinarly, the normal thick (1.5mm) shield couples inductively and is heated in the same manner as the lid and susceptor. In order to reduce this coupling effect, the periphery of the shield was slitted, as shown in Figure 17. The reduction in coupling to the shields is quite evident visually and is confirmed from actual measurements of shield temperatures (see section 3.2.3).

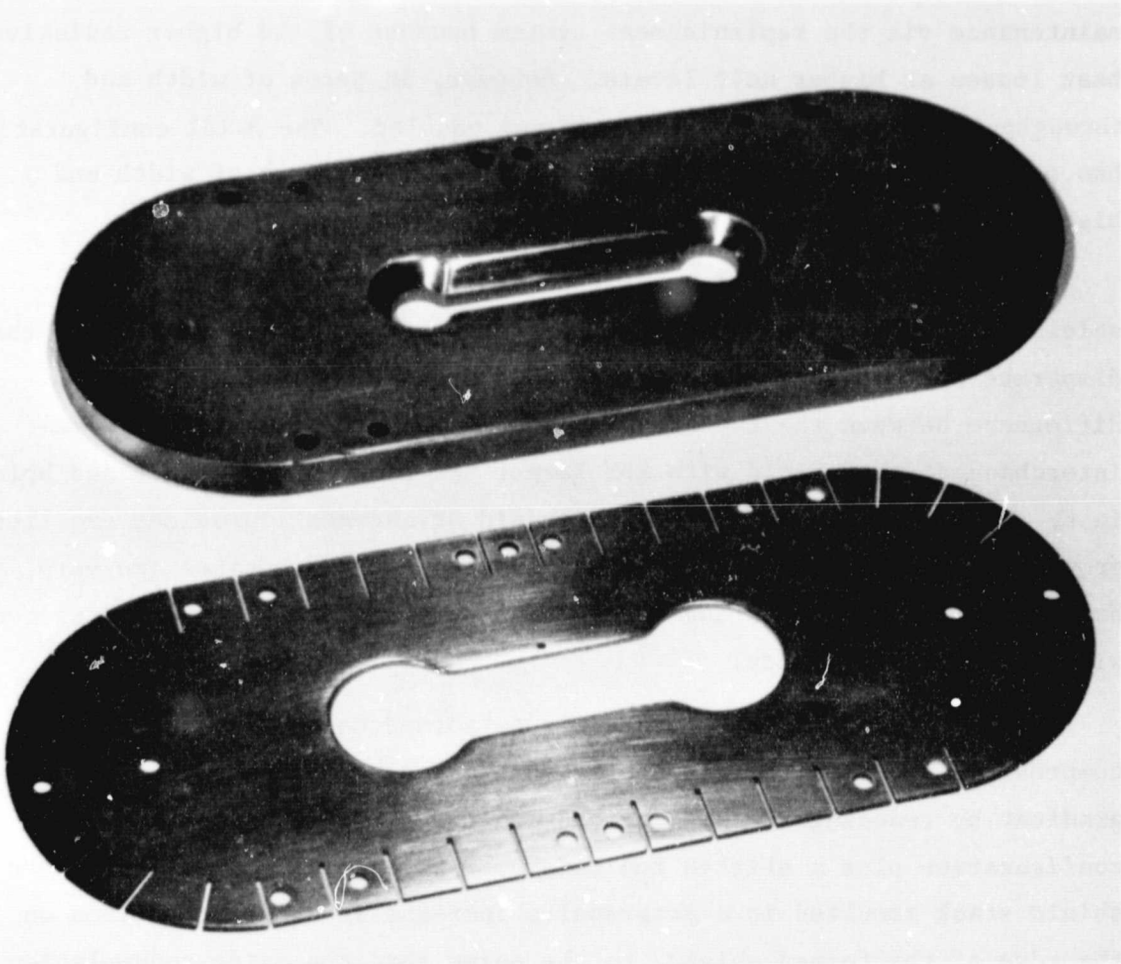

Figure 17 The J-181 lid and a slitted top shield designed to reduce inductive coupling effects.

A series of experiments utilizing one or more slitted shields with the J-181 lid configuration, (Figure 18) showed that very stable growth conditions could be achieved with easy and reproducible growth initiation at relatively high melt levels. This has positive implications in terms of increasing growth velocity when coupled with melt level maintenance via the replenishment system because of the higher radiative heat losses at higher melt levels. However, in terms of width and throughput the previous results were not equaled. The J-181 configuration has overall been the most consistent performer in terms of width and high thruput.

One further example of the magnitude of the effect of top shield configuration on growth behavior can be noted with respect to the disparate performances of configurations E and F, Figure 16. The difference between the two arrangements is that the two shields were interchanged; the shield with the larger set back is above in F and below in E. Configuration E, (RE-1 Type shield arrangement) provides excellent growth stability, whereas with configuration F the dendrites are very non-uniform in thickness and spontaneous pullouts or extra dendrites occur with excessive frequency.

A series of experiments was performed to test the effects of compressing the total height of the shield stack and thus the vertical gradient by reducing the spacing between the shields, using the J-181 configuration plus a slitted top shield. Systematic compression of the shield stack resulted in a progressive increase in oxide deposition on the edge of the formed shield, to the point that the oxide accumulation interferred with otherwise very stable growth. With close spaced shield configurations the use of barrier type separators between the shields (instead of washers) to inhibit gas flow between the shields reduced the rate of oxide deposition somewhat, but did not extend the available growing time sufficiently to fully evaluate the effects on growth behavior of close spaced shields.

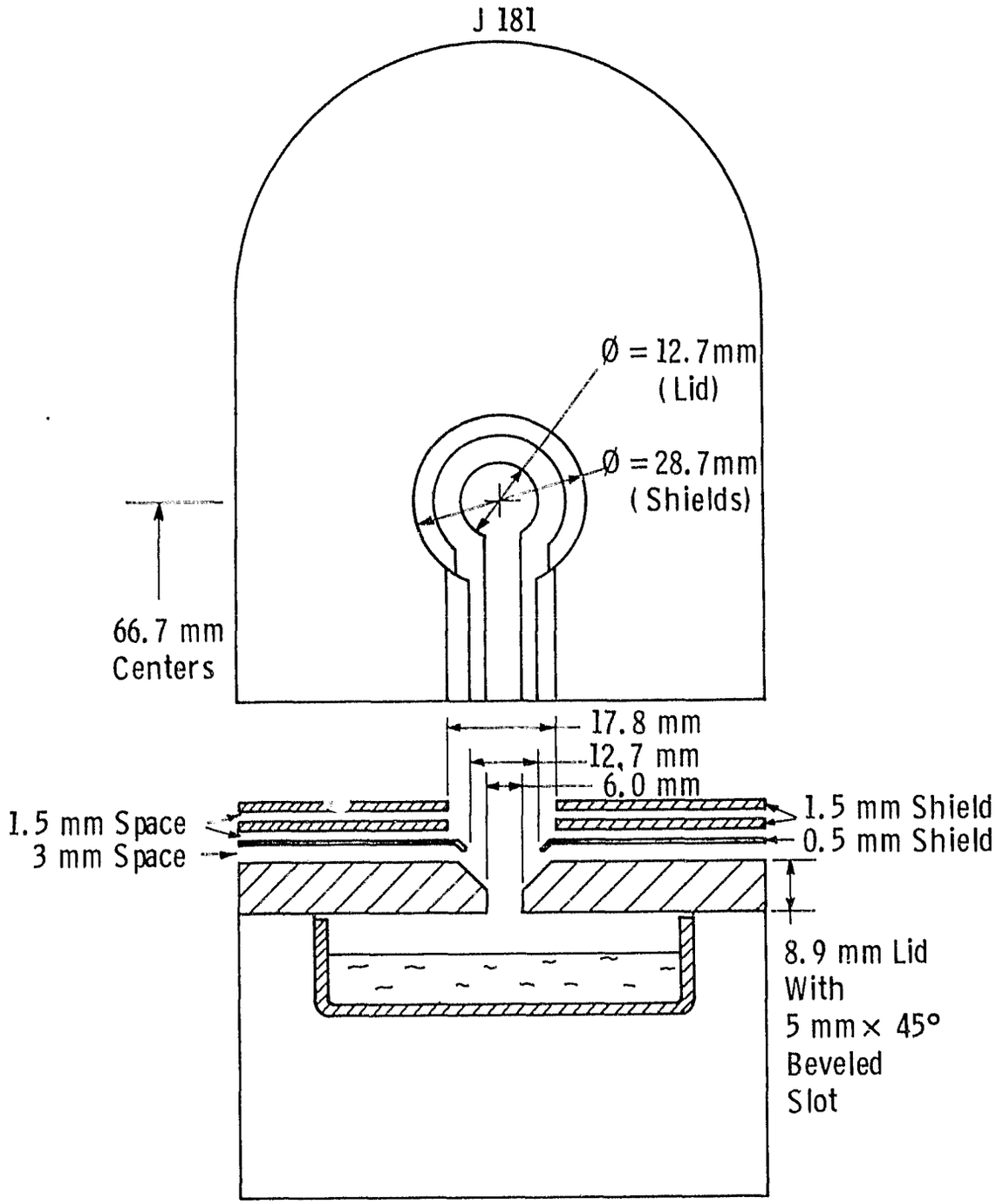

Figure 18 The J-181 baseline lid and top shield configuration

Recently, the J-furnace was modified for melt replenishment, incorporating all the features successfully tested and utilized in the RE-facility except the melt level sensor (which may be incorporated later). The purpose is to grow web with high throughput geometries under conditions which are 1) thermally compatible with and 2) may be improved by melt replenishment.

3.2.4 Width Control

Control of the crystal width in dendritic web growth depends on a balance between lateral heat loss from the bounding dendrites and the temperature profile in the melt, as discussed in Appendix 9.3. The importance of width control lies in the capability of growing very long crystals of a width compatible with a specific device requirement. Since most of the experimental effort in the present phase of the contract has been targeted at maximizing ribbon width, only a small effort has been expended on experiments with constant width growth, especially since feasibility had been established in the previous phase of the work.[1]

The earlier experiments with width control were carried out in a small, round crucible geometry and thus the design could not be carried over directly to the long crucible systems. The basic design criteria - low lateral losses and a "dished" melt profile - were used to design several lid/shield configurations. The experimental resulsts indicated that the basic concept was correct and a number of crystals were grown which approached a steady state width, but a true steady state was not achieved. Some of the deficiencies of the present designs are becoming evident and will be eliminated in future work.

3.2.5 Growth System Characterization and Thermal Modeling for Equipment Design

An important adjunct to the web growth studies themselves is development of a data base characterizing specific system configurations and analysis techniques to provide design guidance for future improvements. Thus we recently have been evaluating and improving the correlation between observed web growth behavior and the mathematical models which describe the growth process. As noted earlier, qualitative agreement between the computer simulation[1] and measurement has been good but quantitative agreement is hindered because some parameters, such as lid and shield temperatures, used in the model are known only approximately. The purpose of the work described below is to give better insight into the relationship between the imposed growth conditions and the way web actually grows and to identify directions for improved system design.

The first step toward developing system designs with enhanced output rates is to evaluate just how well the model used for design guidance actually describes the performance of a specific growth geometry. To accomplish this, actual temperatures at critical regions had to be measured, and a suitable growth parameter to compare with the model had to be identified.

The most important system parameters seem to be the temperature at the slot in the susceptor lid and the concomitant temperature of the top susceptor shield. The choice of growth parameter is less direct. The most appropriate data would be the temperature distribution along a growing web. However, the task of measuring this profile with the necessary accuracy in both temperature and position is formidable. A relatively simple measurement, that of the ribbon thickness as a function of velocity, provides a great deal of information, especially the initial slope of the temperature distribution. The following subsections describe these measurements as well as the validation of the thermal model.

3.2.5.1 System Temperature Measurements

To provide data for the thermal modeling and lid design effort, thermocouple measurements were made of the lid and the top shield temperatures of a J181 configuration (see Figure 18) with the melt at the "hold temperature". Small holes were drilled in the lid and shield near one side of the mid position of the slot, such that the thermocouple beads were centered in the thickness dimensions. The lid temperature was measured with a Type B (Pt-30%Rh/Pt-6%Rh) couple with the bead inserted deeply into the material; the long "immersion depth" created by running the leads between the lid and the first top shield would minimize temperature measurement errors. The top shield temperature was measured by a Type K (Chromel-Alumel) couple and in this case, the bead was secured in the hole with an alumina slurry cement to assure thermal contact. The thermocouple outputs were fed into a data logger and monitored until a steady state thermal situation was reached.

Two modifications of the J181 configuration were analyzed. In the first configuration (baseline) the 1.5mm thick top shields were solid and thus coupled to some extent with the induction field. In the second modification, the periphery of the top shields was interrupted with slits 12mm deep about 1mm wide and spaced every 12mm as in Figure 19 Section 3.2.5.2.The intent of this modification was to reduce the inductive coupling to the shields, and this was successful as can be seen from the data, Table 2. The data also show that the lid temperature is relatively insensitive to coil height, while the top shield temperature is more strongly affected. When these data were compared with the temperatures previously used in the thermal modeling, it was found that the measured lid temperature was about 50°K to 150°K hotter than had been assumed on the basis of a radiation equilibrium between the lid and shields. Even in the case where the shields were slit, it appears that the top shield is somewhat hotter than anticipated. This may be due in part to conductive transport of heat through the gas and in part to some residual heating by the induction field. In any case, apparently reliable data is now available for use in thermal modeling.

TABLE 2 LID AND SHIELD TEMPERATURES FOR J181 CONFIGURATIONS

Coil Position	Shield Type	Lid Temp., °C	Top Shield Temp., °C
100.0 mm	Solid	1354.7	963.1
102.7	"	1351.3	941.7
105.0	"	1344.6	927.4
101.0	Slitted	(open T.C.)	878.6

Note that in the coil position column, higher numbers mean a lower coil position relative to the susceptor.

3.2.5.2 Velocity-Thickness Measurements

The relation between the thickness of a web crystal and its growth velocity is dependent on the rate at which the latent heat of fusion can be removed from the growth front. As such, both the heat loss to the supercooled liquid and the heat loss through the web itself make a contribution so that the interpretation of measure velocity-thickness (v-t) relation is not completely unambiguous. As will be discussed later, however, the contribution from the supercooled melt can be ascertained with reasonable exactness, so that the web contribution can be extracted from the combined data.

Generation of the experimental v-t data is straightforward; once growth is started, the pull speed on the crystal is varied incrementally to provide segments of different thicknesses. The only major caution is to allow 10 to 15 cm of growth at each speed in order to reach steady state. If the twin planes do not grow out of the ribbon as it thins, then the speed can be set at normal rate and growth continued. There is, in fact, some suggestion that thinning the crystal may improve its quality by eliminating dislocations.

The most convenient means of presenting velocity-thickness data is to tabulate the coefficients a and b in the equation

$$v = a + \frac{b}{t} \qquad (1)$$

where t is the ribbon thickness. This empirical equation not only proves to be an excellent fit to the experimental data but also, as will be seen, is a very good representation of the modeling results. Some representative data on crystals grown from the J181 type lid configurations are given in Table 3. Several minor modifications of the configuration are included and it is evident that there is very reasonable reproducibility between crystals grown from the same configuration and even among the different modifications. Rather than include the correlation coefficient for the data, the root-mean-square deviation for the velocity, S, is given in the table. In most cases S is about 0.01 to 0.05 cm/min which is of the order of accuracy in determining the pull speed setting, i.e about 1 division on the control dial.

TABLE 3 VELOCITY-THICKNESS DATA FOR J181 CONFIGURATIONS

Crystal	Configuration (See Notes)	ΔT °C	a cm/min	b μm-cm/min	S cm/min	REMARKS
J197-1	Std.	4.3	1.33	167	.019	Full (185 gm) crucible
J198-2	M1	3.4	1.17	146	.028	8 gm removed by growth
J199-1	M1	5.0	1.17	154	.029	5 gm removed
J211-1	M2	3.6	1.17	150	.006	Full (185 gm) crucible
J211-5	M2	3.7	1.22	107	.02	45 gm removed by growth

Notes: The lid configuration are as follows

Std. - Identical to Figure 2.

M1 - Added thin shield placed directly on top of J181 (std) top shield

M2 - Added heavy shield; top two shields slitted to reduce coupling.

One particular data set is worth notice. Crystals J-211-1 and J-211-5 were the first and last crystals grown in furnace run J-211. Between the growth of the two crystals, about 45 gm of material had been drawn from the melt causing the melt level to fall about 2mm. This change in melt height is apparently reflected in the "b" coefficient of Eq. 1.

3.2.5.3 Modeling the Performance of Lid/Shield Configuration

The approach we adopted for the modeling effort was to establish a baseline calculation for the J181 growth configuration using the measured lid and shield temperatures. The results of the calculations were then compared with experimental data to evaluate the overall validity of the model. As mentioned in the foregoing section, the simplest data which can be used for this comparison is the relationship between the web thickness and the growth velocity. In order to match the empirical data, two models must be evaluated: first, a calculation of the heat loss to the meniscus and supercooled melt, and second, a calculation of the heat dissipated from the crystal itself. For all intents, these calculations are independent and the results can be conveniently expressed as partial velocities, v_{melt} and v_{web}, with $v_{total} = v_m + v_w$.

Meniscus Heat Loss

The thermal model of the heat loss to the meniscus follows the same approach as the model for the heat loss from the web as described in appendix 6.5 of the 1978 annual report of this project.[3] For this calculation, the most critical geometrical and thermal parameters are the temperature of the susceptor lid near the growth slot, the effective thickness of the lid itself, the width of the slot, the position of the interface below the lid, and of course the melt undercooling.

Although the geometry of the J181 configuration is well defined, a range of parameters were modeled to evaluate the sensitivity of the melt partial velocity, v_m, to changes in the lid configuration. Although the results must be nonlinear over an extended range of ribbon thickness,

the calculations proved to be a very good fit to an equation analagous to equation 1, namely

$$v_m = a_m + \frac{b_m}{t}, \qquad (2)$$

where the subscript, m, implies the coefficients apply to the melt heat transfer.

The results of the current modeling, Table 4, are given in terms of the coefficients a_m and b_m in Eq. 2. The most striking feature of these numbers is that they are relatively independent of the lid geometry and are mainly dependent on the melt undercooling. Furthermore, comparison with some earlier data showed that the coefficients were nearly the same even though the geometrical factors were different. Thus, an almost "universal" set of parameters a_m and b_m can be used to represent the partial velocity due to the melt for both modeling purposes and for analysis of experimental data.

Web Heat Loss

The temperature distribution and concomitant heat fluxes were calculated for the J-181 lid and shield configuration using the experimental lid and shield temperatures in the model. The basic features of the model are shown in Figure 19 in which the actual J181 configuration is compared with the model parameters. Temperature/heat flux data was calculated for three web thicknesses, 100, 150 and 250 μm in order to derive a velocity-thickness curve. The three temperature curves were very nearly the same except for a few millimeters near the interface. Again it was found that for the range of crystal thicknesses involved the data could be represented well by an equation of the form.

$$v_w = a_w + \frac{b_w}{t}. \qquad (3)$$

where the subscript w implies the coefficients are for the web. A fit to the data with $a_w = 0.88$ and $b_w = 64$ exhibited an rms deviation from linearity of 0.014 cm/min.

TABLE 4

COEFFICIENTS FROM MELT PARTIAL VELOCITY CALCULATIONS

ΔT °C	LIN mm	LID mm	SLOT mm	a_m cm/min	b_m μm-cm/min
4	1	6	6	.32	75
4	1	10	6	.31	72
4	2	6	6	.31	74
4	2	10	6	.30	71
2	2	10	6	.19	41
6	2	10	6	.41	99

ΔT = melt undercooling

LIN = interface distance below lid

LID = effective lid thickness

SLOT = slot width

a_m, b_m = coefficients in $v_m = a_m + b_m/t$

TC	TS	TBEVEL	TAS	TLID	ZD	ZH
1623	1460	.6	1213	1.0	1.35	1.85

Dimensions in CM

Temp. in °K

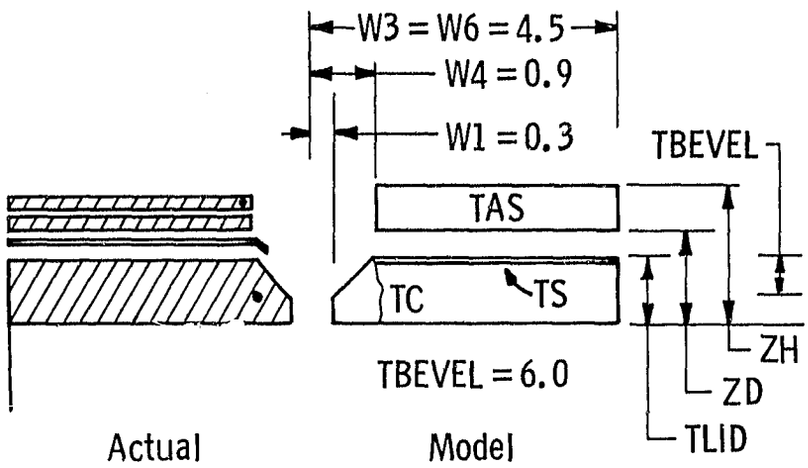

- Thermocouple Location

Figure 19 J181 Thermal Model Configuration

Combined Results

Since the form of the velocity-thickness is the same for both the melt and the web partial velocities, the like coefficients can be summed to give the total velocity as illustrated in Figure 20. The result can be expressed explicity as

$$v_t = (a_m + a_w) + \frac{(b_m + b_w)}{t}. \qquad (4)$$

For the present modeling results, this gives

$$v_t = 1.19 + \frac{137}{t}. \qquad (5)$$

where t is in μm and v is in cm/min.

The model results should be compared with the experimental results given in Table 3. Omitting the data for J211-5, which represents a melt lowered by several millimeters from the other cases, the average coefficients are $a_{expt} = 1.21 \pm .08$ and $b_{expt} = 154 \pm 9$. These numbers can be compared with the model results of $a_t = 1.19$ and $b_t = 139$. The agreement is quite good, especially considering the fact that the experimental data represents a (small) range of melt heights and supercoolings. The present model is apparently a good tool for predicting the velocity-thickness characteristics of new lid designs and is being applied to guide the development of designs for improved output rate performance.

3.3 Silicon Feedstock

With continuous melt replenishment being an important feature of advanced dendritic web growth technology, careful consideration must be given to the feedstock used in the process. Since the growing web crystal apparently rejects solute to the melt with about the same efficiency as a growing Czochralski crystal, there is good reason to expect that less pure, or "solar grade" silicon can be used for web growth technology. In this section, we will present some more recent

$$V_{total} = V_{melt} + V_{web}$$

$$V_i = a_i + \frac{b_i}{t} \qquad i = \text{total, melt or web}$$

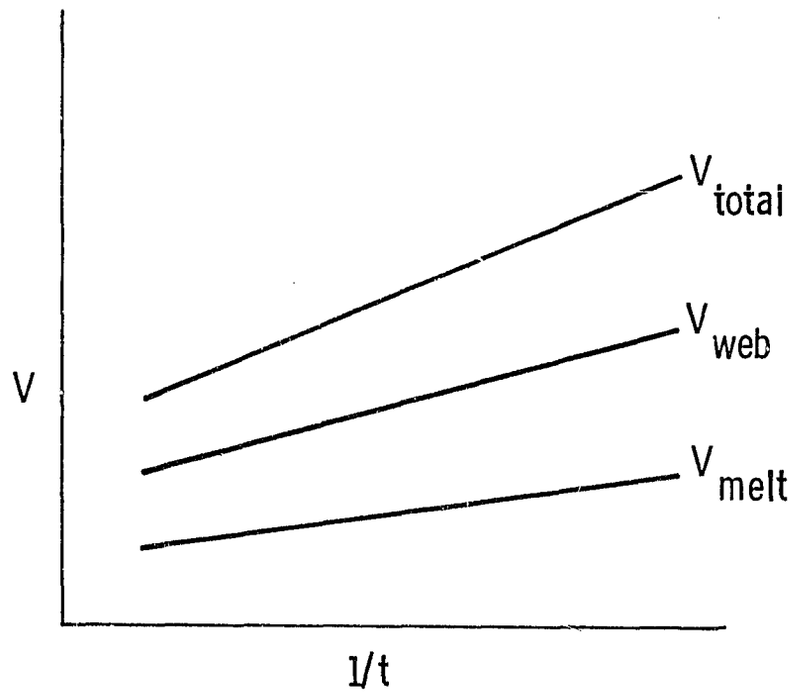

Figure 20 Components of web velocity — thickness relationship

information on the rejection of impurities in dendritic web growth as well as some information on the use of laboratory samples of silicon prepared by processes targeted at terrestrial solar cell technology.

3.3.1 Theory of Segregation in Dendritic Web Growth

A simple theoretical model of solute segregation in dendritic web growth has been published in the open literature,[4] and its general features and conclusions can be reviewed briefly. The geometry of the model is shown in Figure 21 where the liquid meniscus is modeled as a long wedge of included angle 2θ. Liquid flow in the meniscus is equated to the growth rate of the crystal, and the diffusion of rejected impurity is calculated for the moving frame. Under conditions of small segregation coefficient ($k_o < 10^{-3}$) and some stirring outside a diffusion boundary layer, the solution to the diffusion problem becomes

$$k_{eff}/k_o = (1 + vt/2D\sin\theta) \qquad (6)$$

where k_{eff} is the effective segregation coefficient, k_o is the equilibrium (or interface) segregation coefficient, v is the crystal growth velocity, t is the crystal thickness, D is the solute diffusivity in the liquid and θ is the effective half angle of the wedge. Since the true meniscus spreads more rapidly than a wedge, the effective half angle is somewhat larger than the true contact angle of 11°; 20° or more is probably a reasonable estimate. Depending on the parameters of the specific solutes, the ratio of k_{eff}/k_o should be somewhere between about 1.5 and 10; most of the available data to date shows that it is more nearly unity than ten.

3.3.2 Measured solute Segregation Coefficients

Boron. In the 1978-1979 Annual Report on this project, we reported some preliminary data for the segregation coefficient of boron in dendritic web growth.[1] During the past year additional data was generated which changed the measured value of k_{eff} somewhat, but still seemed to support the conclusion that k_{eff} for boron in dendritic web growth is less than k_o for boron as determined from Czochralski growth experiments.

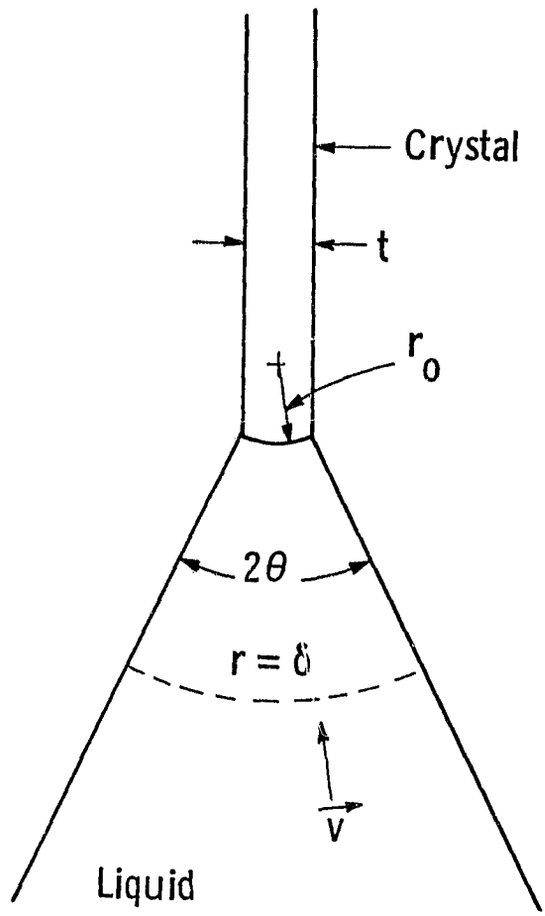

Figure 21 Simplified geometry for calculating solute diffusion in the meniscus of a growing web.

The technique used for the calculation of segregation coefficients was the same as reported previously[4] with the exception that a slightly more precise procedure was used for the four probe resistivity measurements. With a number of samples, the probe voltage was found to be illumination dependent, so that the measurements were made with the samples covered with a black cloth. In addition, voltage measurements were obtained for several different currents and the slope of the curve, dV/dI was used instead of the ratio V/I in the resistivity calculations.

In addition to slightly improved measurement techniques, a much larger data base was accumulated. As before, DopeSil* pellets were used to add specified amounts of boron to the silicon melt. The doping pellets were obtained from a number of different lots and presumably there could be a lot-to-lot variation in the actual boron content as well as a pellet-to-pellet variation within a given lot. The averaged segregation coefficients arranged by pellet lot number are given in Table 5. The data would seem to indicate that the lot-to-lot variation is insignificant compared with the pellet-to-pellet variation. Further, the value of $k_{eff} = .70$ is closer to the accepted value of 0.8 than our preliminary value of 0.59.[1]

Phosphorus. Although most of the web crystals which have been grown were doped with boron, four crystals were grown using phosphorus doping (also in the form of DopeSil pellets). In this case, the effective segregation coefficient was found to be $k_{eff}(P) = .36 \pm .02$ compared with the commonly accepted value of $k_o = 0.35$. In calculating the effective k-value from the resistivity data, a concentration dependent mobility was derived from

$$\mu_N = 55.3 + \frac{1332.92}{1 + (N_D/1.072 \times 10^{17})^{.733}}$$

*Trademark of Hemlock Semiconductor Co. (Dow Corning)

TABLE 5

MEASURED BORON SEGREGATION COEFFICIENTS FOR SILICON WEB GROWTH

Dopant Lot Number	Nominal Boron Content	Number of Samples	Resistivity Range	Effective Segregation Coefficient
WPD-006	$2x10^{17}$	15	6.5-10.3	.72±.09
WPD-007	$3x10^{17}$	12	1.7-4.6	.67±.07
WPD-023	$2x10^{17}$	7	6.5-9.5	.69±.12
WPD-026	$2x10^{17}$	21	5.9-10.5	.72±.14
"Master Dope"		2	4.3-4.4	.68±.01
		Grand Average		.70±.03

taken from the paper of Antoniadis et al.[4] In addition, a correction was made to the raw value of k to account for the effect of melt depletion. On the basis of this data it would appear that the effective segregation coefficient for phosphorus in dendritic web growth is very nearly the same as the accepted equilibrium value.

Transition Metals. Any "solar grade silicon is likely to be contaminated with metallic impurities from the transition element group. Although no work was conducted on this problem under the present contract, investigations were carried out at this laboratory as part of the LSA Task I (Contract 954331),[5] and will be summarized here for completeness.

Dendritic web crystals were grown from melts doped respectively with $1.77 \times 10^{18} cm^{-3}$ Ti, $1.5 \times 10^{18} cm^{-3}$ V and $2 \times 10^{18} cm^{-3}$ Mn. Additionally, boron was added to the melt to give about 8 ohm-cm resistivity material so that diagnostic solar cells could be fabricated. Impurity concentrations in the web crystals were determined from both the solar cell performance and deep level transient spectroscopy (DLTS) measurements. Since both techniques evaluate only the electrically active impurity concnetrations, the total concentration was determined by using the ratio, C_{elect}/C_{total}, from previous work on Czochralski crystals.

Reasonably good results were obtained from the titanium and vanadium doped crystals, however no DLTS data were obtained from the manganese doped material and only the solar cell data could be used to estimate the concentration. The final results can be summarized as follows:

Titanium: $k(web) = 4 \times 10^{-6} = 2k(CZ)$
Vanadium: $k(web) = 1.7 \times 10^{-5} = 4.2k(CZ)$
Manganese: $k(web) = \quad = 2.5k(CZ)$, approximately.

These values for the segregation coefficients are in good agreement with model presented in Section 3.3.1, and suggest that the dendritic web process is compatible with the use of solar grade silicon.

3.3.3 Web Growth from Non-Semiconductor Grade Silicon

Although segregation coefficient measurements indicate that the dendritic web process should be amenable to starting material other than semiconductor grade silicon, direct evidence to corroborate this is important. During the report period, two types of starting material were evaluated:

1. A potentially low cost silicon produced by the Battelle Laboratories and,
2. Recycled dendrites which were removed from web crystals both before and after they had been processed into solar cells.

The economic implications of both these materials are significant. In the first case, a possible low cost starting material was directly evaluated for dendritic web growth, and in the second case the material utilization efficiency of the process was evaluated.

Battelle Silicon. The material used in this growth experiment was an early laboratory sample produced by the Battelle Memorial Institute under an LSA Task I contract. The sample which we evaluated was supplied to us by JPL through Dr. R. Kachare, the technical monitor for the present contract. The fine granular character of the material made it of particular interest since it would be quite suitable for melt replenishment applications as well as being of potentially low cost.

The Battelle process utilizes the reduction of silicon tetrachloride by zinc in a fluidized bed technique, and as a result the material as received had a high concentration of zinc. Before utilizing the sample for web growth it was heated at about 1200°C in argon for 6 hours to remove entrapped zinc; this was the only pre-treatment. There was no difficulty with web growth from the melt, and samples from the crystals were fabricated into solar cells (crystals W180-1, -2, and -3). Boron doping was also added to melt to give material with a resistivity of 12 ohm-cm based on the use of semiconductor grade silicon.

The resulting web crystals had a resistivity of 0.25 ohm-cm indicating that some p-type impurity (possibly zinc?) was initially present. Nevertheless, the resulting solar cells, fabricated from crystal W180-1 and W180-3 had efficiencies of 8.9% and 9.0% respectively without AR coating (estimated to be 12.6% and 12.8% had AR coatings been applied). In summary, even this preliminary sample of a possible low cost silicon can be fabricated into reasonably good solar cell material by the dendritic web process.

Recycled dendrites. One factor which reduces the material utilization of dendritic web is the dendrites which remain attached to the ribbon during the solar cell processing. These dendrites serve to greatly strenghten the thin ribbons and permit relatively easy handling of the material, but unquestionably reduce the "yield" of the growth process. This yield could be increased if these dendrites were recycled, and several experimental runs were made to demonstrate the feasibility of the approach.

In the first experiment, dendrites were removed from unprocessed web and used to make up a portion of a growth charge. The dendrites were first given a light cleaning etch in $HF-HNO_3-H_2O$ and then 18.4 gm were added to the usual semiconductor grade silicon to make up a total charge of 185 gm. Crystals grown in this run, J266 were processed into solar cells which then showed an AM1 efficiency (uncoated) of 9.8% (14% coated). The resistivity of the material was 5.7 ohm cm, as expected from the boron dope added to the melt.

In the second experiment, dendrites were obtained from the cell fabrication facility. These dendrites had coatings of aluminum and copper from the metallization process as well as diffused layers of aluminum and phosphorus doped silicon from the junction formation steps. The cleaning was therefore a little more complex. The scrap dendrites were first cleaned with hot HNO_3 to remove the AR coating and copper metallization and then with NaOH to remove the aluminum back metal. Finally 3:1 $HF:HNO_3$ was used to remove diffused surface layers of

phosphorus and aluminum doped silicon. Again 18 gms of these reprocessed dendrites were added to semiconductor grade silicon to make up a total melt of 181 gms (Run J269). Samples from crystal 269-1 from this run were processed into diagnostic solar cells which had an average uncoated efficiency of 8.5% (∿ 12.1 precoated).

These results indicate that the scrap dendrites from the solar cell processing step could be recycled into the growth process if it were cost effective to do so. The desirability of such an approach would depend upon the identification of an appropriate recycling sequence and an economic analysis of such a sequence. The economics of recycling dendrites are addressed in Section 4.2.

3.4 Semi-automated Growth

A continuously maintained silicon melt level is the key requirement for the semi-automated growth of dendritic web. Essentially equilibrium thermal environment and growth conditions can be maintained for long periods (many hours) when the melt level is fixed. The equipment to provide a continuously maintained melt level has been designed, built and operated in this reporting year. The two major components of this system have already been described in section 3.2 of this report. These are the laser based melt level sensing system (Figure 6) and the melt replenishment system which is a motor driven pellet feeder and a tube delivery system which guides the pellets into the replenishment compartment of the crucible. A batch feeder has also been assembled (Figure 3) which serves as a reservoir of pellets to reload the motor driven feeder. These elements in combination with the compartmented crucible provide a feed, sensing, and crystal growth function concurrently.

Each of the elements has been operated independently and it requires an appropriate circuit to close the loop and use the output of the laser/sensor component to control the rate of feed of pellets into the melt. This element then provides closed loop control of the melt level during web crystal growth. A photograph of this element is shown in Figure 22. The system was installed and operational testing begun near the end of this reporting year.

A block diagram of the closed loop system developed to continuously maintain a fixed silicon melt level during web growth is shown in Figure 23. This loop utilizes a two milliwatt helium-neon laser mounted such that the coherent beam of light reflects from the melt to strike a solid state position detector. A bandpass filter and a focussing lens are used to improve the signal to noise ratio and consequently to provide a useful electrical output signal. The signal is subsequently amplified and conditioned to provide suitable level and zero reference. It is then fed to a voltage sensing relay which, in effect, differentiates between melt levels slightly ($\sim$ .1mm) above or below the intended level. Hence a dual speed motor control circuit operates a motor driven polysilicon

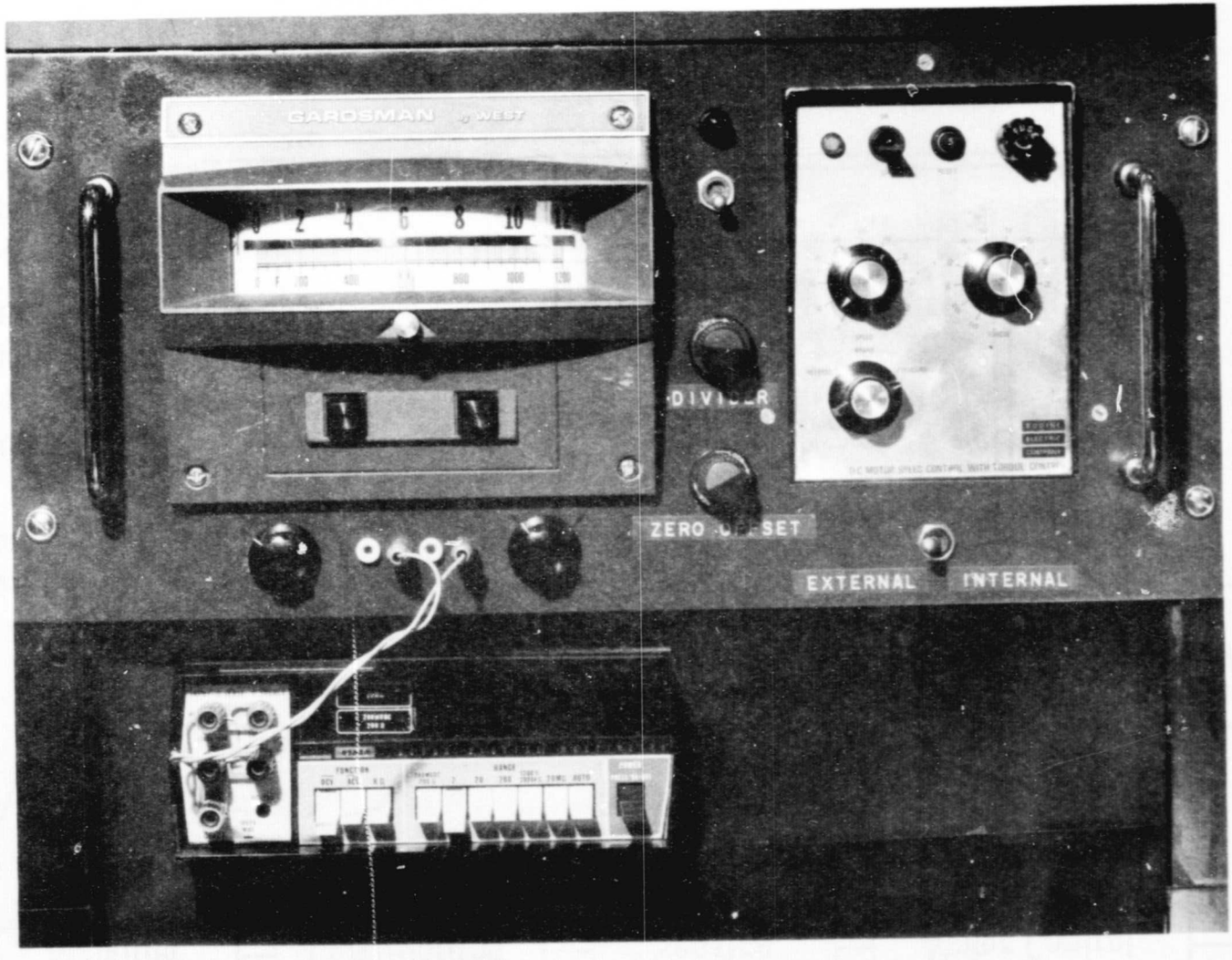

Figure 22 Closed Loop Circuit for Pellet Feed Control

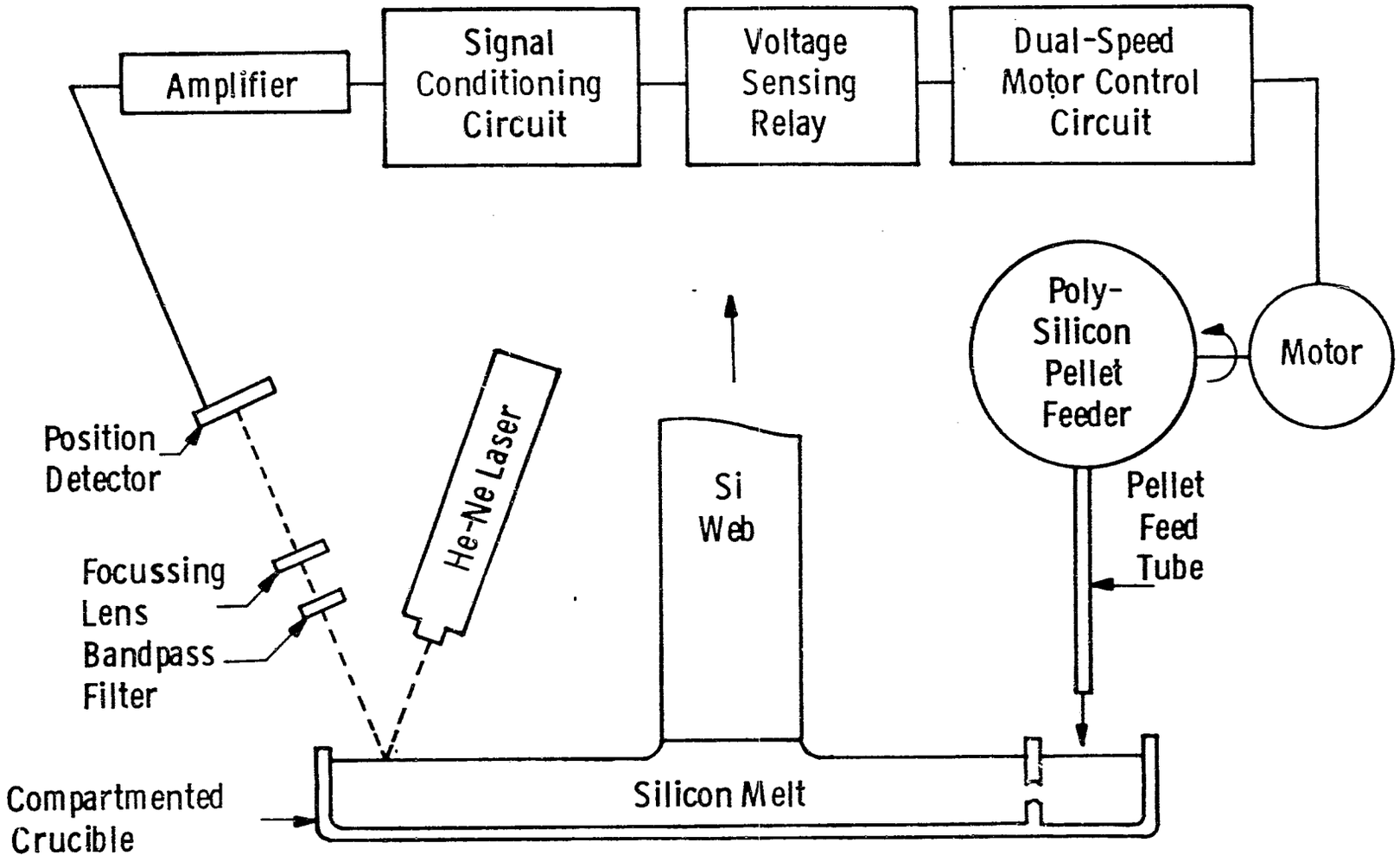

Figure 23 Block diagram of closed loop circuit for control of melt level

feeder at selected pellet feed rates either appreciably greater than or less than a rate sufficient to maintain melt level equilibrium while silicon is being removed in the form of growing web ribbon. This loop is capable of maintaining the melt level within ∿.1mm, indefinitely during web growth. During initial testing, 3 1/2 hours of closed-loop constant-melt-level semi-automatic web growth have been attained.

3.5 Material Evaluation

Material grown during the period has been evaluated in a variety of ways. Generally, all large crystals were electrically characterized by measuring resistivity and by evaluating the performance of diagnostic solar cells fabricated from each crystal. In other instances, residual stress was measured on representative crystals from new lid configurations. Additionally, thickness-velocity data were taken as necessary to evaluate the lid performance as discussed in Section 3.2.3.

3.5.1 Solar Cell Characteristics

Since the ultimate utilization of the dendritic web material is in the fabrication of solar cells, the characteristics of diagnostic solar cells provide an operational evaluation of the crystals. In the present program, all of the ribbons large enough to be useful in solar cell experiments were characterized by fabricating 1x1 cm diagnostic solar cells. A detailed description of the cell processing procedure was given in the previous Annual Report[1] but can be briefly summarized here. The blanks are first cleaned to remove any surface oxide and then diffused in BBr_3 to produce a back surface field region, and then in $POCl_3$ to form the front junction. The contact grid pattern is then evaporated through a photoresist mask and silver plated to build up the finger thickness. Finally, a .400x.400 in. square mesa is etched on the front junction to give a $1.032cm^2$ cell. All processing and measurements are done with the dendrites attached to the blanks.

The cells are tested using a quartz-halogen lamp to simulate an AM1 spectrum with a power density of 91.6 mW/cm^2. Five voltage-current points are measured on each cell, and the data used to derive the parameters I_o, N and R in the equation

$$I = I_{SC} + I_o \left(1 - \exp(V+IR)/V_{th}\right)$$

where I_{SC} is the short circuit current, V and I are the terminal voltage and current, and $V_{th} = kT/q$. The maximum power point is then calculated from this equation to give the efficiency and fill factor. All measurements are made without any antireflection coating on the cells in order to remove that variable from the data.

In order to convert the efficiency without an antireflective coating to the efficiency with one, a factor of 1.43 can be used for the coatings usually prepared in this laboratory. The validity of this factor can be seen from Figure 24 which plots the measured efficiency of 16x40 mm solar cells with an AR coating against the data for 10x10 mm diagnostic cells from the same crystals converted by use of the factor. Although the data are somewhat scattered about the 1:1 line, the general agreement is very good and in fact the center of weight appears to be slightly above the line. Not only does the data suggest that the data obtained from the 10x10 mm cells is a fair measure of the performance to be expected from larger devices, but also that 1.43 is the appropriate factor.

The cell data for about 190 crystals are given in Appendix 9.2; each crystal entry represents the average values for four cells. Most of the entires in the table are self explanatory, however the WEB QUAL column gives the processing run in which the cells were fabricated, and the entry CP in the NOTES column indicates that the wafers had a slight chemical polish before fabrication. Similarly, SINTER indicates that the metallization was given special sintering treatment in order to reduce the series resistances of the cells.

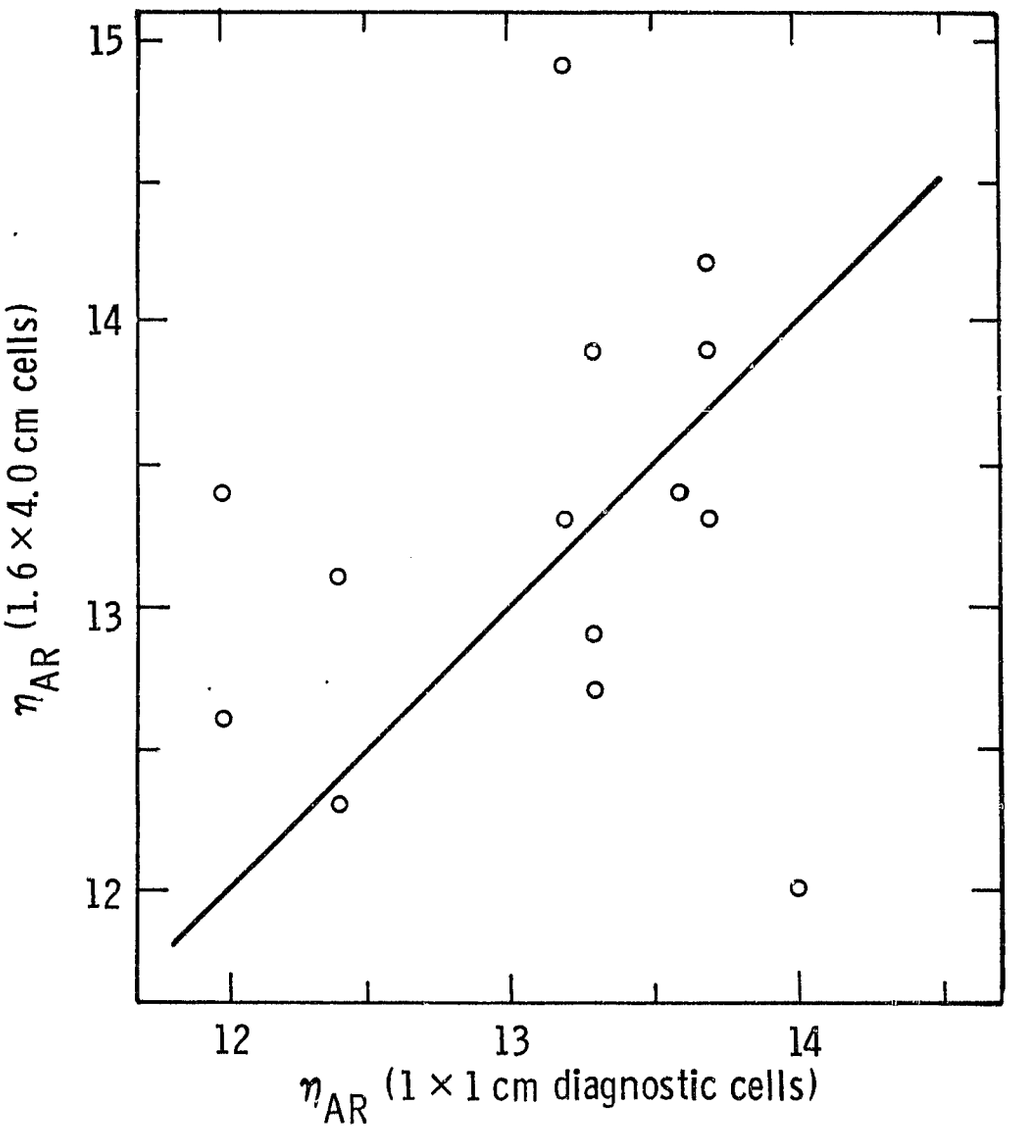

Figure 24 Comparison of cell efficiency for 16x40 mm and 10x10 mm solar cells made on the same web crystals.

In some instances, the crystal number has the letters STD appended to it; this designation indicates that this material was used as a standard material which was included in a number of processing runs to evaluate the fabrication. Generally, the characteristics of these standard samples were very consistant from run to run, however in some instances, the characteristics changed drastically indicating a processing problem. In such cases, the samples had to be reprocessed and in such instances, the cell characteristics always improved indicating the validity of the standard web data.

Within the cell data, some of the results have particular interest. For example, furnace run W180 was made using the Battelle silicon as an example of potentially low cost solar material. The cell characteristics of W180-1.3 and -3.7 indicate that uncoated efficiencies of about 9% (anticipated AR efficiencies of about 13%) can be achieved with this material.

Another group of cell data of interest is the group of WA crystals between WA7 and WA20. These cells have an average uncoated efficiency of about 8.5% and OCD lifetimes of about 2 μs. During this period of growth runs, this furnace was plagued with sporadic deposits of a black "fuzz" which analysis showed to be primarily molybdenum. Analysis of the web material showed that indeed there was a relatively large surface "skin" of molydenum on the crystals which is reflected in the poor cell performance. Subsequently, several leaks were found in the system and when these were corrected and an improved start-up procedure was initiated, then the cell performance improved as shown by cells from runs WA51 through WA68.

Still another group of cell data of note is associated with crystals RE258-1 through -6. These crystals were grown in a long run during which the melt was continuously replenished. The cell averages for the six crystals were all 9% or better indicating that excellent efficiency was maintained during feeding process. Further, the resistivity of the material monotonically increased as would be expected from the fact that undoped, semiconductor grade silicon was used as the replenishment material.

3.5.2 Structure Studies

Only a relatively small effort was spent on structure studies during the period, however several interesting results were obtained with regard to both the seed perfection and the etch pit density in web crystals.

Dendrite Seed Studies

In some instances, it has been found that web crystal growth is difficult to initiate, but that the problem is solved by removing a short length of seed. In other instances, a crystal has poor structure from the start. Both of these conditions suggested that the seed itself may be faulty, and some studies were conducted of the twin configuration in a number of seeds. Two techniques were employed: fractographic, in which the seed was carefully broken to reveal the twin planes, and a standard metallurgical polish and etch process.

In a large majority of the cases, there were no discernable differences between the twin structures of the seed, even though they were grown at different times in different furnaces. In the larger sense, the twin structure of seed used in the present program has been propagated throughout the program. In a few instances, however, structural faults were found which could adversely affect web growth. Sometimes, these defects appeared to be an extra twin lamella or the failure of a twin lamella to propagate completely across the width of the seed. In one instance, Figure 25, a twin on another (111) system was observed.

Fortunately, these degraded twin structures are quite rare and are characterized by difficulties in the seeding phase of growth. The cure to the problems are thus both quick and easy-either remove a portion of an already mounted seed, or at worst, substitute a new seed for the defective one.

Dislocation Studies

The present dislocation etch pit studies are a continuation of the work reported in Section 3.4.3 of the previous Annual Report.[1] The same preparation and Sirtl etching process was used to reveal the dislocation etch pits and a similar but improved automatic counting technique was used to determine the etch pit density.

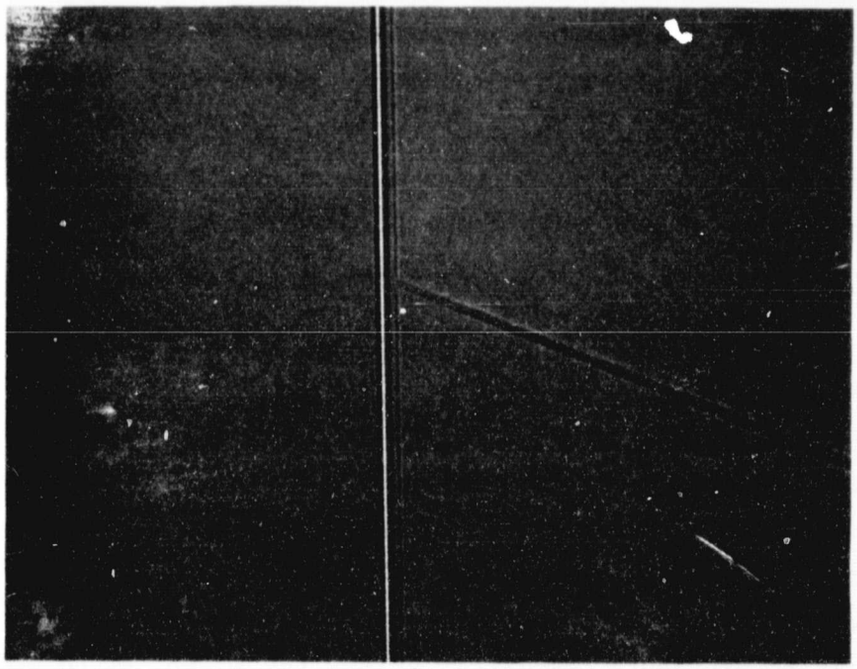

Figure 25 Seed #1 - Twin structure at 800X

Generally, the present results confirmed the earlier conclusions; the etch pit density, particularly the value at the central maximum if one existed, was directly related to the residual stress in the crystal measured in a strip adjacent to the etched sample. A new feature was observed, however, when etch pit counts were made on both the front and the back of the same sample. Again, generally the etch pit counts were similar, if not identical, on both sides of the sample, but in some instances there was a dramatic difference. Such a situation is illustrated in Figures 26a and 26b for a sample from crystal W187-1.3. One side of the crystal is almost dislocation free, while the other side shows a central maximum of about 150 counts (1 count = 250 pits/cm^2). The residual stress measured on the adjacent material was -2.5 ± 3.1 Mdyn/cm^2, essentially zero, which would be consistent with the very low dislocation density observed on side B. This would suggest that the high central peak on side A may have been due to a twin plane fault rather than to a stress induced plastic deformation. A more thorough study of some of these crystalline defects should be conducted with regard to their effect on very high efficiency solar cells, but is not in the scope of this program.

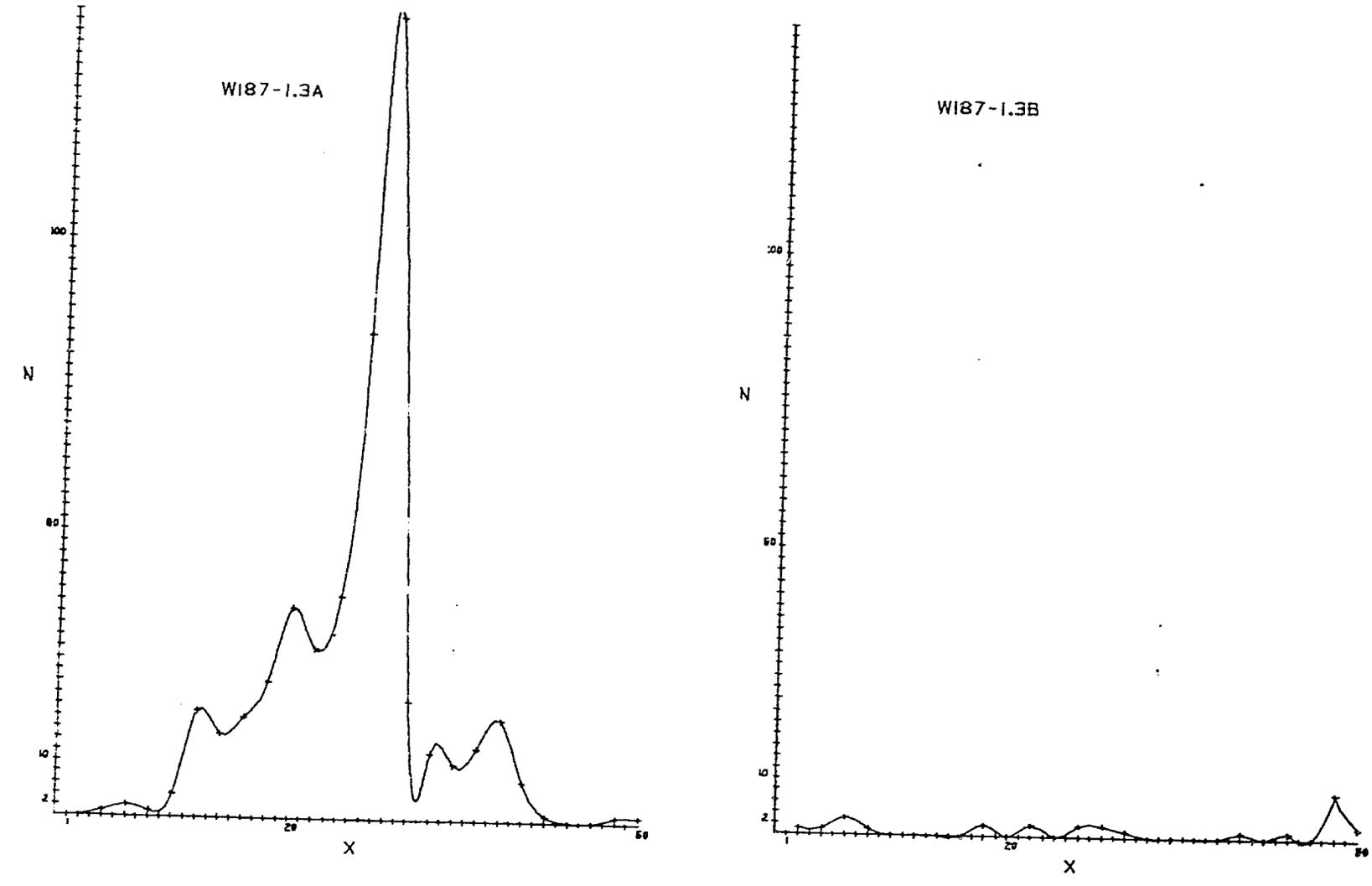

Figure 26 Etch pit counts on two sides of a web sample (1 count = 250 pits/cm^2). Width of count area is full width of web.

3.6 Hardware Improvements

In addition to the specific improvements to growth furnaces as discussed earlier, other more general improvements have been performed. These developments are discussed in the following paragraphs.

During the past year two web growth furnaces of improved design have been placed in service and each have been used in the performance of this program. These furnaces were built at Westinghouse expense and represent an interim design having some cost advantage over the previous design. They do not represent the ultimate in web cost effectiveness but rather an interim design. A photograph of these furnaces is shown in Figure 27.

The design of a newer and further improved web growth furnace is now in progress and will be completed in the next quarter of this program. The major improvement of this design is that it will have the functional features of the growth conditions included in the SAMICS-IPEG economic projection for the silicon web process.

A solid state high frequency generator circuit developed under Westinghouse funding was evaluated as a possible power source for induction heating in silicon web growth. The intent of this evaluation was limited to determining the technical capability of the generator in web growth application. The generator, in a breadboard version prepared for this evaluation, was found to perform well in all respects during actual web growth. The generator is comparatively small in physical size and can be mounted on a standard 19 inch wide rack panel. Although no actual costing of the generator was performed, rough estimates indicated that the cost would at worst be competitive and possibly would provide as substantial cost reduction compared with a motor generator. A photograph of the breadboard version of the generator used in our test is shown in Figure 28.

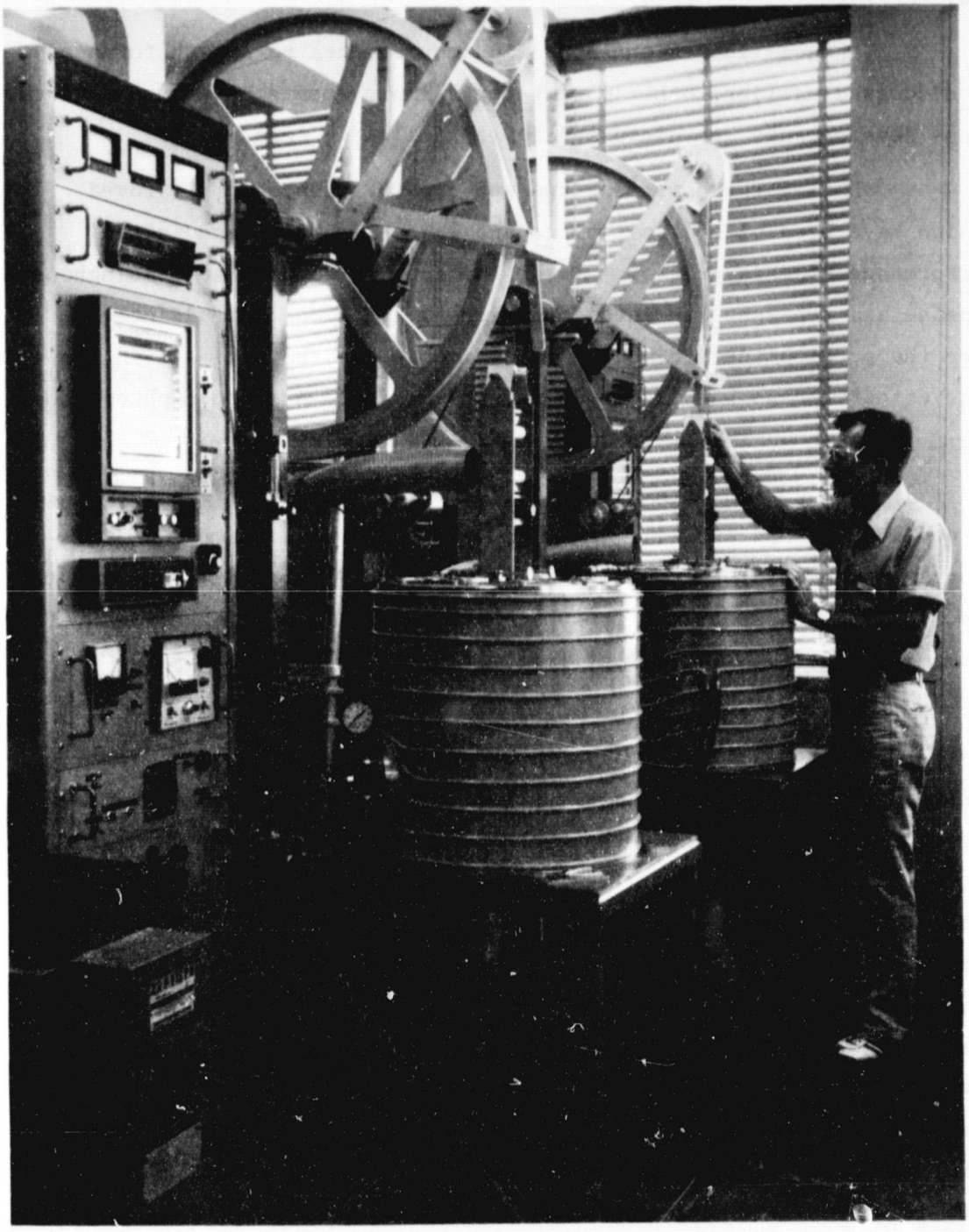

Figure 27 Improved Design Web Furnaces

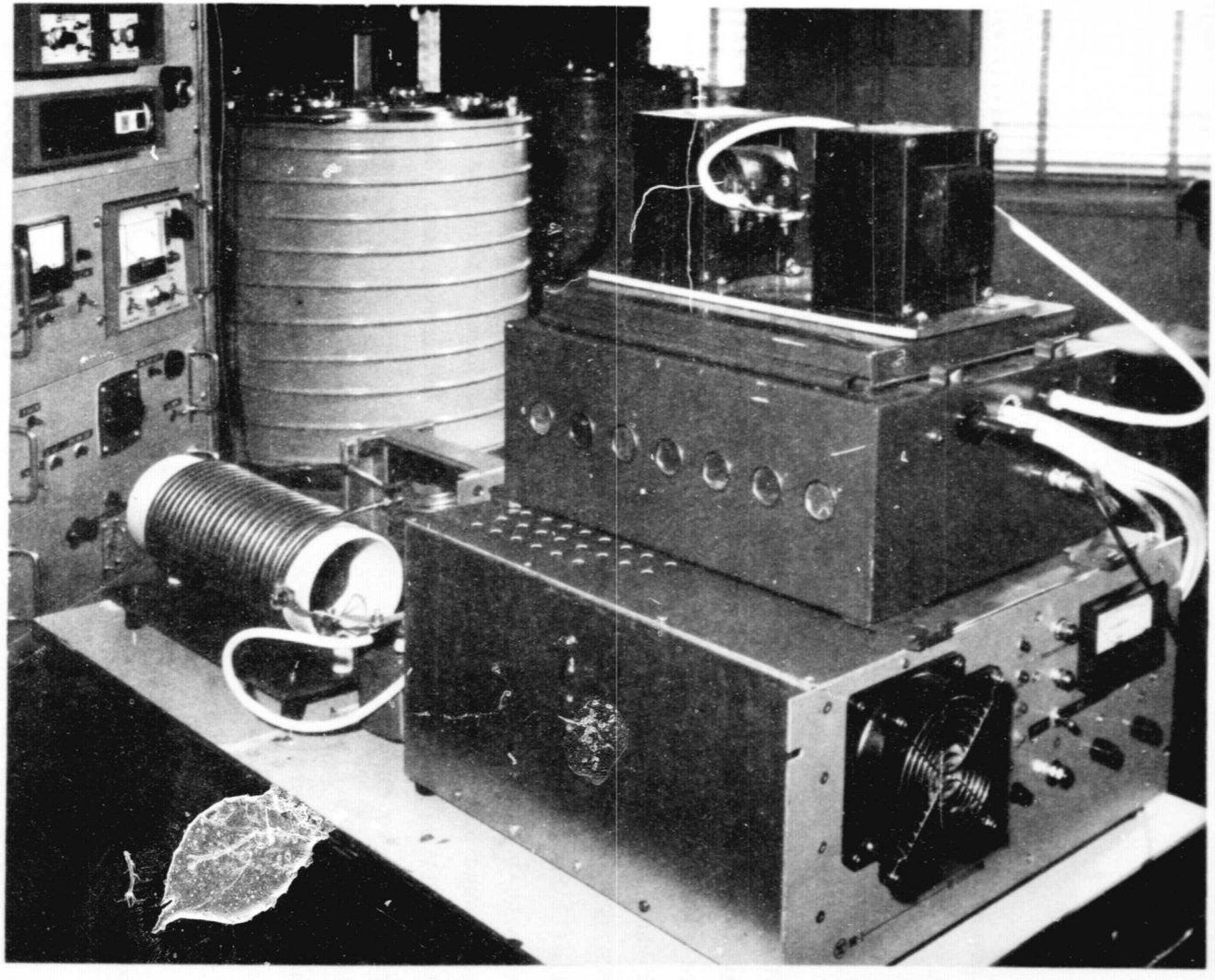

Figure 28 Breadboard Solid State Power Supply

4. ECONOMIC ANALYSIS UPDATE

The original version of the economic analysis[3] of the silicon web growth process was updated in several respects during this contract year.

4.1 Capital Equipment Cost Sensitivity

The total wafer cost for any sheet process comprises the costs for polysilicon and the value-added cost of processing the polysilicon into wafer form. The SAMICS/IPEG economic analysis accumulates all of the value-added costs within five categories. The categories are: capital equipment, floor space, direct labor, materials, and utilities. The SAMICS/IPEG analysis for silicon web[3] projects that the total wafer cost will be 17.3 cents per peak watt in 1980 dollars. This analysis assumes that the long range technical goals of the process will be met or surpassed and that the DOE/JPL 1986 polysilicon price goal of $14/kg (1980$) will be met. The analysis further indicates that the cost attributable to capital equipment is 4.6¢/Wpk, or 26.8% of the total wafer cost. The capital cost is thus not a dominant factor. In the event that the capital cost were to be increased by one half beyond the assumed figure, the wafer cost would increase to 19.6¢/Wpk. Furthermore, if the capital cost were to double the amount used in the economic analysis the wafer cost would increase to only 21.9¢/Wpk, which is appreciably below the DOE/JPL 1986 wafer goal of 22.4¢/Wpk.

4.2 Cost Effects of Dendrites

Although the economic impact of dendrites in web growth is small (see below), options are open with respect to their reuse. These options and their economic merit are discussed in the following cases. All costs are shown in 1980 dollars.

Case I - Dendrites Not Salvaged

General Assumptions:

Area rate of growth - $25cm^2/min$

Thickness of web - 6mils (150μm)

Width of usable web - 2 inches (5cm)

Polysilicon price - $14/Kg (1980$)

Cell efficiency - 15% AM1

Growth cycle period - 3 days

Dendrite dimensions:

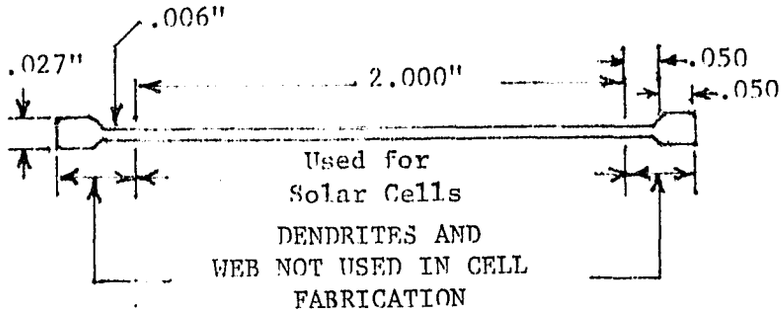

The total cross sectional area of the dendrites and unused web is seen to be (2.050x.006) + (2x.050x.027) = $.0033in^2$. Also, the area of the web used for solar cells is (2.000x.006) = $.012in^2$. Thus, if dendrite and unused web area are not salvaged an additional amount of polysilicon, will be required. The total cost of web then becomes:

Cost of polysilicon actually used for solar cells per SAMICS-IPEG[1] =	.0386$/Wpk
Cost of unsalvaged web and dendrites (27.5% of .0386) =	.0106
Value-added wafer cost per SAMICS-IPEG = (cost of converting polysilicon to web)	.1330
Total combined polysilicon and wafer cost =	.1822
	≈ 18.2¢/Wpk

(DOE/JPL 1986 goal = 22.4¢/Wpk)

Case II - Dendrites Salvaged Before Cell Fabrication (Returned to Melt)

General Assumptions: same as Case I

In this case essentially no silicon is lost because the dendrites and un-used web are returned to the melt. Before the dendrites and un-used web are returned to the melt a light cleaning etch is required. Because the etch is very light essentially no silicon is lost. The cost of the etch can be determined from the economic analysis prepared under DOE/JPL contract 954873 which was for Phase II of the Array Automated Assembly Task for the Low Cost Solar Array. In that analysis a cost was determined for cleaning web for solar cell fabrication. A portion of that cleaning, the etching, was found to be suitable for cleaning dendrites for return to the melt. Using the etching portion of that cost and correcting for the different dimensions an etching cost for dendrites and un-used web is found to be .0011$/Wpk. The total cost for web then becomes:

Cost of polysilicon used for solar cells, (same as Case I)	= .0386$/Wpk
Cost of cleaning dendrites and un-used web	= .0011
Value-added wafer cost (same as Case I)	= .1330
Total combined polysilicon and wafer cost	= .1727
	≈ 17.3¢/Wpk
(DOE/JPL 1986 goal	= 22.4¢/Wpk)

Case III - Dendrites Salvaged after Cell Fabrication (returned to melt)

General assumptions: same as for Case I and Case II.

Dendrites and un-used web must have the metals from cell fabrication removed before remelting. Additionally, some of the silicon must be removed in order to eliminate impurities diffused and/or alloyed into the dendrites and un-used web. Thus, the cost of salvaging the dendrites and un-used web will include two separate etches and a loss of silicon through etching which we estimate at 25%. Again using economic data from DOE/JPL contract 954873 and correcting for the area involved, a cleaning cost of .0023$/Wpk is obtained. The cost of silicon lost through etching will be 25% of that lost in Case I, or .25x.0106 = .0026$/Wpk. The total cost of web then becomes:

Cost of polysilicon used for solar cells (same as Case I and Case II)	= .0386$/Wpk
Cost to clean dendrites and un-used web for return to melt	= .0023
Cost of polysilicon lost via etching	= .0026
Value-added wafer cost (same as Case I and Case II)	= .1330
	= .1765$/Wpk
Total combined polysilicon and wafer cost	≈ 17.7¢/Wpk
(DOE/JPL 1986 goal	= 22.4¢/Wpk)

Comparison of the Three Cases

Comparison of the three cases indicates that a small cost advantage can be attained by salvaging dendrites and un-used web. Case II may not be attainable since the development of solar cell fabrication techniques has concentrated on fabrication with the dendrites attached for handling purposes. The cost effect of cell fabrication without dendrites would have to be taken into account if Case II were to be considered for commercial use. While Case III is less economically attractive than Case II it is cheaper than Case I and has the advantage that developed solar cell fabrication techniques are not altered. Web has been grown under the conditions of Cases II and III without any change of growth behavior as compared to Case I.

4.3 Cost Sensitivity of Melt Replenished Growth Period

Economic analysis indicates a melt replenished growth period of the order of two days is necessary to satisfy the DOE/JPL 1986 cost goal for silicon wafers.[1] The dependence of the time length of the growth period, Figure 29, also shows that the cost improvement diminishes rapidly as the growth period extends beyond a period of three days. Note that the growth cycle consists, in all cases, of seven hours of nongrowth time which is required for such activities as furnace loading, heat-up, start of growth, cool-down and cleaning. Thus, for example, the actual time available for growth in a one day cycle is 24-7 = 17 hours. The growth period of a two day cycle would be 41 hours.

Including the key assumptions for this analysis, $25 cm^2/min$ throughput rate and \$14/kg polysilicon price, the economic analysis predicts that the silicon web process can produce wafers at a cost substantially below the DOE/JPL 1986 goal when a three day growth cycle is used.

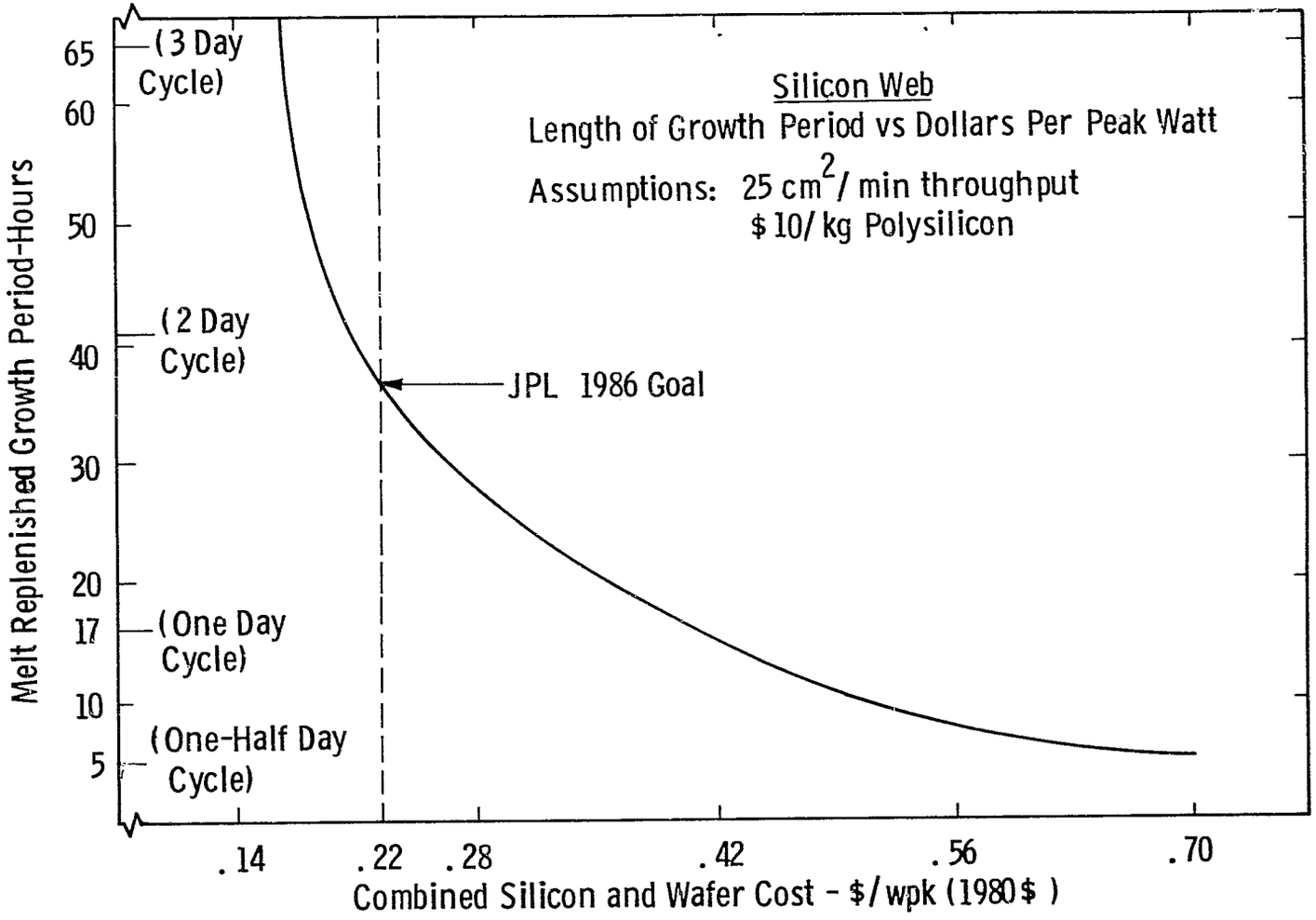

Figure 29 Variation in web wafer cost (including polysilicon) with replenished growth cycle time

4.4 Summary

Capital equipment cost was shown to be comparatively insensitive as related to the 1986 cost since it comprises only 4.6 cents per peak watt as projected by the economic analysis. In the very unlikely event that actual capital cost were to double the projected amount, the resulting wafer cost would nevertheless be expected to fall below the 1986 DOE/JPL goal.

Three options considered for dendrites show that a small but significant cost advantage can be attained by recycling dendrites by either of two options. The less advantageous of the recycling options, Case III, may in the broader sense be the more desirable. For Case III the cell fabrication activity may profit considerably as compared to CAse II by having the dendrites in place for added structural strength during fabrication.

Economic analysis projects that a web growth cycle of almost two days is required in order to satisfy the DOE/JPL 1986 cost goal. It is further shown that the projected three day growth cycle will result in a wafer cost well below the 1986 goal.

5. SUMMARY, CONCLUSIONS AND FUTURE WORK

5.1 Summary and Conclusions

5.1.1 Melt Replenishment

Summary of Work in Phase III

- Manually controlled one-day growth cycle demonstrated.
- Cells of web grown during one-day cycle show excellent efficiency.
- Pellet feeder design improved.
- Batch feeder added to pellet feeder to allow longer period of growth.
- Improved crucible barrier for reliable melt distribution.
- Melt level sensor installed and operating.
- Adjustable thermal shields added to provide dynamic thermal trimming.
- 2nd web growth furnace converted to melt replenishment.

Conclusions

The development of new hardware for melt replenishment is complete. Refinement of the hardware and thermal environment is continuing in order to improve growth conditions during melt replenishment. The demonstrated one day growth cycle is within a factor of two of the minimum requirement necessary to satisfy the Phase III goal.

5.1.2 Throughput Rate

Summary of Work in Phase III

- Throughput rate of $27 cm^2$/min demonstrated.
- High cell efficiency demonstrated with web grown at high throughput rate.

Conclusions

The throughput rate goal of 25cm^2/min has been exceeded (27cm^2/min). Also, the quality of high throughput rate web has been verified by the preparation of high efficiency (∿ 13% AM1) solar cells. Routine and continuous growth at high throughput requires routine melt replenishment. Refinement of the growth conditions during melt replenishment has begun as melt replenishment is now a reproducible operation.

5.1.3 Silicon Feedstock

Summary of Work in Phase III

- Web grown from solar grade (Battelle) polysilicon. Solar cells from this web have demonstrated high efficiency.
- Dendrites removed from web have been re-melted and grown into new web. Web grown from re-melted dendrites produced solar cells of high efficiency.

Conclusions

The web growth process has demonstrated acceptance of one type (Battelle) of low cost polysilicon. Web was grown from this material (pre-treated) without any growth difficulty and was found to produce high quality solar cells (∿ 13%). Also, no loss of efficiency occurred when solar cells were prepared from web grown from melts which contained cleaned and re-melted dendrites salvaged from web crystals. The web growth process is comparatively insensitive to melt impurities and rejects impurities similar to the Czochralski growth process.

5.1.4 Economic Analysis Update

Summary of Work in Phase III

- Two-day growth cycle shown to satisfy the program economic goal. A three-day cycle is optimum; a longer cycle provides minimum added benefit.
- The capital cost of the growth equipment is not dominant.

- A minor cost advantage can be attained by re-melting dendrites.

Conclusions

The economic analysis which was prepared earlier in this program was refined and updated in some respects. These changes did not alter the original analysis but instead more accurately defined the cost sensitivities of the length of growth cycle and the capital cost of the equipment. Also, the cost effectiveness of recovering dendrites was identified and shown to offer a significant but small economic advantage.

5.1.5 Semi-Automatic Web Growth

Summary of Work in Phase III

- Closed loop system for control of melt replenishment installed and operating.
- Semi-automatic web growth demonstrated for 3 1/2 hours.

Conclusions

The closed loop system was installed as this reporting period ended. Initial operation has shown that the system performs as intended and semi-automatic web growth for up to 3 1/2 hours has been demonstrated.

5.1.6 Web Growth Equipment

Summary of Work in Phase III - In addition to the apparatus changes listed in sections 7.1.1 through 7.1.5 the following substantial progress was made:

- Two new Westinghouse web growth furnaces of improved design were built and operated.
- A compact solid state 10 kHz generator of unique design was evaluated and found technically suitable for web growth.

Conclusions

Two new Westinghouse furnaces of advanced design were built and placed in operation on behalf of this program. A Westinghouse developed solid state 10 kHz generator was found to be technically

suitable for web growth. Although no detailed cost analysis for the generator was prepared, a rough analysis of the cost indicates that the expected cost may be competitive with conventional 10 kHz generators.

5.2 Future Work

5.2.1 Planned During Remainder of Phase III (Through 7/23/80)

Work performed through the conclusion of Phase III will concentrate on experimental semi-automatic web growth runs with emphasis on increased length of growth time and throughput rate.

5.2.2 Recommended After the Conclusion of Phase III

The primary goal should be to design, build, and demonstrate the operation of a new web growth furnace having the functional features, performance and low cost identified in Phase III of the present program. This should lead to a successful demonstration of technology readiness for the web process. A second major recommended goal is to develop and demonstrate higher throughput to the range of 30 to 35cm^2/minute.

6. NEW TECHNOLOGY

1. Method for continuous melt replenishment during silicon web growth.

2. Method for silicon melt level sensing.

3. Method for controlling temperature gradients in the susceptor, crucible and melt during dendritic web growth.

4. Barrier for use in melt replenishment for silicon web growth.

7. REFERENCES

1. C. S. Duncan et al., "Silicon Web Process Development Annual Report. April 1978-April 1979." Contract NAS954654, DOE/JPL 954654-79/2.

2. C. S. Duncan et al., Silicon Web Process Development, Quarterly Report.

3. C. S. Duncan et. al., Silicon Web Process Development Annual Report April 1977-April 1978 Contract NAS 954654 DOE/JPL 954654-78/1.

4. R. G. Seidensticker, A. M. Stewart and R. H. Hopkins, "Solute partitioning During Dendritic Web Growth," J. Crystal Growth 46, p. 51-55, (1979).

5. D. A. Antoniadis, A. G. Gonzalex and R. W. Dutton, J. Electrochem. Soc. 125, 813, (1978).

6. R. H. Hopkins, et al., "Effects of Impurities and Processing on Silicon Solar Cells. Phase III Summary and Seventeenth Quarterly Report. Vol. 2: Analysis of Impurity Behavior." Contract 954331, DOE/JPL-954331-80/9.

8. ACKNOWLEDGEMENTS

We would like to thank P. A. Piotrowski, H. C. Foust, L. G. Stampahar, E. P. A. Metz, W. B. Stickel, J. M. Polito, A. M. Stewart, J. P. Fello, and C. H. Lynn for their contributions to the web growth studies and P. Rai-Choudhury, R. B. Campbell, E. J. Seman, J. B. McNally, W. Cifone, D. N. Schmidt, and H. F. Abt for the processing and testing of the web solar cells. The report typescript was prepared by D. Labor and edited by S. Farukhi, and we gratefully acknowledge their important contribution to this effort.

9. APPENDICES

9.1 Growth Run Summary-Report Period April 1979-April 1980.

GROWTH RUN SUMMARY

RUN	NO. OF CRYSTALS	LENGTH (cm)	MAX. WIDTH (mm)	DESCRIPTION/RESULT
RE-138	5	460	31.4	This was the first run made with aspirators in an elongated susceptor system. The first 40 cm of web pulled had almost no oxide coating, but after another 40 cm the oxide coating was about normal. After the run the aspirators were blocked with oxide. Used RE-1 lid with feed and aspirator holes.
RE-139	4	433	25.5	Repeat of RE-138 set up, but with a decreased aspirator argon flow. The aspirators became blocked with oxide sooner than in RE-138.
RE-140	1	94	21.3	The aspirators were set up to pull gases from between the lid and the shields. The aspirators did not become blocked, but they did not reduce oxide build-up either.
RE-141	4	579	30.7	The purpose of this run was to determine what effect an additional shield in the RE-1 arrangement would have. Growth was easy, but "ice" from oxide spalling and entering the melt ended each crystal, preventing determination of maximum width possible.
RE-142	3	298	26.2	This was the first run made with the milled channel aspirator. The corner with the feed hole and aspirator was too cold; ice from the corner ended several crystals. The lid used had an RE-1 slot.
RE-143	1	216	30.2	Repeat RE-142, with a partial shield on the left end of the susceptor. This solved the problem of freezing in the corner, but some floating ice occurred. A temperature profile of the melt end of the susceptor showed that the feed corner was still too cold.
RE-144	1	169	29.9	Set up as in RE-142, with manual feeder. Several small crystals were started; ice caused pull outs whenever feeding was tried. On the last crystal feeding achieved for 15 minutes before ice appeared.

GROWTH RUN SUMMARY

RUN	NO. OF CRYSTALS	LENGTH (cm)	MAX. WIDTH (mm)	DESCRIPTION/RESULT
RE-145	2	163	20.9	The RE-1 lid with the milled aspirator was used. A partial shield on the right end and a full shield on the left end were used to make the ends of the crucible hotter. The dendrites were choppy and growth was difficult. Twenty five minutes of continuous feeding was performed.
RE-146	2	212	21.4	Set up as in RE-145; Thermal measurements made both with and without feeding. Feeding appeared to drop the temperature on the feed end about 1°. Fed pellets at 1 per minute for 53 minutes before ice appeared.
RE-147	3	473	32.4	Set up as in RE-145, but no argon flow through the feed tube. Heating coil position varied. For one crystal, 83 minutes of feeding at 1 pellet per minute was done before oxide on the lid caused pull out. For the second 85 minutes at 2/min and 33 minutes at 3/min was done before ice appeared. On the third crystal 4 pellets/min were added for 40 min before any ice occurred.
RE-148	3	437	31.1	Set up as in RE-147. For one crystal pellets were added at 3/min for 105 minutes. The crystal was ended because of deformation (problem not caused by feeding).
RE-149	Nonproductive			Set up as in RE-147. Crystals tended to form thirds or pull out easily.
RE-150	2	272	26.3	A growth run, using lid which gave 4cm web. Ice was a major problem; clean-up revealed that there had been a large amount of oxide spalling.
RE-151	6	635	43.1	Set up like RE-150. The first crystals went poly, but after that the crystals grew well.
RE-152	Nonproductive			Run with a lid similar to the RE-1 lid, but with a 1/2" shorter slot. The purpose of running with a shorter slot is to develop more uniform width for feeding experiments.
RE-153	2	268	27.9	Set up like RE-147, but with a lower feed tube position. Oxide collection on the end of the feed tube and in the feed hole prevented successful pellet feeding.

GROWTH RUN SUMMARY

RUN	NO. OF CRYSTALS	LENGTH (cm)	MAX. WIDTH (mm)	DESCRIPTION/RESULT
RE-154	3	338	24.5	First run in development of width control in elongated susceptor. Used J-98A lid and shield arrangement. Growth was difficult; the thermal gradient was quite steep.
RE-155	2	370	29.2	Development of width control; J-98B lid and shield arrangement. Crystals grew well and were easily controlled. Width was stabilizing when the crystal pulled out.
RE-156	1	256	39.1	Lid for wide crystal growth with melt replenishment. No feeding was done; the run checked the ease of growth without replenishment. Web growth was typical; however oxide collected on the bottom shield and brushed against the crystal.
RE-157	3	288	30.9	Repeat of RE-156 lid configuration. Again there was a large amount of oxide on the shield, but during this run oxide fell into the melt ending the crystals.
RE-158	Nonproductive			Used J98-B lid arrangement to try to further develop width control. Ice prevented crystal growth; spalling was the probable cause.
RE-159	Nonproductive			Run aborted when furnace oxidized.
RE-160	Nonproductive			Used J98-B lid arrangement; ice was a problem whether feeding was used or not. Some spalling was evident.
RE-161	2	346	26.7	Used J98-B lid arrangement for width control. There was some ice, but not as much as previously.
RE-162	1	103	19.8	Used same lid as in RE-156, but used a higher aspirator flow; again there was a large amount of oxide growth on the shield. Oxide fell into the melt, ending several crystals rapidly.

GROWTH RUN SUMMARY

RUN	NO. OF CRYSTALS	LENGTH (cm)	MAX. WIDTH (mm)	DESCRIPTION/RESULT
RE-163	Nonproductive			Used same lid as in RE-156, raised the shields by 1/16 inch. This kept the bottom shield clean. Several crystals were polycrystalline; when feeding was tried with several other crystals ice occurred ending growth.
RE-164	3	18.9	31.6	Used same lid as in RE-156; raised shield as in RE-163. A molybdenum block was placed over one dogbone hole in the lid to determine whether this could be used for width control. The block did not collect oxide, and did force crystal to steady state width. Feeding was tried, but resulted in ice.

GROWTH RUN SUMMARY

RUN	NO. OF CRYSTALS	LENGTH (cm)	MAX. WIDTH (mm)	DESCRIPTION/RESULT
RE165	3	351	18.6	Molybdenum blocks were placed on the ends of the wide growth slot to evaluate for use in width control. Oxide grew on the blocks and caused ice throughout the run.
RE166	2	420	18.6	This run was a repeat of the set up of RE165. Although oxide grew on the blocks, ice was not a problem. One of this run's crystals held a width within 2 mm for 90cm, a positive result for width control.
RE167	3	191	23.2	This was another run like RE165. Again oxide on the blocks caused ice and prevented good crystal growth.
RE168	2	275	19.9	To try to keep the lids blocks hotter, and oxide free, blocks were placed on the shields above the other blocks. The result was oxide along the slot of the shield as well as on the moly blocks.
RE169	NONPRODUCTIVE			Run aborted because of water pressure problems.
RE170	1	105	20.9	Wide grow lid and shields, with feeding. The feed tube was coiled to slow the pellets, to decrease the impact wave. Ice occurred when feeding was tried.
RE171	3	402	23.8	A lid with a long straight slot (no dogbone) was tried with the moly blocks to see if the gas flow would be sufficiently different. However, oxide on the blocks was as bad as with the dogbone lid.
RE172	2	260	26.4	Wide grow lid and shields for feeding, using a solid end shield on feed side. Feeding resulted in ice; experiment ended when pellets became stuck in feed coil. Enough web was pulled out that the melt shifted near the end of the day. Incomplete wetting of the quartz was evident in the feed chamber.

GROWTH RUN SUMMARY

RUN	NO. OF CRYSTALS	LENGTH (cm)	MAX. WIDTH (mm)	DESCRIPTION/RESULT
RE173	1	147	29.4	Set up like RE172, using a different feed coil. A large amount of silicon was pulled before the recorded crystal was grown. This was necessary because the melt level was higher than normal, due to a failure of wetting in the feed chamber. Suspected cause: the arrangement of the polysilicon in the crucible.
RE174	1	92		Set up like RE172, except using the perforated end shield. The aspirator flow was varied throughout the day as about 10 crystals were started. This was done to find the flow which would be the most effective in the prevention of ice.
RE175	2	393	41.5	Wide growth slot in lid and shield. The lid had slots milled into the bottom. These slots act as aspirators, allowing the silicon oxide an alternative to the growth slot as an exit from the crucible region. With this lid the oxide deposited on the web was largely a hard oxide, but the bottom of the lid was perfectly clean.

GROWTH RUN SUMMARY

RUN	NO. OF CRYSTALS	LENGTH (cm)	MAX. WIDTH (mm)	DESCRIPTION/RESULT
RE-176	7	546	32.6	J-181 configuration for feeding, perforated shield on left end. Oxide on the lid was the most significant problem, preventing long growth periods. One 40 min. feed period was achieved before the oxide caused ice.
RE-177	2	231	28.2	Set up like RE-176. Oxide again was a problem, but not as much as in RE-176. Ice occurred several times while feeding, but generally these particles could be melted while crystal growth continued on one crystal 1 hr 23 min. of feeding was achieved before ice ended growth.
RE-178	1	102	23.1	Set up like RE-176. There was no oxide on the lid, but ice was a problem. Feeding was not practicable this run because the feed end of the crucible had "dewetted" and held no silicon.
RE-179	Nonproductive of Web			An error in the furnace setup resulted in conditions that made crystal growth impossible.
RE-180	3	209	-	Set up like RE176. The thermal profile was peculiar; the ends of the crucible seemed colder than normal, relative to the center temperature.
RE-181	3	394	27.8	J-181 lid and shields for feeding; solid shield on feed end of susceptor to increase the end temperature. There was some oxide on the lid in the beginning of the run, but it was a temporary problem. When feeding was tried, this proved to be the most successful run yet. No feed related problems were encountered all day. Of the crystals grown, the longest grew for 2hr. 23min. with feeding. (Over 5 hours of feed time, 3 crystals was obtained without ice.)
RE-182	1	93		Repeat setup of RE181. This run was not successful; the feed chamber had dewetted and so held no silicon except the pellets which were added later.

GROWTH RUN SUMMARY

RUN	NO. OF CRYSTALS	LENGTH (cm)	MAX. WIDTH (mm)	DESCRIPTION/RESULT
RE-183	1	170	33.6	Repeat set-up of RE181. A different coil position was tried in the meltdown, but again the feed chamber was empty.
RE-184	Nonproductive of Web			Repeat setup of RE181. A more extreme coil position was tried, successfully wetting the feed chamber of the crucible. However the other end of the crucible did not web properly, and no good crystals were obtained.
RE-185	2	223	-	Repeat lid and shield of RE181. The barrier used had a 3mm ridge along the bottom of the crucible with a 3mm gap above the ridge. The furnace components were slightly oxidized during the run, affecting the thermal gradients. Ice occurred throughout the run.
RE-186	1	106	20.0	J-181 lid configuration perforated end shield; ice occurred with feeding.

GROWTH RUN SUMMARY

RUN	NO. OF CRYSTALS	LENGTH (cm)	MAX. WIDTH (mm)	DESCRIPTION/RESULT
RE188	3	355		J-181 lid and shields, not set up for feeding.
RE189	1	204	21.8	J-181 lid and shields; solid end shield; "fence" barrier. Misalignment of feed tube resulted in ice when pellets rolled across the lid into the growth slot. Three crystals were grown for periods of up to 1 hr 15 min. with feeding with no other ice problems.
RE190	2		23.6	J-181 lid and shields,solid end shield. Ice was a problem in this run; the cause is uncertain.
RE191	1	90	22.2	J-181 lid and shields; solid end shield. Ice was a problem with and without feeding.
RE192	Nonproductive of Web			J-181 lid and shields for feeding; solid end shield. Ice was a problem with and without feeding.
RE193	1	96	23.1	J-181 lid and shields for feeding; solid end shield. Ice was a continuous problem; there was evidence of spalling on the lid.
RE194	Nonproductive of Web			J-181 lid and shield. This was not a feed run. Ice was a problem, generally occuring within an hour after a crystal was begun. Again there was evidence of spalling, despite the heavy sand blasting the lid received before the run.
RE195	Nonproductive of Web			J-181 lid with slotted bottom. Continual oxide growth on the lid prevented crystal growth. The probable cause of the oxide was an improperly cleaning of the lid.
RE196	Nonproductive of Web			J-181 lid for feeding, solid end shield. Whenever feeding was tried ice occurred. From the shape of the ice and from the varied times before ice appeared, oxide particles were the probable cause.
RE197	Nonproductive of Web			J-181 lid with milled bottom. Ice was again a problem.

GROWTH RUN SUMMARY

RUN	NO. OF CRYSTALS	LENGTH (cm)	MAX. WIDTH (mm)	DESCRIPTION/RESULT
RE198	Nonproductive			J-181 lid with melted bottom; solid end shield; barrier made with 2mm rod and microscope slide. Ice occurred several times; other times poor starts led to polycrystalline growth.
RE199	5	414	19.6	J-181 lid for feeding, solid end shield. The run purpose was to determine whether ice occurred without feeding; it did. However after the run it was seen that the feed chamber was empty, which made the presence of ice inconclusive.
RE-200	4	438		J-181 feed lid and shields; no barrier. Run purpose again was to determine whether ice occurred without feeding. Several specks of ice were picked up.
RE201	Nonproductive			Repeat set up of RE-200 to verify problem. Again ice was a problem, preventing crystal growth.
RE202	Nonproductive			J-181 lid and shields used from J-furnace. This was done to eliminate the feed lid as the cause of the ice problems.
RE203	1	109		J-181 lid and shields. Ice was not a problem. Before this run the furnace was leak tested and several leaks were repaired.
RE204	1	172	22.9	Repeat of RE-203 to verify results. Ice was not a problem.
RE205	Nonproductive			J-181 feed lid and shields. Ice was a problem from a leak in the pellet feeder.
RE206	2	210	18.9	J-181 feed lid. Ice was a problem; there was strong evidence of spalling.
RE207	2	335	39.0	J-181 feed lid arrangement. A misalignment of the feed tube prevented replenishment experiments. One speck of ice occurred, but did no damage to the crystal which picked it up.

GROWTH RUN SUMMARY

RUN	NO. OF CRYSTALS	LENGTH (cm)	MAX. WIDTH (mm)	DESCRIPTION/RESULT
RE208	Nonproductive			J-181 feed lid, straight feed tube. The barrier end of the crucible was reworked-this may have caused the problem of an empty feed chamber.
RE209	Nonproductive			J-181 feed lid, straight feed tube. Again the feed chamber was empty.
RE210	Nonproductive			J-181 feed lid and shields. Ice was a problem; suspect particulate blow over from between shields.
RE211	Nonproductive			J-181 feed lid and shields. A piece of molbydenum tubing was placed on the lid around the feed hole to try to prevent ice.

GROWTH RUN SUMMARY

RUN	NO. OF CRYSTALS	LENGTH (cm)	MAX. WIDTH (mm)	DESCRIPTION/RESULT
RE212	Nonproductive of Web			First run with movable end shield. Run purpose was primarily for measurement of effects of various shield positions.
RE213	2	359	29.7	J-181 feed set-up, low barrier in crucible, movable end shield. The end of the feed tube was below the level of the top shield and was quickly blocked with oxide. This prevented melt replenishment.
RE214	Nonproductive of Web			J-181 feed set up. The run purpose was to measure temperatures along the slot with various end shield positions using Ircon.
RE215	Nonproductive of Web			J-181 feed set up. Pellet feeding was done with end shield not in shielding position. As a result, the feed chamber froze and the run was ended.
RE216	2	257		J-181 feed arrangement. The run purpose was to make thermal measurements in melt and in susceptor at various end shield positions.
RE217	3	473	35.6	J-181 lid and shields, not a feed run.
RE218	2	175	-	J-181 feed lid arrangement. Thermal measurements of the melt were made with varied end shield positions.
RE219	Nonproductive of Web			J-181 feed lid arrangement.
RE220	Nonproductive of Web			J-181 feed lid arrangement. Thermal measurements were recorded as end shield position and feed rates were varied.
RE221	1	115	20.5	J-181 feed arrangement, high barrier in crucible, movable end shield. When argon was blown through the feed tube, ice occurred both with and without feeding. When this flow was stopped there were no ice problems.

GROWTH RUN SUMMARY

RUN	NO. OF CRYSTALS	LENGTH (cm)	MAX. WIDTH (mm)	DESCRIPTION/RESULT
RE-222	3	417		J-181 feed lid and shields; barriers between shields, movable end shield. About 1 1/2 hr. ocessful feeding was achieved before a failure in the feeder occured
RE-223	Nonproductive of Web			Set up like RE-222. The feed chamber did not wet, resulting in a poor thermal situation and preventing successful feed experiments.
RE-224	3	246		Set up like RE222. Again the feed chamber did not wet.
RE-225	2	233		J-181 feed lid and shields with laser holdes; movable end shield. Feeding was done for 1 hr. at a 2 pellet/min rate; the rate was then increased, freezing the feed chamber.
RE-226	Nonproductive of Web			Same set-up as in RE-225, shield in a lower position. Several hours of feeding were achieved as short crystals were grown. A source of ice was seen to be oxide on the web guides. The web rubbed oxide off the guides, dropping it into the melt where it nucleated ice. This contributed to the absence of long crystals.
RE-227	1	136	26.1	J-181 feed lid and shields with laser holes; fixed solid end shield; high barrier. Fed at 2 pellets/min for over 4 1/2 hours with no feed related problems. Several crystal starts were made during this period.
RE-228	5	536	21.4	Set up of RE227. Fed at 4 pellets/min for 5 hr 20 min.

GROWTH RUN SUMMARY

RUN	NO. OF CRYSTALS	LENGTH (cm)	MAX. WIDTH (mm)	DESCRIPTION/RESULT
RE229	1	183	29.8	J-181 lid and shields with feed and laser holes; solid end shield. Oxide growth on the lid caused some ice problems.
RE230	Nonproductive of web			Furnace was oxidized; resulted in early shutdown. A leak was found on an argon line.
RE231	4	538	26.9	J-181 feed/laser lid and shields; moveable end shield; high barrier Nearly 5 hr. of feeding, at approximately 2/3 the optimal replenishment rate. During this time 3 crystals were grown.
RE232	3	351	20.3	J-181 feed/laser lid and shields; solid end shield. No apparent feed related problems.
R233	3	352	26.6	J-181 feed/laser lid and shield; solid end shield on left; partial perforated shield on right. Crystals had a tendency to extra dendrites; ice occurred several times.
RE234	3	215		Repeat RE-33 set up. Oxide on the lid provided some growth problems. Later in run, pull outs occurred, primarily resultant from the fluctuating dendrite size.
RE235	Nonproductive of Web			Repeat RE233 setup. Ice occurred several times; the source seemed to be the web guides or the furnace's top plate.
RE236	Nonproductive of Web			After the silicon was melted the crucible cracked. Necessitated susceptor repairs.
RE237	Nonproductive of Web			J-181 feed/laser lid and shields; solid end shield. One crystal pulled out; two were polycrystalline; several were ended by ice.
RE238	5	705	22.3	Repeat RE237 setup. Ice occurred once. Fed silicon pellets for 3 hours
RE239	3	361	21.8	Repeat RE237 setup. Ice was a reoccuring problem in the later part of the run.
RE240	3	361	27.0	Repeat RE237. Ice was a problem throughout the run. Part of the problem could have been due to incomplete wetting of both the feed and the growthcompartments of the crucible.

GROWTH RUN SUMMARY

RUN	NO. OF CRYSTALS	LENGTH (cm)	MAX. WIDTH (mm)	DESCRIPTION/RESULT
RE-241	4	384	-	J-181 feed/laser lid. Ice was a problem; source unknown.
RE-242	3	427	33.2	RE-1 feed lid; purpose of run was to determine whether recent ice problems were related to the slot being used. Since ice continued to be a problem, with and without feeding, the J-181 slot is not the problem.
RE-243	NONPRODUCTIVE			J-181 lid and shields; not for feeding, no end shield. Ice was a recurring problem.
RE-244	1	211	17.5	J-181 feed/laser lid. Perforated shields were on both ends of the susceptor; a barrier was in each end of the crucible.
RE-245	NONPRODUCTIVE OF WEB			J-181 feed/laser lid. Tests were made at various feed rates to determine effect on buttoning.
RE-246	NONPRODUCTIVE			
RE-247	4	451	28.0	J-181 feed/laser lid, solid end shield. Oxide on the lid caused some problems; mostly growth was adequate, although-thermally displaced from center.
RE-248	3	420	35.7	J-181 feed/laser lid; solid end shield, on left end tabe on right end. Good growth run; however a multiple pellet drop plugged the feed hole of the lid, preventing further feeding.
RE-249	4	426	29.4	Repeat set up of Re-248. On this run the left wall and barrier became totally devitrified; the side walls between the barrier and the end were partly devitrified. Crystal growth appeared unaffected.
RE-250	2	375	30.0	J-181 feed/laser lid. Tab on right; moveable shield on left. A cold spot on the right caused growth problems which included occassional ice with and without feeding.
RE251	3	357	28.7	Repeat of RE-250 set-up. Ice appeared twice, bottom shield was oxidized.

GROWTH RUN SUMMARY

RUN	NO. OF CRYSTALS	LENGTH (cm)	MAX. WIDTH (mm)	DESCRIPTION/RESULT
RE252	2	313		J-181 feed/laser lid and shields. moveable shield on left, fixed tab on right. Ice was a reoccuring problem.
RE253	4	498	23.6	J-252 feed lid and shields. Ice was an increasingly severe problem as the 12 hr. feed run continued. The source of ice appeared to be from oxide spalling from the top shield. This was confirmed after the run.
RE254	1	153	22.9	J-259 feed/laser lid and shields. Oxide on lid and ice were problems of this run.
RE255	1	227	27.2	J-252 feed lid and shields. Several other crystals were started. but became polycrystalline.
RE256	Nonproductive			Repeat RE255 setup. Oxide on the lid was a problem source most of the run. Longest crystal was 79 cm.
RE257	3	382	21.7	J-252 lid, J-181 shield on top, J-252 middle shield. Ice was an occasional problem, still suspect spalling from top shield.
RE258	6	713	23.7	J-252 lid, 2 J-252 mid-shields. 17 hours of feeding; no apparent feed-related problems.
RE259	4	364		J-252 feed lid; solid shield on left, perforated shield on right. Several crystals pulled out; others were polycrystalline.
RE260	3	418	26.2	J-259 feed/laser lid and shields. The laser holes became blocked with oxide early in run, preventing melt level monitoring.
RE261	3	236	22.1	Repeat RE-260 set-up. Ice was a recurring problem.
RE262	1	142		RE258 set up. Oxide on lid caused some problems. Some specks of ice were picked up in two crystals.
RE263	3	254	19.3	J-252 lid and mid-shields; raised lower shield 1/16". Ice in run may have been due to a low barrier in the crucible.

GROWTH RUN SUMMARY

RUN	NO. OF CRYSTALS	LENGTH (cm)	MAX. WIDTH (mm)	MAX. SPEED (cm/min)	DESCRIPTION/RESULT
J-163	3	355	32.5	6.75	Test effect of adding fourth top shield to beveled slot and top shield arrangement of RE-126. Problems with ice suggest that extra shield makes center to end ΔT too small. Reached thruput of 21.7 cm^2/min.
J-164	3	532	35.1	5.74	Return to 3 top shields, beveled lid. Attempt to grow wide web. Improved growth behavior. Max. thruput 20.0 cm^2/min.
J-165	1	305	40.5	1.7	Repeat J-164 configuration. Problems with oxide falling into melt from lid.
J-166	2	180	24.0	1.7	Repeat J-164 Configuration. Difficult to initiate growth. Pull outs. Jumpy melt.
J-167	3	223	24.2	7.5	Repeat J-164 Configuration. Vary growth speed. 18.1 cm^2/min thruput.
J-168	3	292	30.0	5.0	Repeat J-164 configuration. Floating ice problems all day.
J-169	Not Productive of Web				Repeat J-164 configuration. Constant ice problems. Believe this due to oxide particle which fell from lid and attached to crucible wall. Ice spikes from crucible wall.
J-170	1	82	19.1	1.6	Repeat J-164 configuration in attempt to determine cause of erratic behavior. Difficult to get thermal symmetry even with coil adjustment at extreme position.
J-171	3	220	21.2	1.6	Modify top shielding by replacing upper 1.5mm thick shield with one 0.5mm thick in attempt to reduce coupling and run top shield cooler. Consistent ice from left. Coil adjustment (lateral) severely binding to the extent that its function is compromised.

GROWTH RUN SUMMARY

RUN	NO. OF CRYSTALS	LENGTH (cm)	MAX. WIDTH (mm)	MAX. SPEED (cm/min)	DESCRIPTION/RESULT
J-172	2	145	21.6	1.9	Repeat J-171 configuration. Poor growth behavior. After run, coil positioning mechanism overhauled so that it moves freely. However, due to some alignment problems which have apparently increased over a period of time, the range of motion is limited. This will be corrected when time permits.
J-173	3	454	32.8	6.7	Repeat J-171 configuration. Better growth behavior than previous runs, but crystal deformation occurs at narrower widths than in configuration with thick upper top shield. Reached thruput rates of 17.1 and 22.0 cm^2/min.
J-174	2	122	22.2	1.7	Return to J-164 configuration, i.e. 1.5mm Top shield instead of 0.5mm. Difficult to start. Tendency to go poly early.
J-175	3	132	20.1	1.7	Repeat J-174, with similar results. Present inconsistency of behavior of this configuration is not well understood. Perhaps the well used shields have changed sufficiently to perturb thermal behavior. Changes will be made in future runs.

GROWTH RUN SUMMARY

RUN	NO. OF CRYSTALS	LENGTH (cm)	MAX. WIDTH (mm)	MAX. STRAIN (cm/min)	DESCRIPTION/RESULT
J-176	2	233	34.2	1.7	Test configuration modification. Overlap of formed lower shield of J-175 configuration increase 1mm. Late start due to servicing of generator. Web deformed at narrower widths than J-175 configuration.
J-177	2	117	29.3	1.7	J-175 configuration. Floating ice in P.M. Dendrites very smooth. Dendrite probe indicated good melt profile.
J-178	No Significant crystal production				J-175 configuration modified by raising upper top shield 1.5mm. Difficult to grow. Web; quality rapidly degenerated.
J-179	No useful crystal production.				Repeat J-178 configuration. Web crystals consistently turned polycrystalline, initiated by formation of a line and subsequent breakdown. Conclude this modification has negative results.
J-180	2	403	40.1	3.3	J-175 configuration modified to uniform 1.5mm shield spacing No argon flow tubes. Good growth, but oxide collected on lower shield.
J-181	3	549	42.1	3.0	J-175 configuration without argon flow tubes. Run terminated due to exhaustion of silicon melt.
J-182	2	434	44.3	1.7	J-181 configuration modified by adding a 0.5mm thick shield on top. New width record, 4.43cm.

GROWTH RUN SUMMARY

RUN	NO. OF CRYSTALS	LENGTH (cm)	MAX. WIDTH (mm)	MAX. VELOCITY (cm/min)	DESCRIPTION/RESULT
J-183	2	286	38.5	1.7	Repeat J181 configuration. Early starts tended to generate lines in crystals. Growth good later.
J-184	3	409	33.1	1.7	J-181 configuration. Similar to previous run.
J-185	3	431	33.5	1.7	J-181 configuration. Good crystal terminated by pull out.
J-186	3	266	28.9	1.7	To produce lower resistivity material for evaluation, ($6x10^{17}$ total boron) J-181 configuration. Crystals terminated because of degeneration in quality.
J-187	4	513	33.4	1.6	Test new configuration. Insert additional 0.5mm thick full shield with slight bevel overlap into J-181 shield stack. Total 4 top shields. $6x10^{17}$ total boron. Growth behavior generally good. Crystals terminated by pull out.
J-188	No significant web production				Repeat J-187 configuration. Most of day spent video taping of growth initiation.
J-189	2	494	36.9	3.1	Repeat J-187configuration. Peached thruput values of 15.8 and 16.6 cm^2/min.
J-190	3	525	30.1	1.6	Repeat J-187 configuration. Early crystals terminated by pull out or quality degeneration. Conclude this configuration not improvement over J-181 in terms of width capabilities.
J-191	3	378	33.9	6.6	J-181 configuration. Crystal quality poor early, good later in day.
J-192	3	534	36.0	3.2	J-181 configuration modified by addition of 0.5mm thick shield directly on top. Max thruput of 18.7cm^2/min.
J-193	Not Productive of Web.				J-181 configuration. Piece of oxide fell into melt early and attached to crucible wall, causing ice nucleation.

GROWTH RUN SUMMARY

RUN	NO. OF CRYSTALS	LENGTH (cm)	MAX. WIDTH (mm)	MAX. VELOCITY (cm/min)	DESCRIPTION/RESULT
J-194	3	445	30.5	1.6	J-181 configuration. Crystals terminated by pull out. Attempt was made to minimize undercooling during growth.
J-195	3	499	35.8	6.0	J-181 configuration. Max. thruput 21.5 cm^2/min.
J-196	2	421	35.7	7.6	J-181 configuration with additional thin top shield. Reached record thruput of 27.1 cm^2/min.

GROWTH RUN SUMMARY

RUN	NO. OF CRYSTALS	LENGTH (cm)	MAX. WIDTH (mm)	MAX. VELOCITY (cm/min)	DESCRIPTION/RESULT
J-197	2	202	19.7	3.3	Purpose: To measure lid and top shield temperatures of J-181 configuration. See text for results. Thickness-velocity data. Doped to ∿ 2 ohm-cm.
J-198	4	336	20.8	3.3	Test J-181 configuration with addition of 0.5mm thick shield spaced 1.5mm above upper thick shield. Doped to ∿ 2 ohm-cm. Thickness-velocity data. Growth behavior generally poor.
J-199	3	260	19.9	3.3	Repeat J-198, with spacing of top most shield increased to 4.5mm. Thickness velocity data. Difficult to start and grow.
J-200	2	538	47.2	3.3	J-181 configuration. New width record. Thruput rate of 15.8cm^2/min.
J-201	4	325	27.2	2.8	J-181 configuration. Some difficulty starting growth early in day.
J-202	3	338	29.1	1.8	J-181 configuration. Dendrites somewhat choppy.
J-203	2	463	39.2	1.7	J-181 configuration. Some starting difficulties early good growth during afternoon.
J-204	2	441	35.6	1.6	Test modification of J-181 configuration. Middle Top shield slitted around periphery to limit r.f. coupling. (See Text)
J-205	3	410	28.4	1.6	Another J-181 modification with slitted shield on top. Doped to ∿ 2 ohm-cm. Crystals terminated by pullouts.
J-206	Not Productive of Web				Repeat J-205. Melt very unstable for no apparent reason.
J-207	2	167	24.1	3.3	Repeat J-205 configuration. Thickness-velocity data. Coil raised to improve dendrite penetration. Improved growth behavior, but crystal terminated when reel tape tension wire failed.

GROWTH RUN SUMMARY

RUN	NO. OF CRYSTALS	LENGTH (cm)	MAX. WIDTH (mm)	MAX. VELOCITY (cm/min)	DESCRIPTION/RESULT
J208	2	470	33.7	1.6	J-181 configuration. Radiation shields below susceptor replaced. Nominal 175gm melt as opposed to standard 185gms to start at slightly lower melt level. Generally good growth behavior.
J-209	2	305	38.4	1.6	Modification of J-181 configuration. Two upper shields slitted around periphery. To minimize r.f. coupling and thus reduce temperature. Very stable growth.
J-210	3	696	38.4	1.6	Modification of J-181 configuration, extra top shield, upper Two slitted to reduce r.f. coupling. Good growth behavior.
J-211	5	380	24.0	3.3	Repeat J-210 configuration. Thickness-velocity data. Growth behavior poor relative to J-210. After run, it was discovered that Si melt had not wetted one end of crucible, and pulled away further as run progressed.
J-212	3	586	32.9	5.0	Repeat J-210 configuration, except starting melt increased to 185gms. Thickness velocity data. Reached 16.5cm^2/min thruput.
J-213	4	432	32.0	5.2	Repeat J-210 configuration. Thickness-velocity data early and late in day. 16.6cm^2/min max. Thruput.
J-214	2	220	18.5	3.3	Test different to shield configuration. J-181 lid with RF-1 type shields, except upper slitted. Thickness-velocity data. Unstable melt. Poor growth behavior.
J-215	No significant web production				J-210 configuration with lid and topmost shield instrumented. Melt unstable. Thermocouple feed through evidently leaked, causing partial oxidation of side shields.

GROWTH RUN SUMMARY

RUN	NO. OF CRYSTALS	LENGTH (cm)	MAX. WIDTH (mm)	MAX. VELOCITY (cm/min)	DESCRIPTION/RESULT
J-216	2	401	33.5	3.3	J-181 modification with added shield, Total 4, upper two slitted. Overhang of lower formed shield increased by 1mm. V-T data. Easy growth initiation, stable growth. Oxide forced termination of growth.
J-217	4	427	22.6	3.3	J-216 modified by bringing shield stack 1.5mm closer to lid. V-T data. Oxide problems.
J-218	Not productive of web				Lid and shield configuration shown in Figure 2. modified by adding two additional top shields in effort to improve growth behavior. Oxide accomulated in slot growing from bottom edge of folded over (lower) shield.
J-219	3	482	36.7	3.3	Same lid as J-218, but the J-181 shield stack, upper two slitted was used. Oxide deposition minimal, able to grow most of day, although early starts (high melt) were poly.
J-220	4	494	36.2	3.3	Repeat J-219 configuration. Very similar growth behavior.
J-221	No significant web production				Test RE-1 configuration with top shield slitted to provide cooler view to web. V-T data indicated this configuration faster than others tested, but oxide deposition and icing prevented any significant web growth.
J-222	No significant web production				Modification of J-218 in attempt to alter convective gas flow patterns. J-181 shield stack placed directly on full formed shield. Excessive oxide build up prevented growth.

GROWTH RUN SUMMARY

RUN	NO. OF CRYSTALS	LENGTH (cm)	MAX. WIDTH (mm)	MAX. VELOCITY (cm/min)	DESCRIPTION/RESULT
J-223	4	367	30.7	3.3	Test of the 4 shield J-181 mod., with stack condensed by spacing between shields at 0.5mm instead of 1.5mm. T-V data. Generally stable growth. Oxide deposited on lower shield.
J-224	2	439	36.0	1.7	Repeat J-223. Good growth, except for oxide deposition on lower shield.
J-225	2	170	17.3	3.3	Test J-218 lid. Gap between formed shield and lid lip increased in effort to reduce oxide build up. Three full top shields, upper two slitted. Early crystals poly, oxide growth on lower shield, falling into melt.
J-226	1	93	21.7	2.7	Repeat J-225 with the additon of alumina barriers between lid and lower shield in effort to change gas flow and reduce oxide accumulation. Not successful., oxide, poor growth.

GROWTH RUN SUMMARY

RUN	NO. OF CRYSTALS	LENGTH (cm)	MAX. WIDTH (mm)	MAX. VELOCITY (cm/min)	DESCRIPTION/RESULT
J-227	2	∿ 200	-	3.3	Four shield modification of J-181 with compressed shield spacings. 1.5mm between lid and formed shield, 0.5mm between rest. Top two shields slitted. Oxide grew rapidly from edge of formed shield forcing premature termination of growth. Thickness velocity data.
J-228	1	147	-	5.0	Repeat J-227 except a solid barrier was used as spacer between lid and formed shield in attempt to inhibit gas flow. Oxide still grew from lower shield, inhibiting growth and forcing early termination. Grew 105 cm at constant 5 cm/min. before crystal terminated by oxide growth.
J-229	4	360	23.8	3.3	Test J-98B configuration for widening characteristics and thickness-velocity behavior. Crystals picked up ice particles and degenerated. Ice caused by oxide spalling from bottom of lid.
J-230	No significant crystal production.				Repeat J-229, with extra care with lid preparation. Similar ice problems.
J-231	3	225	25.9	5.0	Repeat J-228 configuration. Oxide growth from lower shield inhibited growth. Overall growth behavior poor. V-T data.
J-232	3	280	26.8	3.3	Repeat J-228 except overhang of lower top shield decreased. Growth behavior poor, even though oxide less.
J-233	2	253	19.1	1.8	J-98B (short slot) configuration. Test for width control. Feed hole plugged. Lid upside down to present different surface to melt in effort to control spalling. Ice in afternoon, due to spalling.

GROWTH RUN SUMMARY

RUN	NO. OF CRYSTALS	LENGTH (cm)	MAX. WIDTH (mm)	MAX. VELOCITY (cm/min)	DESCRIPTION/RESULT
J-234	3	437	28.4		Modify J-228 configuration using 0.5mm barriers instead of washers as spacers between shields. Better growth. Oxide growth on right end limited growth duration to about 1.5 hours per crystal. T-V data.
J-235	Not productive of web crystals.				Modification of J-234, in which lid is ported on lower edge around periphery, in effort to modify convective gas flow and oxide deposition. Oxide deposition and ice formation prevented growth.

GROWTH RUN SUMMARY

RUN	NO. OF CRYSTALS	LENGTH (cm)	MAX. WIDTH (mm)	MAX. VELOCITY (cm/min)	DESCRIPTION/RESULT
J-236	2	172	22.7	2.0	Test J98B configuration with new lid. Partial lower shield. Growth hampered all day by ice fronts moving in from left.
J-237	No significant web growth				Test new thin lid. 3mm thick, RE-1 slot geometry, RE-1 lower shield + 3 J-181 shields, upper two slitted. Fast growth configuration, but floating ice prevented significant web growth.
J-238	1	82	14.7	2.4	Repeat J-237, except narrower slot in lower shield in effort to make lid slot hotter. Severe and rapid oxide accumulation in slot prevented significant growth.
J-239	No significant web growth				3mm thick lid with 3 full top shields. T-V data. Rapid oxide deposition along slot inhibited growth.
J-240	1	126	-	-	J-181 configuration. Repeated ice nucleation prevented growth. Post-mortem showed heavy spalling on bottom of lid.
J-241	1	325	39.7	1.9	Repeat J-240. Ice particles in morning. Good growth during afternoon.
J-242	No significant growth				Repeat J-240. Ice nucleation all day prevented growth.

GROWTH RUN SUMMARY

RUN	NO. OF CRYSTALS	LENGTH (cm)	MAX. WIDTH (mm)	MAX. SPEED (cm/min)	DESCRIPTION/RESULT
J-243	No significant web production				J-181 Configuration. Ice problems from both ends. Susceptor probe indicated end temperatures too low.
J-244	3	144	19.1	1.9	J-181 Configuration with the addition of end shields with 1/3 area coverage. Thermal profile improved, but had problems with floating ice particles. Suspect atmosphere purity.
J-245	1	210	33.9	1.6	Diffusion pump repaired and back in operation. J-244 Configuration. Grew well in afternoon.
J-246	No significant web production				Report J-245. Poor growth behavior.
J-247	2	168	-	2.9	J-98B configuration, to test width control characteristics. End shields, 1/3 coverage, in place. Floating ice problems
J-248	2	177	24.4	1.9	Repeat J-247. Temperature probe of melt. No ice problems but difficult to control pull out.
J-249	No significant web production				J-181 configuration with 4th top shield, slitted end shields. Poor growth behavior. Discovered malfunction in electronic balance, giving over weight starting loads, (odd account for some of the growth problems in this and some previous runs.)
J-250	5	495	35.6	1.9	Repeat J-249. Growth behavior much improved.
J-251	No significant web production				Repeat J-249. Poor growth behavior, difficult starting.
J-252	4	455	22.8	2.0	New lid. Modification of RE-1 for width control. Good growth behavior, but crystals terminated by ice.
J-253	2	321	20.7	1.9	Repeat J-252 with the addition of end-shields with 1/3 coverage. Some problems with oxide on lid.

GROWTH RUN SUMMARY

RUN	NO. OF CRYSTALS	LENGTH (cm)	MAX. WIDTH (mm)	MAX. SPEED (cm/min)	DESCRIPTION/RESULT
J-254	3	128	-	-	J-252 configuration with addition of end shields with 1/3 coverage. Considerable trouble with pullouts, unstable melt. Bottom shields oxidized. Leak suspected.
J-255	3	338	23.1	2.2	Repeat J-254 configuration. New bottom shields under susceptor. Floating ice.
J-256	5	649	27.6	2.2	Repeat J-254, with end shielding increased by 33%. Attempt at width control Good growth during afternoon.
J-257	2	344	27.7	2.0	Repeat J-256 configuration. One end shield moved off center during heat up, making growth more difficult. 270 cm long crystal late in day.
J-258	2	67	-	3.4	Repeat J-256. Thickness velocity data. Difficulty in starting.
J-259	3	263	21.2	2.0	J-252 lid slot lengthened by 3mm. Problems with oxide on slot.
J-260	2	136	-	-	Repeat J-259. Starting problems. Unstable melt.
J-261	1	220	27.4	2.0	Repeat J-259. Good growth a.m. Melt very unstable, difficult starting p.m.
J-262	3	406	26.0	2.0	Add third top shield to J-259 configuration. Early starting difficult. Good growth later, but crystals terminated by floating ice.
J-263	4	395	26.2	5.0	Repeat J-262. Easy to start, but problems with oxide on lid slot. Thickness velocity data.
J-264	3	115	-	-	Repeat J-262. Ice problems terminated crystals.

GROWTH RUN SUMMARY

RUN	NO. OF CRYSTALS	LENGTH (cm)	MAX. WIDTH (mm)	MAX. SPEED (cm/min)	DESCRIPTION/RESULT
J-265	1	232	25.7	2.0	Repeat J-262. Ice and poor starting until late in day.
J-266	1	238	-	1.9	Test inclusion of 10% by weight recycled dendrites in melt. J-262 configuration. Grew well. Web growth similar to that with all semiconductor polysilicon charge.

GROWTH RUN SUMMARY

RUN	NO. OF CRYSTALS	LENGTH (cm)	MAX. WIDTH (mm)	DESCRIPTION/RESULT
J-267	2	267	25.7	J-259 Lid with 3 top shields, raised to 3mm above lid. Test different coil heights.
J-268	1	101	28.6	J-181 configuration, new susceptor 5cm end shields. Repeated pull outs prevented much growth. Control problems during p.m.
J-269	1	105	19.1	Same configuration as J-268. 10% of Si load consisted of dendrites removed from processed solar cells. Control problems. Controller replaced.
J-270	1	104	21.2	Same configuration as J-268. Poor growth.
J-271	Not productive			Susceptor modified for melt replenishment. J-252 lid configuration. Severe icing problem forced early shut down.
J-272	Not productive			J-181 lid configurations. Test coil positions. Barrier crucible. Ice problems all day.
J-273	Not productive			Repeat J-272. Ice due to spalling from underside of lid.
J-274	1	100	25.5	J-181 configuration adapted for melt replenishment. New pellet feeder and feeder loader mounted on furnace. Feeder operated during gorwth. Ice late in day due to spalling from underside of lid.
J-275	2	174	-	J-181 feed configuration susceptor end shields, solid left perforated right. Feeding melt. Oxide from lid caused termination of growth. After run, shields slightly oxidized indicating trace of air in system at some point.
J-276	5	382	-	Repeat J-275 feeding. Oxide from lower top shield caused premature termination of crystals.

GROWTH RUN SUMMARY

RUN	NO. OF CRYSTALS	LENGTH (cm)	MAX. WIDTH (mm)	DESCRIPTION/RESULT
J-277	3	249	–	Repeat J-275. Feeding. Could not achieve symmetric temperature profile.
J-278	Not productive			Attempt to improve profile by perforating side shields near crucible barrier. Poor growth stability and ice.
J-279	Not productive			Repeat J-278. Same results.

GROWTH RUN SUMMARY

RUN	MAX. WIDTH (mm)	TOTAL LENGTH (cm)	DESCRIPTION/RESULT
WA-1	*	*	RE-1 lid configuration. Oxide from lid and shields caused icing problems. May have been due to melting down too rapidly and overheating. Lateral coil position adjusted until buttoning was symmetrical.
WA-2	*	*	RE-1 lid configuration. Initially difficult to get dendrite penetration. Coil raised to achieve dendrite formation and first web grown.
WA-3	*	*	J-181 lid configuration. Oxide and icing problems. Further coil adjustments to improve buttoning.
WA-4	*	*	J-181 lid configuration. Various coil heights tested obtained better growth initiation and dendrite penetration. Oxide deposition prevented significant web growth.
WA-5	*	*	J-181 lid configuration. Again, oxide interfered with web growth.

*First five runs primarily for leak check, coil test, controller and speed calibration. Growth was secondary objective.

GROWTH RUN SUMMARY

RUN	MAX. WIDTH	TOTAL LENGTH (cm)	DESCRIPTION/RESULT
WA-6		112	Growing with vented lid in J181 configuration, to help eliminate oxide problems. Oxide was not a problem and growth was good. There was some polycrystalline growth and choppy dendrites until the melt was lowered by about 10 grams. Coil was adjusted for more symmetric growth.
WA-7		170	Using standard J181 configuration with a slower melt down to help prevent oxide development. This run was free of oxide and growth was good. Some additional coil movements were made to improve button symmetry and dendrite penetration.
WA-8		120	Standard J-181 configuration using normal melt down procedures. The more rapid melt down previously used seemed to be a cause of oxide formation. No long pieces were grown because of oxide falling in the melt causing ice.
WA-9		435	Repeat WA-7 using slow melt down to prevent oxide development. This run was again free of oxide, and oxide formation appears to be definitely related in part to melt down procedure. Growth was good with very few adjustments being required.
WA-10	Not Productive of Web		J-181 configuration being used for pull speed calibration. A more rapid melt down was used which resulted in oxide formation again. Future runs should be made with the slower melt down procedure. Oxide formation prohibited growth, but pull speed calibration was made, as intended.
WA-11	Not Productive of Web		Repeat WA-10 run, repeating pull speed calibration. Problems with melt down and lid preparation resulted in some oxide. Polycrystalline growth was a problem early in the run. Past experience suggests a lower starting melt weight will offset this difficulty.

GROWTH RUN SUMMARY

RUN	MAX. WIDTH (mm)	TOTAL LENGTH (cm)	DESCRIPTION/RESULT
WA-12	Not Productive of Web		Using J-181 configuration with a vented lid, repeat WA-6, to determine if vented lid will prevent oxide deposition. Oxide did not deposit on lid but did form on shields. Growth was prohibited by the oxide.
WA-13	24.7	184	J-181 configuration using slow melt down to control oxide deposition on components. Some oxide did form on upper shields this may be due to inadequate lid preparation. These lids will be prepared using the usual procedures and run in the J furnace to see if oxide forms. The oxide problem was not a severe as usual and some growth was possible.

GROWTH RUN SUMMARY

RUN	MAX. WIDTH	TOTAL LENGTH (cm)	DESCRIPTION/RESULT
WA-14	3.0 cm	109 cm.	J-181 configuration with 1/16" raised top shield. Clean and oxide free, raising shield helped prevent oxide. Problems were with polycrystalline growth, may be due to high argon flow rates.
WA-15	Not Productive of Web		Repeat WA-14 configuration. Clean and oxide free, raised shield appears to eliminate oxide. Lower argon flow appears to have corrected polygrowth problem, except at higher speeds.
WA-16	3.4 cm	160 cm.	Repeat WA-14, this run was clean and oxide free. Thickness velocity data for the J181 configuration was obtained. The melt weight was increased again to 185 grams but polycrystalline growth resulted early in the run.
WA-17	3.3 cm	150 cm	This run used a 30° beveled lid with a J181 shielding configuration to improve the radiation losses from the web. Growth was good and the run was clean. Thickness velocity data was taken and thickness was increased by 20% for a given pull speed as compared to the standard J-181 lid.
WA-18	Not Productive of Web		Repeating WA-17 configuration to get additional thickness-velocity data on the new lid. This run was again clean and oxide free. Several short crystals were grown and thickness data recorded. The higher melt level is still resulting in polycrystal line growth early in the run.
WA-19	Not Productive of Web		Repeating WA-17, thickness velocity data was recorded for several short crystals and the thickness is still greater as compared to the standard J-181 configuration.
WA-20	3.8 cm	182 cm	Repeat WA-14 using J-181 configuration to get thickness-velocity data. This run was clean and free of oxide.

GROWTH RUN SUMMARY

RUN	MAX. WIDTH (mm)	TOTAL LENGTH (cm)	DESCRIPTION/RESULT
WA-21	3.20	281	Running a 30° beveled lid with J-181 top shields to get thickness–velocity profile. Had some difficulty with polycrystalline growth early in the run. This run is to repeat WA-17.
WA-22	3.50	307	Repeating WA-17 to get thickness velocity data. First run using the new solid state generator. Furnace was clean and free of oxide.
WA-23	Not Productive of Web		Repeating WA-17 to get additional thickness velocity data. Run was shut down early when web fell in melt and caused freeze out.
WA-24	Not Productive of Web		Repeating WA-17 to get thickness–velocity data. Had problems with polycrystalline growth throughout the run. New operator was being trained to run.
WA25	Not Productive of Web		Repeating WA-17 with first shield lowered 1/16" to cut down on view between lid and web. This run had difficulty with oxide and icing. New operator was being trained.
WA26	Run Aborted		Run was terminated during melt down when the generator malfunctioned.
WA27	3.30	256	Repeating WA-17 with first shield lowered 1/16". Oxide and ice formation were again a problem but some data was obtained.
WA28	3.45	293	Repeating WA-25 and WA-26 to get additional thickness–velocity data. New operator had some difficulty growing but data was obtained.
WA29	Not Productive of Web		Repeating WA-25 to obtain additional thickness velocity data. Oxide and icing problems limited growth but some data was obtained.

GROWTH RUN SUMMARY

RUN	MAX. WIDTH (mm)	TOTAL LENGTH (cm)	DESCRIPTION/RESULT
WA-30	3.65	324	Using J-181 configuration to obtain thickness velocity data for comparison with WA-17 configuration. This run was clean and free of oxide.
WA-31	No run		Problems were incurred during meltdown and the run was terminated. Susceptor was damaged by silicon and had to be replaced.

GROWTH RUN SUMMARY

RUN	MAX. WIDTH (mm)	TOTAL LENGTH (cm)	DESCRIPTION/RESULT
WA-32	215	260	The purpose of this run was to obtain thickness-velocity data for the open configuration, with a 30° bevel, shown in Figure 1. This run had difficulties with polygrowth but some data was obtained.
WA-33	Not Productive of Web		This run was to repeat WA-32 to obtain additional T-V data. Silicon dewet a portion of the crucible during this run, resulting in polygrowth throughout the run. This run will be repeated.
WA-34	265	310	This was a repeat of WA-32. Growth during this run was relatively good and T-V data was obtainable. These preliminary results show that the open configurations has significant effects on improving thickness at relatively high growth speeds.
WA-35	310	290	Repeating WA-32 for additional T-V data. This run was good and T-V data was obtained. The results correlated with those for the previous run and preliminary findings were supported. More work at higher speed should be performed with this configuration.
WA-36	Not Productive of Web		This run involved the use of an overlapping shield on the 30° beveled lid as shown in Figure 2. Icing from the right side of the crucible was a continual problem during this run and no T-V data could be obtained.
WA-37	Not Productive of Web		Repeat WA-36 to obtain T-V data for new lid-shield configuration. This run had recurring problems with oxide on the shields and with poly growth. This run will be repeated.
WA-38	Not Productive of Web		Repeating WA-36, this run again had problems with oxide and poly growth throughout the day. This run will be repeated. No evidence of crucible dewetting was found and the source of poly growth is not clear.
WA-39	Not Productive of Web		Repeating WA-36, problems were again associated with oxide formation and with poly. growth in particular. A J-181 configuration will be run to help isolate the source of poly growth. Malfunctions in the temperature control system may be contributing to this problem.

GROWTH RUN SUMMARY

RUN	MAX. WIDTH (mm)	TOTAL LENGTH (cm)	DESCRIPTION/RESULT
WA-40	Not Productive of Web		This is a baseline J-181 configuration for furnace shakedown tests. This run was unsuccessful because of temperature instability in the furnace. The controller appears to be malfunctioning.
WA-41	Not Productive of Web		This is a repeat of the J-181 baseline run. Temperature controller problems prevented long term growth. Some material was grown that was not polycrystalline, but only in short lengths. This run was not conclusive and will be repeated.
W-42	Not Productive of Web		Repeating the J-181 baseline configuration. Reseting and adjusting the temperature controller system did not correct the temperature stability problems. More checking of the controller must be performed.
WA-43	Not Productive of Web		This is another repeat of the J-181 baseline run. The source of temperature instability is still not clear. Growth was still unsuccessful because of this problem.
WA-44	Not Productive of Web		This objective of this run is to try and isolate the source of temperature instability within the control network. Adjustments were made to attempt to improve stability, but were not successful.
WA-45	Not Productive of Web		This run is to further isolate temperature control problems within the control system. Adjustments to the controller have not corrected the problem. The coil itself appeared to move during this run and may be effecting temperature stability.

GROWTH RUN SUMMARY

RUN	NO. OF CRYSTALS	LENGTH (cm)	MAX. WIDTH (mm)	DESCRIPTION/RESULT
WA-46	Not productive of web			Repeating WA-36, this run had control problems and temperature was constantly changing. Growth was unstable and the electronic controller had to be adjusted.
WA-47	Not productive of web			Repeating WA-36 configuration. This run also had some temperature control problems. The control was improved later in the day when a light pipe sensor adjustment was made. Growth was limited by the temperature instability.
WA-48	Short segments of web grown			Using a J-181 configuration to isolate the problems in growth. Icing and choppy dendrites were still a problem. Growth improved later in the day as the melt was lowered.
WA-49	Not productive of web			Repeating J-181, with a new melt down procedure to prevent oxide from forming on the susceptor. Choppy dendrites and icing were still a problem during growth. The melt was probed for temperature symmetry and an assymetry was found the new melt down procedure eliminated the oxide on the susceptor.
WA-50	Short segments of web grown			Repeating J-181 with new melt down procedure. Oxide on the shields was a problem early in the day. The susceptor was clean and free of oxide. Choppy dendrites and icing still lead to early pullouts. This run will be repeated.
WA-51	1	180cm	34.0	Repeating WA-50, this run was clean and free of oxide. Dendrites were choppy early in the day but growth improved as the melt was lowered.
WA-52	Not productive of web			Running RE-1 configuration, oxide on the lid and shields was a continual problem, and resulted in icing throughout the day.

GROWTH RUN SUMMARY

RUN	NO. OF CRYSTALS	LENGTH (cm)	MAX. WIDTH (mm)	DESCRIPTION/RESULT
WA 54	2	310	-	RE-1 configuration. Lid and susceptor free of oxide.
WA 55	Short lengths of web			RE-1 configuration. Test variations in coil height. Poor growth behavior.
WA 56	Short lengths of web			J98B configuration. Test short slot for width control. Unstable melt pullouts. Control instabilities.
WA 57	Not productive of web			J98B poor growth behavior. Conclude J98B lid. Too difficult to control for width control purposes.
WA 58	Not productive of web			J252 lid configuration. Seed broke, web fell shorting coil causing early shut down.
WA 59	1	268	22.5	J252 configuration. Ice problems. Width held to within 2mm for over 1 meter.
WA 60	Not productive			J252 configuration. Generator cut out due to temporary water pressure drop.
WA 61	No significant web production			J252 configuration. Continual ice problems throughout day caused early termination of crystals.

GROWTH RUN SUMMARY

RUN	NO. OF CRYSTALS	LENGTH (cm)	MAX. WIDTH (mm)	DESCRIPTION/RESULT
WA 62	4	384	19.7	J-252 configuration. Test width control. Some oxide and control problems. Growth generally good.
WA 63	3	449	25.8	J-252 configuration. Good growth except some ice late in day. Width approimated desired value.
WA 64	1	130	23.5	J-252 configuration. Recurring ice problems limited growth.
WA 65	2	244	25.0	J-252 configuration. Ice terminated crystals.
WA 66	1	96	19.5	J-252 configuration. Ice problems all day.
WA 67	2	481	26.9	J-252 configuration. Good growth with one crystal 3.3 meters long
WA 68	1	291	27.0	J-252 configuration.
WA 69	Not Productive			RE-1 configuration. Crystals terminated by pullouts and thirding.

APPENDIX 2

9.2 Average Solar Cell Data on Web Crystals (Report Period April 1979 to April 1980)

The tables in this appendix give the averaged solar cell performance for cells fabricated from the crystals listed. Each entry in the table represents the average value for approximately four cells. Measurement conditions were a simulation of AM1 illumination at a power density of 91.6 mW/cm^2 as determined by a standardized solar cell. The cells were nominally 10x10 mm square (actual area 1.032 cm^2), and had an active area of about 92.5%. The cell efficiency reported is for a device WITHOUT an antireflective coating; experience with TiO_2-SiO_2 coatings indicates that an average increase in efficiency by a factor of 1.43 occurs.

CRYSTAL NUMBER	WEB QUAL	THICK MIC-M	RHO OHM-CM	ISC MA	VOC VOLT	FF	EFF %	OCD MIC-S	NOTES
J10-3.3	WQ29	255	8.5	19.63	.511	.719	7.64	1.6	
J133-1.6	WQ28	200	7.4	19.18	.510	.724	7.49	1.2	
J134-3.5	WQ28	190	7.6	17.80	.516	.733	7.12	1.4	
J135-3.4	WQ29	210	7.5	20.70	.528	.753	8.79	4.0	
J164-1.3	WQ28	270	9.5	20.28	.527	.764	8.64	2.5	
J164-2.4	WQ29	200	8.8	19.70	.524	.744	8.11	2.7	
J168-3.3	WQ28	220	7.2	20.78	.533	.778	9.11	5.5	
J173-3.4	WQ29	180	10.3	20.28	.522	.740	8.28	3.0	
J176-2.6	WQ30	300	7.95	21.08	.534	.752	8.95	6.5	
J180-2.3	WQ56	320	7.5	21.65	.519	.760	9.03	2.8	
J180-2.5	WQ49	320	7.5	20.93	.518	.722	8.28	2.0	
J181-2.4	WQ35	220	8.3	21.70	.555	.755	9.61	11.1	
J181-2.4	WQ49	220	8.3	20.93	.522	.754	8.70	2.3	
J181-3.3	WQ56	225	10.6	21.10	.517	.749	8.65	2.1	
J182-1.3	WQ36	365	7.78	21.60	.526	.737	8.85	3.9	
J182-2.3	WQ56	190	8.3	20.43	.499	.732	7.89	1.3	
J182-2.4	WQ31	191	8.3	18.40	.503	.728	7.13	.9	
J182-2.8	WQ31	309	8.3	19.30	.495	.724	7.32	1.7	
J183-1.2	WQ56	275	8.34	21.42	.517	.749	8.76	3.4	
J183-2.1	WQ31	256	8.3	19.23	.511	.740	7.69	1.4	
J183-2.4	WQ31	308	8.3	19.78	.523	.743	8.13	2.4	
J184-3.4	WQ49	245	7.5	21.60	.535	.723	8.85	2.8	
J185-1.2	WQ56	320	8.4	20.92	.506	.736	8.24	1.9	
J185-1.3	WQ33	320	8.4	22.60	.522	.695	8.65	4.8	
J185-2.2	WQ56	205	7.95	21.15	.524	.757	8.87	2.3	
J185-2.4	WQ33	200	8.0	22.30	.506	.712	8.50	3.3	
J187-2.3	WQ33	290	3.1	21.75	.547	.750	9.43	4.6	
J187-3 STD	WQ54	205	2.9	20.97	.553	.768	9.43	2.3	CP
J187-3 STD	WQ55	210	2.9	20.80	.550	.765	9.25	3.0	
J187-3 STD	WQ56	205	2.9	21.30	.544	.768	9.40	2.8	

CRYSTAL NUMBER	WEB QUAL	THICK MIC-M	RHO OHM-CM	ISC MA	VOC VOLT	FF	EFF %	OCD MIC-S	NOTES
J187-3STD	WQ53	190	2.9	20.90	.550	.759	9.22	2.9	
J187-3STD	WQ57	190	2.9	21.32	.546	.762	9.38	2.4	
J187-3.4	WQ33	200	2.9	22.05	.555	.750	9.70	4.8	
J189-1.5	WQ33	260	8.4	21.48	.506	.710	8.16	2.2	
J189-2.2	WQ56	255	8.1	20.40	.512	.747	8.25	1.5	
J190-1.3	WQ33	220	2.9	18.15	.486	.713	6.56	1.0	
J190-1.3	WQ44	230	2.9	21.75	.571	.780	10.24	7.3	
J191-2.3	WQ35	250	8.9	21.60	.526	.737	8.85	2.8	
J194-3.4	WQ35	192	12.4	21.97	.543	.748	9.44	10.6	
J195-2.4	WQ56	250	9.7	20.70	.515	.755	8.51	2.3	
J196-2.4	WQ56	160	10.2	21.25	.517	.749	8.70	3.0	
J196-2.6	WQ49	155	10.2	20.67	.510	.731	8.15	1.7	
J197-2.2	WQ36	235	1.43	20.75	.558	.723	8.85	2.4	
J198-2.5	WQ38	244	1.48	20.73	.556	.760	9.26	2.1	
J202-3.5	WQ37	256	8.6	21.23	.531	.769	9.18	3.1	
J203-2.5	WQ37	200	11.9	20.85	.522	.757	8.70	2.7	
J203-2.11	WQ37	206	10.9	19.83	.506	.730	7.74	2.1	
J204-1.5	WQ37	289	11.5	20.55	.517	.759	8.54	2.2	
J204-2.5	WQ37	211	12.2	20.23	.504	.717	7.73	1.2	
J205-3.3	WQ38	260	1.60	18.08	.523	.753	7.53	.8	
J208-1.4	WQ41	234	9.55	22.50	.528	.743	9.32	5.1	
J209-2.4	WQ41	205	3.09	20.10	.535	.747	8.50	.9	
J210-3.6	WQ41	120	8.28	20.85	.521	.737	8.47	.9	
J212-2.5	WQ45	135	8.47	20.18	.532	.759	8.61	2.0	
J212-3.4	WQ56	140	8.5	20.25	.509	.741	8.08	1.1	
J213-3.2	WQ55	220	3.2	20.17	.535	.761	8.68	1.9	
J213-3.2	WQ57	220	3.2	20.80	.530	.758	8.84	1.6	
J216-1.3	WQ55	233	2.9	20.33	.530	.759	8.65	2.1	
J216-2.3	WQ47	190	4.4	20.40	.525	.738	8.37	2.0	
J220-2.4	WQ49	220	3.4	20.88	.537	.759	8.99	2.8	

CRYSTAL NUMBER	WEB QUAL	THICK MIC-M	RHO OHM-CM	ISC MA	VOC VOLT	FF	EFF %	OCD MIC-S	NOTES
J220-3.4	WQ47	140	3.4	19.10	.512	.642	6.64	.8	
J223-3.3	WQ45	188	9.8	20.53	.529	.732	8.40	2.0	
J223-4.6	WQ45	119	10.54	20.60	.529	.763	8.79	2.2	
J224-1.3	WQ47	300	9.3	17.37	.456	.682	5.71	.7	
J224-2.[illegible]	WQ47	175	10.3	17.45	.450	.688	5.70	.8	
J245-1.4	WQ47	300	8.38	20.15	.515	.735	8.07	1.1	
J248-2.2	WQ50	250	11.1	20.15	.511	.739	8.05	1.4	
J248-2.2	WQ55	265	7.32	20.60	.531	.758	8.77	2.8	
J250-4.4	WQ49	205	8.9	22.18	.551	.765	9.88	10.5	
J252-2.5	WQ50	215	5.6	21.25	.555	.766	9.54	6.0	
J256-2.3	WQ50	205	16.8	21.60	.552	.745	9.39	14.5	
J256-5.3	WQ50	195	16.4	21.53	.545	.756	9.37	11.2	
J257-2.5	WQ50	205	22.6	21.65	.540	.756	9.34	10.3	
J263-4.2	WQ57	210	6.8	21.40	.529	.756	9.04	3.3	
J266-1.2	WQ57	170	5.7	22.20	.543	.771	9.82	5.7	
J267-1.2	WQ53	210	7.47	19.98	.503	.726	7.72	1.3	
J267-1.2	WQ55	255	7.5	19.62	.499	.729	7.56	1.2	
J267-2.1	WQ55	205	6.6	18.82	.487	.728	7.06	1.0	
J267-2.2	WQ53	210	6.58	19.15	.488	.715	7.06	1.0	
J268-1.1	WQ55	290	7.5	21.20	.530	.764	9.08	4.2	
J268-1.2	WQ53	330	7.48	21.18	.529	.765	9.07	3.3	
J269-1	WQ53	275	7.99	21.00	.523	.732	8.50	3.0	+DENDRITES
RE12-3.1STD	WQ25	300	16.5	21.18	.518	.732	8.49	8.0	
RE12-3.1STD	WQ26	300	16.5	22.30	.536	.753	9.53	20.6	
RE54-1.2STD	WQ25	227	23.7	21.08	.518	.719	8.30	9.0	
RE54-1.2STD	WQ27	230	23.7	21.08	.546	.723	8.80	19.0	
RE54-1.2STD	WQ28	230	23.7	21.93	.543	.741	9.33	18.4	
RE54-1.2STD	WQ29	230	23.7	21.38	.520	.727	8.55	7.4	
RE54-1.2STD	WQ30	217	23.7	21.25	.536	.727	8.75	19.6	
RE56-3STD	WQ30	210	14.9	21.27	.537	.724	8.64	11.1	

CRYSTAL NUMBER	WEB QUAL	THICK MIC-M	RHO OHM-CM	ISC MA	VOC VOLT	FF	EFF %	OCD MIC-S	NOTES
RE56-3STD	WQ31	200	14.9	21.95	.558	.753	9.74	23.7	
RE56-3STD	WQ33	220	14.9	23.80	.566	.731	10.40	28.0	
RE56-3STD	WQ34	206	14.9	22.18	.536	.758	9.54	11.9	
RE56-3STD	WQ35	202	14.8	23.08	.561	.749	10.25	32.5	
RE56-3STD	WQ36	210	14.8	23.47	.555	.726	9.99	23.8	
RE89-2.3	WQ55	135	19.7	20.95	.529	.741	8.69	4.3	
RE91-2.3	WQ39	216	7.01	22.13	.563	.760	10.02	13.0	
RE91-2.3	WQ55	200	7.0	20.95	.541	.766	9.20	5.5	
RE91-3.2	WQ55	190	7.9	20.45	.536	.764	8.87	3.9	
RE96-3.1	WQ55	180	16.8	21.12	.524	.754	8.83	6.3	
RE108-3.3	WQ39	255	9.36	20.65	.533	.745	8.66	3.4	
RE116-6.3	WQ27	190	7.5	19.25	.528	.736	7.91	1.7	
RE123-5.5	WQ29	205	9.5	20.73	.528	.732	8.47	4.1	
RE126-3.3E	WQ58	280	6.5	22.05	.539	.752	9.44	4.5	CP
RE128-1.1	WQ54	315	7.3	21.57	.534	.759	9.25	6.2	CP
RE128-1.2	WQ26	271	7.3	20.83	.533	.752	8.83	5.7	
RE129-2.3	WQ27	185	12.5	20.78	.533	.738	8.64	5.7	
RE130-1.4	WQ26	175	6.3	19.60	.522	.743	8.03	1.8	
RE130-2.3	WQ26	175	5.9	19.90	.522	.739	8.13	1.5	
RE131-2.3	WQ26	285	9.6	21.08	.527	.752	8.82	4.0	
RE131-3.4	WQ26	280	11.9	20.68	.520	.753	8.55	2.3	
RE131-4.3	WQ26	210	10.6	19.25	.500	.724	7.36	.8	
RE132-1.4	WQ26	195	10.5	20.45	.523	.739	8.35	3.9	
RE132-2.5	WQ29	220	10.6	20.48	.518	.728	8.16	1.9	
RE133-2.4	WQ25	263	8.6	20.20	.522	.728	8.12	3.2	
RE133-2.11	WQ25	223	8.6	18.30	.502	.718	6.97	.8	WIDE
RE134-1.3	WQ27	280	8.1	20.48	.535	.746	8.64	3.9	
RE134-2.4	WQ29	220	7.7	20.50	.520	.721	8.13	3.0	
RE135-2.4	WQ27	250	9.7	19.70	.527	.732	8.02	1.8	
RE136-2.4	WQ27	175	7.8	20.80	.549	.752	9.09	6.7	

CRYSTAL NUMBER	WEB QUAL	THICK MIC-M	RHO OHM-CM	ISC MA	VOC VOLT	FF	EFF %	OCD MIC-S	NOTES
RE137-2.4	WQ27	200	8.3	19.58	.513	.733	7.85	2.5	
RE137-3.1	WQ27	205	8.4	19.85	.505	.724	7.68	1.5	
RE138-1.3	WQ27	370	7.5	22.25	.537	.760	9.60	10.4	
RE141-1.4	WQ27	270	8.1	21.18	.546	.752	9.20	9.8	
RE141-4.4	WQ27	195	7.1	19.23	.516	.725	7.60	1.4	
RE143-1.5	WQ27	230	8.6	20.70	.544	.736	8.76	7.5	
RE143-1.5E	WQ27	180	8.6	20.85	.543	.750	8.98	9.9	CP
RE144-1.3	WQ27	310	8.6	20.90	.546	.761	9.19	10.3	
RE144-1.3E	WQ27	260	8.6	21.00	.542	.735	8.84	4.2	CP
RE151-6.4	WQ29	225	8.2	20.73	.536	.744	8.74	5.6	
RE155-1	WQ30	300	8.14	21.45	.531	.727	8.75	6.2	
RE155-2	WQ30	190	8.36	21.10	.540	.729	8.78	9.0	
RE156-1.5	WQ54	265	8.64	20.40	.519	.746	8.34	2.0	CP
RE157-1.3	WQ30	340	8.07	21.00	.534	.746	8.86	7.9	
RE161-1STD	WQ41	358	7.42	21.45	.543	.742	9.13	3.8	
RE161-1STD	WQ44	380	7.42	21.28	.583	.751	9.27	5.0	
RE161-1STD	WQ45		7.42	21.23	.551	.772	9.55	8.1	
RE161-1STD	WQ47	350	7.42	22.05	.550	.748	9.60	10.6	
RE161-1STD	WQ49	320	7.4	21.18	.533	.748	8.92	3.9	
RE161-1STD	WQ50	400	7.4	20.65	.539	.752	8.84	3.5	
RE161-1STD	WQ57	360	7.4	21.55	.529	.751	9.06	3.4	
RE161-1.6	WQ35	326	7.42	22.35	.558	.775	10.26	15.8	
RE175-2.5	WQ34	211	6.98	20.68	.521	.749	8.53	1.7	
RE177-2.2	WQ36	230	2.29	21.60	.518	.719	8.51	3.1	
RE183-1.4	WQ37	217	8.17	20.25	.527	.763	8.60	1.2	
RE207-2.3	WQ45	217	8.91	19.98	.531	.748	8.38	1.9	
RE213-1.5	WQ47	230	12.3	20.05	.527	.720	8.05	1.0	
RE217-1.5	WQ47	262	11.8	20.50	.520	.739	8.33	1.7	
RE242-3.4	WQ50	220	7.3	20.60	.541	.762	8.98	3.4	
RE250-1.3	WQ57	230	6.85	19.95	.514	.735	7.97	1.0	

CRYSTAL NUMBER	WEB QUAL	THICK MIC-M	RHO OHM-CM	ISC MA	VOC VOLT	FF	EFF %	OCD MIC-S	NOTES
RE251-1.1	WQ54	285	9.37	20.07	.532	.731	8.26	1.7	CP
RE253-1.3	WQ54	300	8.10	22.22	.541	.760	9.66	6.7	CP
RE253-1.4	WQ53	300	8.10	21.80	.550	.753	9.55	9.4	
RE253-2.4	WQ53	290	8.07	20.78	.525	.746	8.60	2.1	
RE258-1.4	WQ54	330	8.68	22.10	.547	.759	9.70	10.4	CP;LNG RN
RE258-2.3	WQ54	300	9.12	22.17	.537	.748	9.43	7.8	CP;LNG RN
RE258-3.2	WQ54	250	10.56	21.65	.537	.739	9.09	6.4	CP;LNG RN
RE258-4.2	WQ54	265	11.70	21.97	.540	.742	9.30	9.5	CP;LNG RN
RE258-5.3	WQ54	240	12.07	22.20	.547	.756	9.72	11.7	CP;LNG RN
RE258-6.2	WQ54	205	12.53	22.02	.525	.736	9.00	6.4	CP;LNG RN
RE266-2.8E	WQ58	280		22.33	.541	.749	9.57	6.7	CP
W128-3.3	WQ39	125	250	23.13	.551	.707	9.52	23.4	STD
W141-1STD	WQ37	201	2.55	21.58	.565	.770	9.92	4.2	
W141-1STD	WQ38	194	2.55	21.90	.567	.774	10.17	6.5	
W141-1STD	WQ44	210	2.54	21.80	.583	.775	10.41	8.7	
W141-1.2STD	WQ34	118	2.54	20.90	.560	.755	9.34	2.9	
W141-2.2STD	WQ29	140	2.6	20.88	.546	.759	9.16	3.6	
W180-1.3	WQ45	131	.25	18.15	.587	.793	8.94	1.1	BATTELLE
W180-3.7	WQ35	115	.25	18.52	.589	.777	8.97	1.3	BATTELLE
W185-1.4	WQ45	135	.0164	11.50	.594	.791	5.71	1.5	
W186-1.6	WQ45	131	5.10	20.65	.553	.767	9.26	7.8	
W187-1.3	WQ47	160	2.10	20.95	.571	.722	9.15	3.8	
W189-2.4	WQ47	110	1.74	20.10	.551	.761	8.92	1.7	
W190-1.3	WQ47	200	30.5	22.22	.520	.738	9.02	8.2	
W192-1.3	WQ49	205	6.3	21.75	.553	.762	9.69	8.5	
W193-1.3	WQ49	190	11.5	20.45	.518	.733	8.21	2.4	
W193-1.3	WQ57	190	11.5	20.70	.502	.724	7.96	1.2	
W196-1.3	WQ57			21.25	.514	.745	8.62	2.5	
W200-1.3	WQ50	210	10.7	20.23	.529	.737	8.33	3.1	
W202-2.4	WQ50	135	3.1	20.50	.541	.754	8.85	2.3	

CRYSTAL NUMBER	WEB QUAL	THICK MIC-M	RHO OHM-CM	ISC MA	VOC VOLT	FF	EFF %	OCD MIC-S	NOTES
W202-3.2	WQ50	150	3.0	20.65	.541	.758	8.96	2.3	
W205-1.1E	WQ58	210	.33	21.00	.582	.758	9.79	1.6	CP
W206-1.1E	WQ58	330	11.0	22.60	.543	.739	9.60	10.9	CP
W206-2.1	WQ58	130	8.51	22.15	.520	.738	8.99	3.2	
W206-2.1E	WQ58	100	8.51	22.10	.547	.736	9.40	5.7	CP
W207-1.2	WQ58	160	10.23	22.20	.516	.742	8.99	3.2	
W207-1.2E	WQ58	140	10.23	22.40	.540	.747	9.55	5.8	CP
W207-2.2	WQ58	130	9.69	21.65	.507	.716	8.31	1.7	
W207-2.2E	WQ58	100	9.69	22.10	.539	.749	9.43	4.9	CP
WA7-1.4	WQ38	250	9.21	20.55	.516	.744	8.34	1.4	
WA9-2.4	WQ38	138	8.37	20.35	.524	.763	8.61	1.9	
WA9-3.2	WQ38	121	8.32	21.00	.524	.730	8.48	2.0	
WA13-1.5	WQ38	145	9.94	20.93	.530	.746	8.74	2.8	
WA17-1.2	WQ45	180	6.75	19.83	.518	.719	7.80	1.6	
WA20-1.4	WQ45	149	3.42	19.80	.553	.758	8.77	1.8	
WA51-1.3	WQ49	290	7.6	22.50	.547	.759	9.88	8.6	
WA54-2.3	WQ50	255	6.5	20.80	.547	.752	9.05	6.0	
WA59-1.3	WQ57	160	5.7	21.72	.530	.763	9.30	3.5	
WA67-2.5	WQ58	190	10.8	21.85	.547	.766	9.60	5.7	CP
WA68-1.5E	WQ58	190	6.08	22.00	.547	.766	9.74	4.6	CP
WB30-1.2	WQ57	150	8.02	19.75	.503	.730	7.67	.8	

9.3 Fundamental Limitations on Dendritic Web Growth

9.3 FUNDAMENTAL LIMITATIONS ON DENDRITIC WEB GROWTH

R. G. Seidensticker
Westinghouse R&D Center
Pittsburgh, PA 15235

1. INTRODUCTION

The dendritic web process has been a viable technique for the production of single crystal silicon ribbons since the mid 1960's when it was used to provide material for solar cells in space applications. Insofar as the Westinghouse Corporation was concerned, the market for space solar cells failed to materialize, and further development of the dendritic web process was discontinued. In the mid 1970's, a growing concern over fuel supplies caused renewed interest in photovoltaic devices and work on the dendritic web process was reinstituted.

The earlier development of dendritic web growth had proceeded to the point where a pilot line operation was producing crystals 10 to 12 mm wide at a speed of about 1.5cm/min although wider and faster growth had been achieved in the laboratory. When the web program was renewed after a hiatus of seven years or so, it was recognized that the area throughput of the prior technology was insufficient to meet the economic requirements for terrestrial photovoltaic power, and the new program had the goals of increased throughput rate, continuous long term growth periods and high material quality. Table 1 summarizes the general results of these recent efforts.

Although significant progress has been made in all aspects of the dendritic web technology, ultimate limits must exist at some point for all the factors. For example, the efficiency of silicon solar cells under air mass one conditions is limited to about 23% by considerations of the solar spectrum and the band gap of the material. Similarly,

dissolution of fused quartz by liquid silicon probably limits the possible continuous crystal growth time to something of the order of several weeks. It is the purpose of the balance of this memo to try to establish some ultimate limits on possible dendritic web throughput rates.

In projecting limits for any process or equipment, several cautions should be observed. First of all, there are two distinct types of limitations: 1. limitations imposed by the sophistication of available technology-these are the "practical" limits, and 2. limitations imposed by the basic laws of nature - these are the "ultimate" limits. Both of these types of limitations can become invalid for various reasons. Practical limitations can be invalidated by advances in technology. For example, the size of integrated circuits has been steadily reduced by the development of new techniques for fabricating smaller and smaller patterns and configurations on the base chips. Similarly, "ultimate" limitations can be circumvented by employing new physical principles such as multijunction/multimaterial configurations for solar cell purposes.

In evaluating the possible limitations on dendritic web throughput, the emphasis will be placed on identifying and evaluating the basic physical factors which limit the process. Relatively little attention will be given here to "practical" limitations of an engineering nature. It is clear from Table 1 that the "practical" limits have been steadily diminished, and there is clear indication that process improvements will continue. Even in the case of the "ultimate" limits, there are some areas where new principles or techniques could circumvent what now seem to be barriers.

TABLE 1

	April 1977	April 1978	April 1979	January 1980
Maximum Demonstrated Area Growth Rate cm^2/min	2.3	8	23	27
Maximum Demonstrated Width cm	2.4	3.5	4.0	4.7
Maximum Demonstrated Solar Cell Efficiency	$\sim$13%	$\sim$14%	$\sim$15%	$>\sim$15%

2. WEB THROUGHPUT FACTORS

The throughput of a web crystal growth system can be defined in two ways: (1) the mass throughput, e.g. gm/min, which is the product of speed, width and thickness, or (2) area throughput, which is the product of only speed and width. The thickness and growth speed of the ribbon are very closely related, as will be discussed later, but these parameters are only indirectly related to the attainable width of the crystal. Since the principal use of the dendritic web crystal is assumed to be for solar cell fabrication, the crystal area is the dominant factor and the crystal need only be thick enough to survive the handling imposed by the cell processing procedure. For the purposes of the subsequent discussion, a practical limitation on thickness will be taken as 100μm (4 mils), although it would seem plausible that cell fabrication procedures could be developed to handle thinner material if the economic incentive were large enough. In fact, efficient solar cells have been fabricated on 50μm thick web. With the understanding that the useful crystal thickness will be determined for the most part by factors other than the growth process, area throughput will be the parameter which we will discuss.

From consideration of the physical processes involved, the growth speed of the crystal and the width of the crystal are completely unrelated. The growth speed (at a given thickness) is determined by the dissipation of latent heat, which in turn is related to the vertical temperature gradient along the length of the crystal and the vertical temperature gradient in the liquid adjacent to the interface. The width of the crystal, for the most part, is determined by lateral temperature gradients in the liquid and some lateral heat loss processes from the bounding dendrites close to the liquid surface. From a practical viewpoint, thermal stresses generated by the vertical temprature profile are an important width limiting factor, but these stresses are subject to manipulation and thus do not represent "ultimate limitations" in the context of this discussion. We shall therefore consider the pull speed and width to be independent parameters.

3. GROWTH SPEED

In any freezing process, the rate of transformation of liquid to solid is controlled by two factors: 1. the mechanism by which molecules (or atoms) from the liquid phase are attached to solid phase - the so called attachment kinetics, and 2. the rate of dissipation of latent heat. In the solidification of silicon, the kinetic factor is negligible if the growth front is not a crystallographic (111) plane. Thus in dendritic web growth kinetic effects do not seem to influence the growth speed, although they are the dominant factor in determining the crystal morphology and probably are important in maintaining the stability of the growth. The thermal effects, on the other hand, are the dominant factors in controlling the speed of growth and the thickness of the ribbon.

The velocity and thickness of a ribbon crystal must be closely related parameters from the physics of the situation. At a given pull speed, the latent heat evolved at the growth front is directly proportional to the thickness of the crystal, as is the thermal conductance of the ribbon. However, the crystal surface area available for dissipation of heat to the ambient is independent of thickness. Thus in order to balance the heat generation with the heat loss, a relationship must exist between the growth velocity and the crystal thickness.

The basic choice in analyzing the heat loss problem lies in what boundary conditions and heat loss mechanisms to include with the governing differential equation, Eq. 1, which is the heat flow equation for a moving reference frame, i.e. a reference frame fixed with respect to the growth front.

$$\nabla\cdot(k\nabla T) - \frac{V}{\rho C}\cdot\nabla T = \dot{Q} \qquad (1)$$

where T is the temperature, k is the thermal conductivity, V is the growth velocity, ρ is the density of the material, C the specific heat and $\dot{Q}$ (T) is the heat loss, (a function of temperature) from the ribbon surface. The case of a wide, thin ribbon simplifies into a one

dimensional problem that has been solved analytically by several workers for a variety of simplified boundary conditions.

All of the analytical solutions included the fact that the thermal conductivity of silicon is a function of temperature having the form of $k = a/T$. The solution of Ciszek[1] used the assumptions that there was no heat flow from the melt at the interface and that heat loss from the crystal was only by radiation to a 0°K environment. The result was expressed as

$$V = \frac{1}{\rho L} \left[\frac{\epsilon\sigma\, T_m^5 k_m}{t}\right]^{\frac{1}{2}} \qquad (2)$$

where T_m is the melting temperature, k_m is the thermal conductivity at T_m, ϵ is the emissivity, σ is the Stefan-Boltzmann constant, ρ is the density L the latent heat and t is the crystal thickness. A similar treatment was done by Swartz, Surek and Chalmers[2] with the assumption that heat loss was not to 0°K but rather to some effective ambient T_o. The resulting expression for V included the effect of heat flow from the melt, but if that term is neglected, their result has the form

$$V = \frac{1}{\rho L} \left[\frac{\epsilon\, \sigma\, T_m^5 k_m}{t}\right]^{\frac{1}{2}} \left[1 - \left(\frac{T_o}{T_m}\right)^4 (1 + 4\ln \frac{T_m}{T_o})\right]^{\frac{1}{2}} \qquad (3)$$

which is essentially the same result as Eq. 2 with a correction for the effective ambient temperature.

Seidensticker[3] arrived at essentially the same result as Eq. 3, however the effective heat transfer was modified by the fact that part of the web was immersed in the growth cavity formed by the slotted susceptor lid. The effect of this immersion was to reduce the growth velocity since the effective temperature is very high in the vicinity of the growth front which reduces the possible heat loss there.

In all cases, the growth velocity is deduced from the temperature gradient at the growth front by means of the heat balance equation

$$LV = k \frac{dT}{dz}\bigg|_o - \dot{Q}_\ell \qquad (4)$$

where L is the latent heat of fusion, $dT/dz\big|_o$ is the temperature gradient at the growth front and $\dot{Q}_\ell$ is the heat flow to or from the melt at the interface. If the liquid temperature near the growth front is higher than the melting temperature, then the heat flow adds to the latent heat and the growth velocity is reduced. If liquid is <u>colder</u> as in the growth of dendritic web, then latent heat can be dissipated to the liquid and the growth velocity is enhanced. In both Eqs. 2 and 3, only the dT/dz term of Eq. 4 is considered.

Both Eqs. 2 and 3 can be evaluated to determine the velocity of a "freely" radiating ribbon when the heat flow to or from the melt is zero. For numerical evaluation, T_m = 1685°K, k_m = .189 W/cm-K, L = 1804 J/gm, ρ = 2.329 gm/cm^3, ε = 0.6 and $\sigma = 5.67 \times 10^{-12}$ W/cm^{2}K^4. In Eq. 3, T_o = 400 K. For web 0.01 cm (4 mil) thick,

Eq. 2 V = .223 cm/sec
= 13.35 cm/min

Eq. 3 V = .221 cm/sec
= 13.22 cm/min

If T_o = 700K, then Eq. 3 gives V = .207 cm/sec
= 12.44 cm/min

Thus the idealized case of a freely radiating web crystal gives a growth velocity of about 13 cm/min for a 100 μm thick ribbon, when all the latent heat is dissipated through the crystal. If, in addition, some latent heat is dissipated to the supercooled melt, then another 1 to 2 cm/min is added to the velocity so that the actual web pull velocity would be about 14 to 16 cm/min.

In practice, the web crystal will not freely radiate to the environment, but will interact with hot furnace components. The situation is shown in Figure 1 which illustrates schematically the thermal interactions of elements of the web and of the meniscus. These thermal interactions are too complicated to handle with analytical approximations. However, they can be easily managed with numerical integration techniques; the details are discussed in Appendix 6.5 of Reference 4. Briefly, the geometry shown in Figure 2 is used to represent the growth system and the radiative view factors are evaluated as a function of a position along the ribbon (or along the liquid surface for the meniscus calculation). Equation 1 can then be integrated numerically to solve for the temperature gradient at the growth front and hence the growth velocity.

Evaluation of the model for the case of a thin (1 mm), cold (700°K) lid with a narrow (3 mm) slot and the web growth front level with the bottom of the lid gives a velocity of 7.88 cm/min for the velocity due to heat flow in a 100μm thick web. Again, several cm/min would be added to this value by the latent heat which would be dissipated to the supercooled melt.

It is instructive to inquire why the model gave a result of about 7.9 cm/min when the analytical results of Eqs. 2 and 3 gave results of about 13 cm/min. The analytical results are essentially the "ultimate" limits while the model result is more of a practical limit. The feature of the model geometry which causes the decrease in speed turns out to be radiation from the hot cavity above the melt through the slot onto the web. If the slot width is reduced so that it closely matches the width of the growing ribbon (200μm slot and 100μm web) then the numerical results of the model are in excellent agreement with the analytical results.

The degree to which the ultimate growth speed can be approached by a practical geometry is very hard to predict. As will be discussed in the next section, the temperature distribution in the crystal indirectly interacts with the obtainable width through thermal stress generation. Further, there are other practical effects in the growth

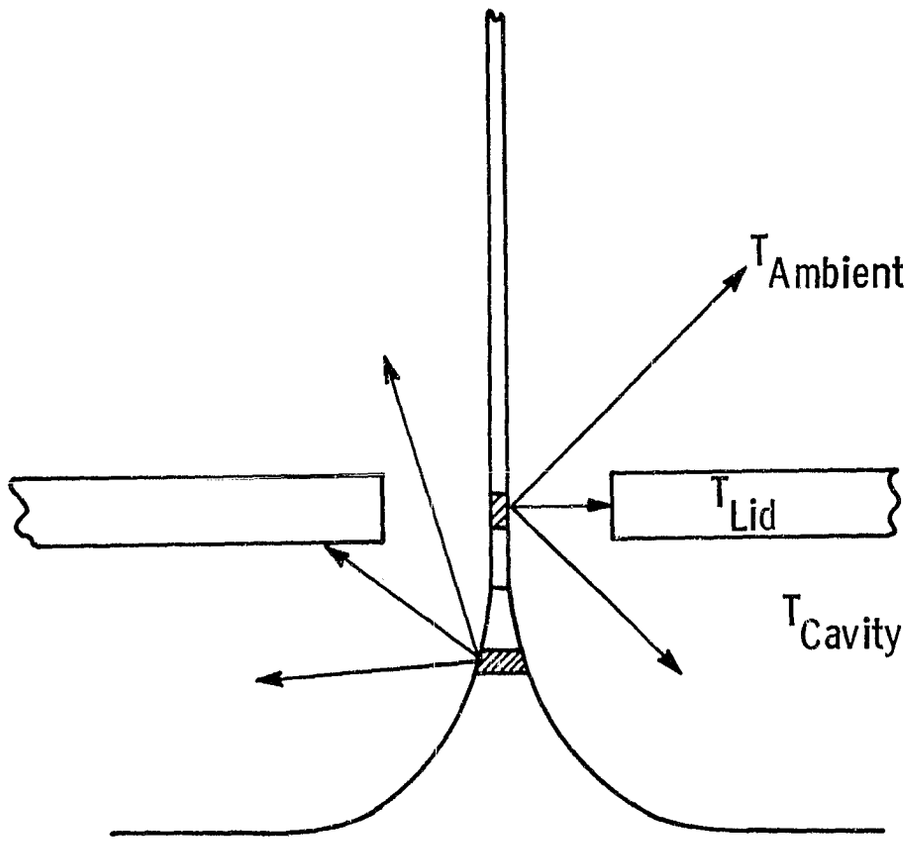

Figure 1 Heat loss factors for thickness velocity mc lel

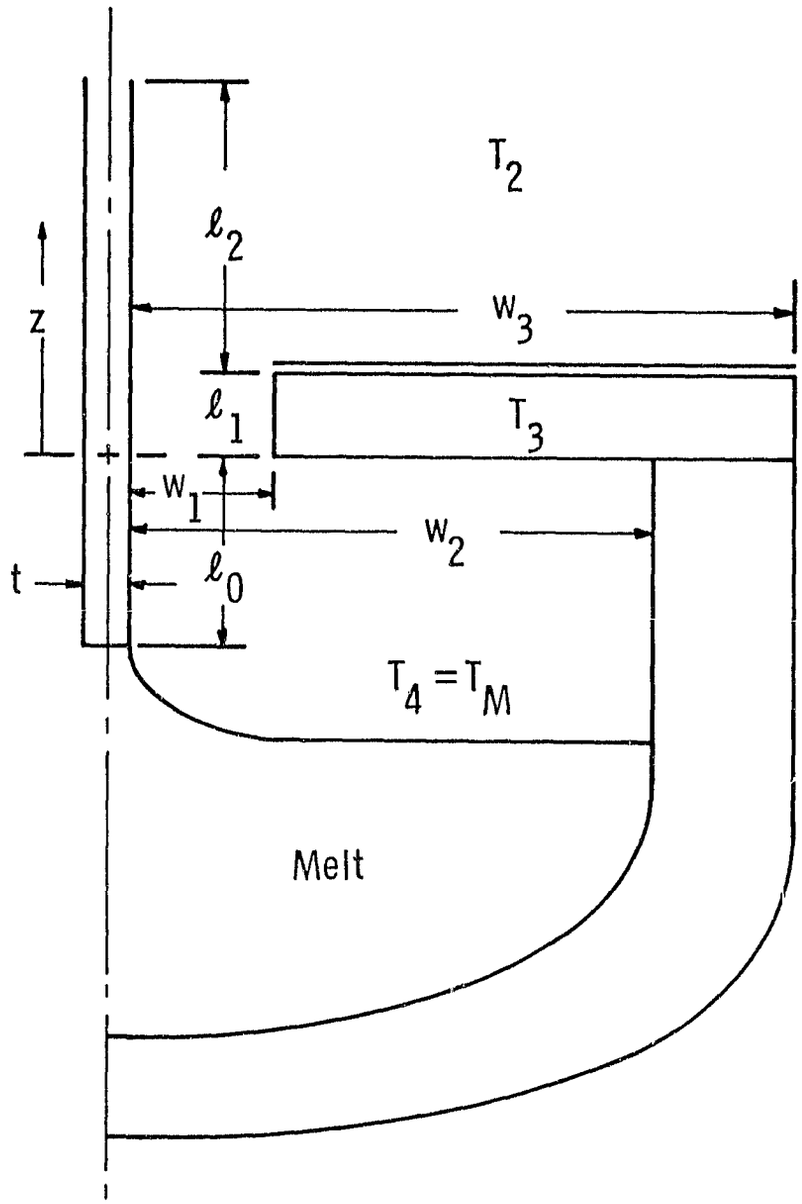

Figure 2 Crucible and web geometry for thermal analysis

process such as the management of the silicon oxide which is evolved by the melt/crucible interaction. Nonetheless, the factors affecting growth speed are identified and continued engineering will narrow the gap between the practical and the ultimate limits.

Summary.

The speed at which a ribbon crystal, including dendritic web, can be grown is determined by the thickness required of the material and by the ability to dissipate the latent heat of fusion. If radiation is the only mechanism considered for removing the latent heat, then a 100μm thick crystal has an ultimate growth speed of about 13 cm/min when all the latent heat must be lost from the crystal itself. In dendritic web growth, some of the latent heat can be removed to the melt as well as to the crystal, and the ultimate velocity for growth should be of the order of 15 cm/min or greater. If additional heat removal mechanisms are introduced such as cold gas jets, then the ultimate velocity is increased even further. Practical limits on the velocity, such as interaction of the crystal with heated regions of the growth system, serve to reduce the velocity.

4. WIDTH

Evaluating the ultimate limit of dendritic web width is a more difficult problem than evaluating the limitations on speed. Not only are the apparent limitations of an indirect nature, but the theory involved is complex and the evaluation of limiting criteria is more difficult.

In order to appreciate the problem, consider the mechanism of widening in dendritic web growth. Figure 3 suggests the way in which the temperature distribution across the melt interacts with the web width. The ribbon part of the crystal grows from a meniscus 6 or 7 mm above the melt surface; however the high liquid curvature required at the edges of the bounding dendrites limits the meniscus height there to only 1 or 2 mm. Crystallographic and heat flow factors cause the growth direction of the dendrites to be very nearly a [211] direction. Lateral heat loss

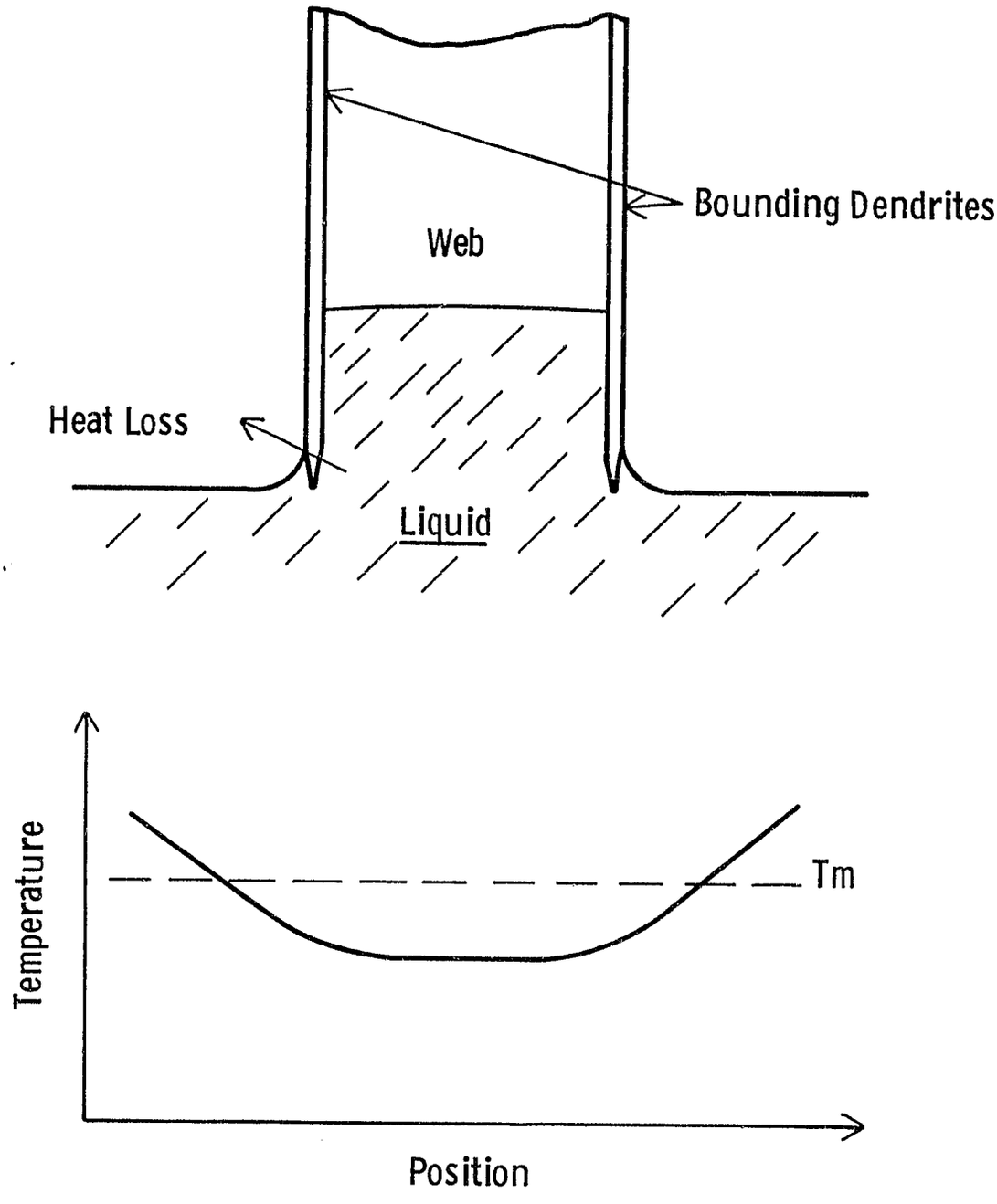

Figure 3 Illustration of the way the lateral temperature distribution in melt and lateral heat loss from the ribbon influence the dendritic web widening process.

from the meniscus, however, perturbs the thermal field near the tip of the dendrite so that there is slightly more growth on the outer edge than on the inner edge. This causes a small deviation of the growth direction from [211] and the crystal widens so long as there is a uniform temperature profile in the melt. When the widening web reaches a region of increasing melt temperature, as shown in the figure, the intrinsic lateral temperature gradient in the liquid counteracts the temperature gradient created by the meniscus heat loss. The web then ceases to widen and continues to grow at a steady state width. Thus, as far as basic growth mechanisms are concerned, a web crystal can grow as wide as it is possible to generate a constant lateral temperature profile in the melt.

From an operational standpoint, the real limitation on the width of dendritic web material arises from deformation of the material during growth. In a usual growth sequence, the crystal is started at a width narrower than its ultimate size. The growing ribbon then widens by the mechanism just discussed until a constant, steady-state width is reached, or until the crystal begins to twist or curl. The primary cause of the deformation observed lies in thermal stresses arising from the temperature profile in the ribbon.

The origin of thermal stress in dendritic web growth has been discussed by Seidensticker and Hopkins[5] and has also been addressed by workers with other techniques for growing silicon ribbons. The analysis of Gurtler[7] is perhaps the most extensive of any, although it is addressed in detail to the "ribbon-to-ribbon" process. Nevertheless, many of his conclusions are more general, and in particular he finds that stresses can be reduced by proper manipulation of the thermal profile. This conclusion is confirmed by developments in dendritic web growth where low residual stress is maintained until elastic buckling occurs. Further, the threshold width for elastic buckling is being continually increased by system thermal design.

Thus thermal stress-induced deformation provides a practical limit to width in the dendritic web process. Characteristic of development studies the practical limit has continually increased as thermal stress was controlled. However, there remains one source of buckling which will provide an "ultimate" limit to ribbon width: surface tension forces acting on the bounding dendrites. As shown in Figure 3, a liquid film (meniscus) is present between the bounding dendrites, and the surface tension of this film acts to pull the dendrites together. This tendency to collapse is balanced by the stiffness of the web and at some combination of width and thickness, the surface tension forces will suffice to cause the web to buckle. This effect provides some measure of an "ultimate" limit on the width attainable in a web crystal of given thickness.

The critical feature of the surface tension limitation is that the force exerted by the surface tension is independent of the separation of the dendrites. In practice, the height of the film is about 0.5cm so that the force $F = 2h\gamma = 720$ dynes. Although this is a small force, it is not negligible and should cause the web to buckle if it is wide and thin enough.

An exact stability analysis for this configuration is extremely complex, if it exists, but some conservative approximations can be made to analyze the situation. The problem was modeled as a thin plate, laterally loaded, with the compressive stress linearly decreasing along the length of the ribbon. Following the treatment of Timoshenko and Gere[8], the critical stress relationship finally yielded a simple relation between the thickness (t) and the width (w) for which buckling would occur, namely:

$$t^3 = 1.8 \times 10^{-11} w^2. \qquad (5)$$

For 100μm thick material, this relation predicts stability (no buckling) for material less than 235 cm wide! For 10μm thick material, however, 7.5 cm represents the limiting width. It would appear that this ultimate limit on width far exceeds the practical limitations imposed by thermal stress.

Summary.

In practice the width of a growing dendritic web is determined by the lateral temperature distribution on the melt surface; the web widens until a balance occurs between temperature gradients produced by heat loss at the dendrite edges and intrinsic temperature gradients in the melt. This situation leads to steady state growth if the web can grow wide enough; however, frequently a second factor occurs: deformation induced by thermal stresses. The thermal stress generation has frequently proved to be the practical limitation to web width. If these practical limitations were removed, an "ultimate" limit has been found in the surface tension forces on the bounding dendrites. An approximate analysis of the ribbon buckling shows that the surface tension effects would not be important for 100μm thick web until the crystal was over two meters wide, so that in fact the thermal stress currently is the effective limiting factor. Increasingly better thermal designs have reduced these stresses and wider web has been grown, so that it is very difficult to predict any real limitation on dendritic web width.

SUMMARY AND CONCLUSIONS

Analysis of the factors controlling dendritic web growth shows that clear limitations on growth speed and ribbon thickness, can be defined but that the limitations on crystal width are much less easily delineated. There is a well-defined relationship between the web growth velocity and its thickness. Changes in the heat loss from the web brought about by the design of the growth geometry alter the thickness-velocity relationship in a well defined manner, and an "ultimate" growth velocity can be specified. For the case of radiative transfer to a 300°K ambient. The heat loss from the web itself accounts for a growth speed of about 13 cm/min (100 μm thick ribbon) while the latent heat lost to the supercooled meniscus adds another 2 or 3 cm/min so that the actual growth speed would be about 15 cm/min. In a real growth system, thermal interaction with hot furnace elements (melt, susceptor, lids) reduces the heat losses and hence the growth speed. In a practical, although still somewhat idealized geometry, we anticipate a growth speed of about 9 to 10 cm/min for the 100 μm thick web.

Because there do not appear to be any inherent restrictions on the widening process itself the limitations on dendritic web width are more difficult to define than are the limitations on speed. The effective width limitations arise from stresses in the crystal which cause it to deform during growth. The closest approximation to an "ultimate" limit is the stress generated by surface tension forces on the bounding dendrites due to the liquid film in the meniscus region. An estimate of these forces gives a limiting width of over two meters for 100 μm web - far in excess of practical width limitations imposed by thermal stresses.

Although the factors governing web speed and width are mainly indepdendent, thermal stresses originate from the same vertical temperature gradients which serve to transport the latent heat of fusion in the ribbon. Therefore from a practical viewpoint the speed and width are interrelated, and the practical limitation on throughput is determined by how well an optimum temperature profile can be engineered. As we noted in the introduction, throughput rates, as well as width and speed,

individually have steadily increased during our program and there is every indication progress will continue.

As of the present time, dendritic web crystals have been grown at a width of almost 5 cm and growth rates over 6 cm/min have been demonstrated. These values represent the current state of the art but are significantly less than any "ultimate" limits calculated above. Although significant engineering effort will be required to push closer and closer to the ultimate limitations of the process, we believe that 5 to 6 cm wide web grown at speeds of 6 to 7 cm/min for a total throughput rate of about 35 cm^2/min. is a reasonable technical objective.

Achievement of a 35 cm^2/min web output rate would also have important economic consequences for the long term reduction in solar cell costs. The implications can be put in perspective as follows. The 1990 DOE cost goal, $0.30 per peak watt (1975$) output power represents about a 40% reduction over the 1986 cost objective of $0.50 per watt. The corresponding reduction in the combined polysilicon plus wafer cost would produce a 1990 target of $0.096 per watt versus about $0.16 per watt for 1986. A SAMICS-IPEG analysis indicates that at a 35 cm^2/min web output rate the wafer plus polysilicon cost would reach the 1990 projected target of $0.096 per watt. If the cost of silicon falls below $10/kg a further cost reduction would ensue. Thus for both economic and technical reasons a target of 35 cm^2/min output rate appears reasonable for future web development activity.

At the current stage of development of dendritic web growth, there is no indication that we have reached the "ultimate" capability of throughput for the process. There are several directions which could diminish or eliminate present practical limitations on the process. These directions involve both extension of the analysis of the process and experimental/engineering implementation of the directions indicated by the analysis. These are:

1. Develop a criterion for the elastic stresses required to cause buckling and deformation of the web. How are width and thickness related to the critical stress distribution?

2. Identify idealized thermal profiles required for both high speed growth and low buckling (elastic) stress.

3. Test the buckling criterion against observed web deformation behaviour.

4. Develop practical system geometries which will generate the desired temperature profiles. Although these designs may involve strictly passive elements (shields and lid) they may require active heating/cooling elements such as gas jets, etc.

REFERENCES

1. T. F. Ciszek, "Maximum Growth Rates for Melt-Grown, Ribbon-Shaped Crystals", J. Appl. Phys. 47, 440 (1976).

2. J. C. Swartz, T. Surek and B. Chalmers, "The E.F.G. Process Applied to the Growth of Silicon Ribbons", J. Electronic Mat. 4, 255 (1975).

3. R. G. Seidensticker, "Thermal Aspects of Dendritic Web Growth", Appendix 6.3 in "Silicon Web Process Development-First Quarterly Report, 20 April (1977-30June 1977" C. S. Duncan et al. Contract NAS 954654 (Westinghouse Report 77-9C4-RIBON-R1).

4. R. E. Kothmann, "Heat Loss from a Silicon Web", Appendix 6.5 in "Silicon Web Process Development-Annual Report, April 20, 1977 April 19, 1978" C. S. Duncan et al., Contract NAS 954654 Westinghouse Report 78-9F4-RIBON-R1.

5. R. G. Seidensticker and R. H. Hopkins, "Silicon Ribbon Growth by the Dendritic Web Process", J. Crystal Growth. To be published.

6. B. H. Mackintosh et. al., "Multiple Silicon Ribbon Growth by EFG", in Conference Record: "13th IEEE Photovoltaic Specialists Conference" IEEE, New York (1978) p. 350.

7. R. W. Gurtler, "Nature of Thermal Stresses and Potential for Reduced Thermal Buckling of Thin Silicon Ribbon Grown at High Speed" J. Crystal Growth. To be published.

8. Timoshenko and Gere, "Theory of Elastic Stability" McGraw Hill, N.Y. (1961), p. 377.

9.4 Publication

DEVELOPMENT OF PROCESSES FOR THE PRODUCTION OF LOW COST SILICON DENDRITIC WEB FOR SOLAR CELLS

C. S. Duncan, R. G. Seidensticker, J. P. McHugh, R. H. Hopkins,

M. E. Skutch, J. M. Driggers and F. E. Hill

Westinghouse R&D Center

Pittsburgh, PA 15235

ABSTRACT

High area output rates and continuous, automated growth are two key technical requirements for the growth of low cost silicon ribbons for solar cells. We have achieved, by means of computer aided furnace design, silicon dendritic web output rates as high as 27 cm^2/min, a value in excess of that projected to meet a $0.50 per peak watt solar array manufacturing cost. We have also demonstrated the feasibility of simultaneous web growth while the melt is replenished with pelletized silicon. This step is an important precursor to the development of an automated growth system. Solar cells made on the replenished material were just as efficient as devices fabricated on typical webs grown without replenishment. Moreover, web cells made on a less-refined, pelletized polycrystalline silicon synthesized by the Battelle process yielded efficiencies up to 13% (AM1).

INTRODUCTION

Dendritic web is a ribbon form of thin (100 to 200 μm) single crystal silicon shaped during growth by crystallographic forces and surface tension, rather than by dies. These characteristics, coupled with the highest demonstrated ribbon solar cell efficiency-15.5%-make silicon web a promising candidate to achieve, or better, the Department of Energy cost objective of 50 cents per peak watt of photovoltaic power. The subject of this paper is the recent demonstration of two key technological steps toward low cost silicon web production: high output rate web growth and the simultaneous growth of silicon web with melt replenishment.

WEB OUTPUT RATE

Web area output (the product of web width and growth velocity) is a key parameter, since as output rate increases, wafer costs diminish. We now have achieved area output rates of 27 cm^2/min, more than triple the 8 cm^2/min maximum rate of a year ago. The accomplishment is the outcome of computer-aided thermal design by which both web width and web speed have been increased. For example, control of the vertical thermal gradient in the web (by means of growth slot and heat shield geometry) reduced stress-induced deformation so that crystals more than 4.5 cm wide have been grown. The growth slot geometry used to accomplish this result is illustrated in Figure 1. Moreover, these wide webs are free of the rippled texture characteristic of the widest crystals grown in the past.

The economic consequences of the recent output rate improvements are put in perspective in Figure 2 where the maximum rate so far achieved is superimposed on a cost projection made using the SAMICS-IPEG methodology.[1] Implicit in the cost calculation are assumptions of a 15% AM1 cell efficiency and a 150 μm web thickness-both of which already have been demonstrated, $10/kg silicon expected within the next few years[2], and a three day continuous growth cycle. (For these conditions web wafer costs equal to the national goal of 16 cents per watt can be achieved at web area output rates about 18 cm^2/min.) At the 27 cm^2/min demonstrated output rate, the projected silicon web wafer plus polysilicon cost is about 12 cents per watt, or more than 4 cents per watt below the 1986 national cost goal of 16 cents per watt in 1975 dollars. Even if the future cost of polysilicon falls only to $25/kg the projected web wafer plus polysilicon cost is 16 cents per watt, which meets the objective.

MELT REPLENISHMENT

To reach the projected 1986 web cost requires not only a demonstration of high output rate operation but that these rates be sustainable for long periods. Beyond this, long term system thermal stability is also necessary to assure optimal growth conditions. Since silicon is continuously removed from the melt as web crystal is grown, the melt height, or more specifically the position of the growth front relative to the lid, will change with time, a feature which would adversely affect web width and velocity (see next section). Thus melt replenishment is necessary for both technical and economic reasons.

Impact of Melt Level on Velocity and Thickness

Changes in melt level affect web output rate most directly through changes in the growth speed necessary to maintain a constant ribbon thickness. If a constant pull velocity is maintained, then the web will steadily decrease in thickness, as shown in Figure 3, unless the melt is maintained at a constant height (replenished). At the start of a run, the growth front of the web is nearly level with the bottom of the crucible lid; small changes in position then have a significant effect on the heat lose from both the crystal and the melt. This is particularly noticable for thicker ribbons, as in Figure 3.

Several papers have treated the relation between the thickness and the growth velocity of growing ribbon crystals,[3,4] and although the results differ in detail, they generally have the form

$$v = C/\sqrt{t} \qquad (1)$$

where C is a constant related to the details of heat loss from the ribbon and t is the ribbon thickness. In the case of dendritic web growth, the latent heat of fusion is dissipated both by the crystal and by the supercooled melt, and a good approximation to both the experimental data and a detailed computer model[5,6] is given by

$$v = a + \frac{b}{t} \qquad (2)$$

where a and b are constants which depend on the detailed system geometry, and hence both change with changes in the interface location. If the latent heat dissipated by the web and by the melt is considered, then a "partial velocity" can be associated with each components. These "partial velocities" both have the dependence given by Eq. 2, and hence the individual a and b coefficients are additive as shown in Figure 4. When the position dependence is examined, however, it is found that the coefficients related to the heat loss through the crystal show the largest changes. Further, by taking the partial derivatives of Eq. 2 with respect to a and b, it is found that both $\partial t/\partial a$ and $\partial t/\partial b$ depend directly on t, so that thicker web shows larger changes with melt height consistent with Figure 3.

It might be thought that the optimum interface position would give the maximum velocity for a given thickness; however, other growth effects also depend on interface position. One of the most important is the thermal stress in the growing crystal, a topic discussed in the following section.

Impact of Melt Level on Web Width

The ribbon width depends on melt height in two ways: through changes in the melt temperature profile and through the generation of width-restricting thermal stresses in the growing crystal as the liquid level varies. The former is a relatively small effect; in practice the effect of melt height on thermal stress is a much more important consideration.

Although the melt itself is relatively far below the lid, Figure 1, the high meniscus typical of liquid silicon brings the web growth front very close to the bottom of the lid. Under these conditions, a liquid level shift of a few millimeters creates a large variation in radiative heat loss and hence in the shape of the temperature profile along the web. Changes in the slope of the temperature curve at the growth front change the velocity-thickness relation discussed in the last section, but in addition there are large changes in the second and higher derivitatives which are responsible for thermal stresses in the ribbon.[6,7,8] Particularly important is the lateral stress developed in the ribbon close to the growth front where the material is hot and the yield point is relatively small. When the thermal stress exceeds the critical yield stress, plastic deformation occurs and the resulting crystal contains residual stress. Since the magnitude of the thermal stress depends on the width of the crystal as well as on the temperature profile, excessive stress generated by melt height changes can limit web widening.

Stress fields in web crystals have been estimated from the calculated temperature profiles for various lid configurations. The lateral stress component σ_{yy} for one geometry is shown in Figure 5. The LIN parameter labeling the different curves is the distance of the growth front below the lid; the accented portions of the curves for LIN= 0 and 4 mm represent regions where the yield point is exceeded and hence plastic deformation would occur. For the intermediate cases, no plastic flow would be expected. In agreement with the model, crystals grown at melt heights for which no plastic flow is expected show very small measured residual stress. Crystals grown after the melt has been greatly depleted (large LIN) exhibit larger (and sometimes negative) stresses as predicted. Thus a range of optimal melt heights exist for a specific growth geometry and melt replenishment is necessary to maintain the level within this range.

Web Melt Replenishment System

We have recently demonstrated the feasibility of simultaneous web growth with replenishment. The approach, which is conceptually and experimentally simple, is illustrated schematically in Figure 6. The feedstock, pelletized silicon, is injected into the melt from a programmable, mechanically-actuated pellet feeder while concurrently pulling a web crystal. The system employs a unique two compartment crucible design in which the melting pellets are separated from the growing web by a quartz barrier. A hole in the barrier located below the melt surface permits equilibration of the melt level in the two compartments as the pellets melt. The pellet feed rate may be programmed so that silicon is replenished at a rate sufficient to replace the melt that is being transformed to crystal.

Some minor adjustments are made to the work coil position and susceptor shielding to compensate for the asymmetric heat load imposed by the feed material. Otherwise, the system is identical to the one used for non-replenished growth. Replenished growth runs of up to five hours have been made with this arrangement. (Growth was terminated by events unrelated to feeding). An optical sensing system using a reflected laser beam will be used for melt height sensing and control of the replenishment rate.

A second key result of these experiments was the demonstration that solar cells fabricated on the replenished material were just as efficient as cells fabricated on typical webs grown without melt replenishment.

SILICON FEEDSTOCK CONSIDERATIONS FOR WEB GROWTH

Projected low-cost grades of silicon may contain levels of contamination significantly greater than in conventional semiconductor grade material.[8,11] With melt replenishment these contaminants could build up during growth to excessive levels,[10] thus we performed some initial tests to ascertain the acceptability of less pure feedstocks for web growth.

Purity Requirements for Web Growth

The dendritic web growth process is very efficient at rejecting impurities; the segregation coefficients for most metals are very small and close to the equilibrium values.[9] Thus most of the impurities present in the feed stock accumulate in the melt. The build up of impurities during the course of a run can affect the output in two ways:[10] (1) the crystal quality can be degraded by structural breakdown, and (2) the suitability of the crystal for device purposes can be compromised by excessive concentrations of undesirable impurities.

We determined the approximate tolerable melt impurity concentrations by observing the growth of webs intentionally doped with large amounts of readily segregated solutes such as nickel, molybdenum, titanium and vanadium.[10] When the solute concentration exceeds about 20 ppma the growth habit of the ribbon deteriorates. The web itself becomes polycrystalline with a uniquely characteristic morphology and extra dendrites occur at random across the growth front. It thus seems that within about a factor of two either way, an upper limit of 20 ppma represents a limiting impurity concentration in the melt for typical metal solutes. If continuous replenishment is done during the course of a run so that the melt is replaced about fifteen times, then the acceptable impurity content of the feed stock is only about 1 to 2 ppma.

The maximum impurity content based on cell performance can be calculated from the impurity-cell performance relationships for silicon. However the process requires knowledge of the electrical effect of the specific impurity as well as an "acceptable" level of device degregation. The topic has been treated in detail elsewhere[10], but for a number of impurities the result is that about 500 ppma represents an upper limit for the total concentration of impurities in the melt assuming that a ten percent degradation in device performance is acceptable. This result leads to an upper limit of about 30 ppma for the total impurity content of the feed stock used for melt replenishment. (Certain impurities, such as titanium and vanadium, are much more deleterious to device performance, and for these impurities, the acceptable concentration is about two orders of magnitude smaller.)

Thus for web, structural breakdown generally sets upper limit on feedstock impurity content. For a three day growth cycle (a conservative estimate from our economic analysis) the total melt impurity content should be less than about 1 ppm. Note that impurity levels of ~ ppb are common in semi-conductor silicon, so the projected requirements for web growth represent a considerable relaxation of present standards.

Device Performance of Melt Replenished Web

Solar cells were made on silicon web crystals grown with replenishment and by more common unreplenished techniques. An $n^+ p p^+$ cell structure was utilized[5] and tests were made at 91.6mW/cm^2 (AM1). Table 1 gives data for solar cells fabricated from a number of web crystals in a single run. Each of the entries in the table is an average of a number of cells; the efficiencies of the cells from the "Feed Runs" where melt replenishment was used were essentially the same as those for cells made on webs grown without replenishment.

Web Growth from Battelle "Low Cost" Silicon

A sample of potentially low cost Battelle pelletized silicon supplied by the Jet Propulsion Laboratory was also evaluated for use in the web growth process. Prior to crystal growth the pellets were heat treated six hours in argon at 1290°C to evaporate any Zn remaining in the material. (It was originally synthesized by Zn reduction of $SiCl_4$.) The material was used without difficulty to grow silicon web. Diagnostic solar cells[5] made on the web exhibited an average AM1 uncoated efficiency of 9.0±0.2% (12.8% est. with AR coatings) with a range from 8.6 to 9.2% (12.3 to 13.2% est. with coatings).

CONCLUSIONS

Our results indicate that most of the major technical requirements to produce silicon web for low cost solar cells-output rate, cell efficiency, ribbon thickness, and tolerance to the type of contaminants likely in solar grades of silicon now have been demonstrated. Implementation of a completely automated growth system for the production of silicon web for low cost solar cells now appears feasible, and the engineering development to achieve this objective is underway.

ACKNOWLEDGEMENT

This paper presents the results of research performed for the Low Cost Solar Array Project, Jet Propulsion Laboratory sponsored under an interagency agreement between the Department of Energy and the National Aeronautics and Space Agency. We would like to thank P. A. Piotrowski, H. C. Foust, E. P. A. Metz, W. B. Stickel, J. M. Polito, A. M. Stewart, J. P. Fello, and C. H. Lynn for their contributions to the web growth studies and P. Rai-Choudhury, R. B. Campbell, E. J. Seman, J. B. McNally, W. Cifone, D. N. Schmidt, and H. F. Abt for the processing and testing of the web solar cells.

TABLE 1

Solar Cell I-V Parameters for Devices made on Silicon Web Crystals Grown with(*) and without Melt Replenishment

CRYSTAL	I_{SC} mA	V_{OC} VOLT	FF	η_o %	η_{AR} %
RE12-3.2	22.18	.548	.737	9.47	13.5
RE102-2.2	20.18	.520	.734	8.15	11.7
J131-2.2	20.98	.537	.746	8.88	12.7
J131-3.4	19.40	.513	.733	7.73	11.1
J134-2.2	21.70	.536	749	9.21	13.2
W141-1.2	21.90	.569	.738	9.73	13.9
*W151-1.2	22.18	.543	.738	9.35	13.4
*W154-1.4	21.58	.542	.722	8.92	12.8
*W154-2.3	21.35	.531	.734	8.79	12.6

NOTE: All devices fabricated concurrently
Cell area 1.039 cm^2
AM1 at 91.6 mW/cm^2
η_{AR} is efficiency with TiO_2-SiO_2 AR coating

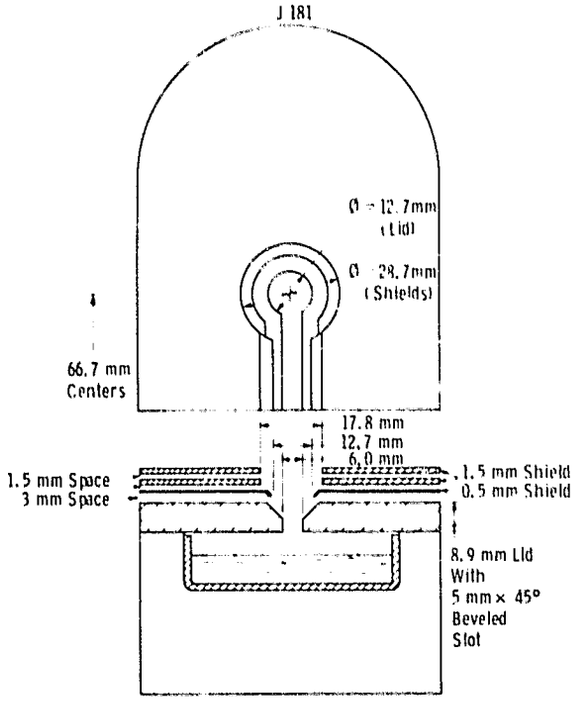

Figure 1 Schematic diagram of susceptor assembly used to grow wide, low stress material.

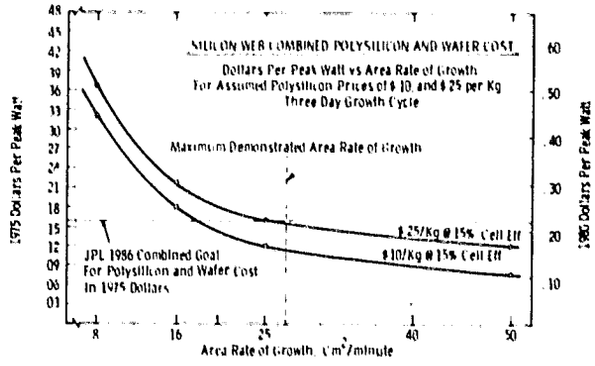

Figure 2 Projected silicon web plus polysilicon cost as a function of area throughput.

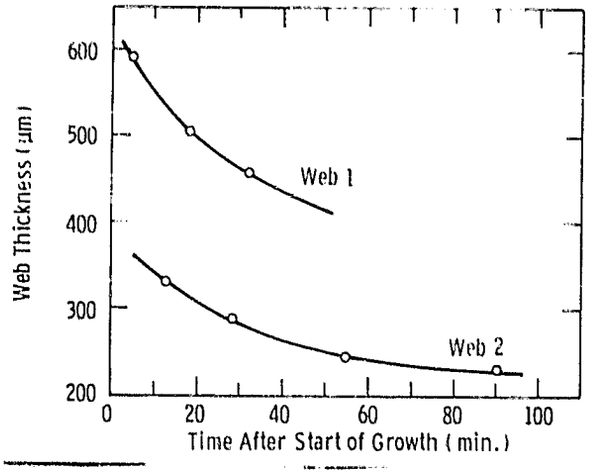

Figure 3 Variation of web thickness with growth time for crystals from two different runs. As the melt is depleted by crystal growth, the crystal thins at a constant growth speed. Conversely, to maintain constant thickness as the melt is consumed, the web velocity must be reduced.

$$V_{total} = V_{melt} + V_{web}$$

$$V_i = a_i + \frac{b_i}{t} \qquad i = \text{total, melt or web}$$

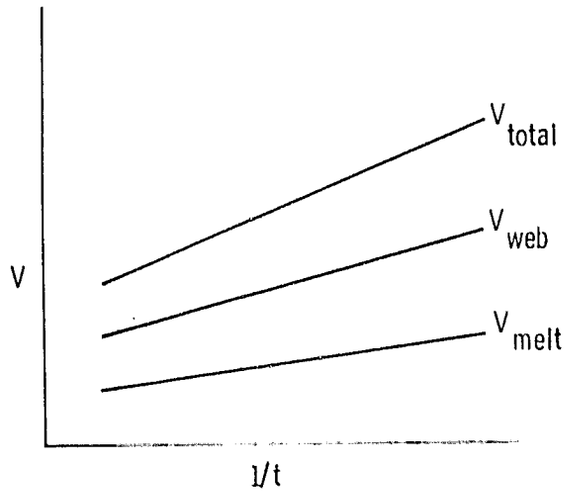

Figure 4 Schematic representation of the relation between web growth velocity and reciprocal ribbon thickness. For analysis, the actual growth velocity, V_{total}, can be considered as the sum of a partial velocity V_{web}, due to latent heat loss from the ribbon and a partial velocity, V_{melt}, due to latent heat loss to the undercooled silicon meniscus. Only the pull speed, V_{total}, and thickness can be measured, e.g., Figure 3.

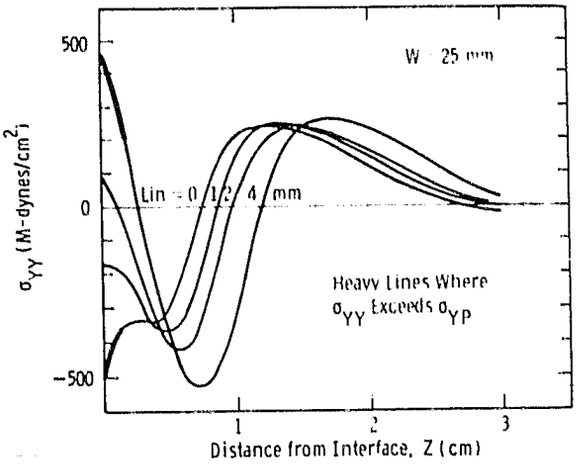

Figure 5 Calculated lateral stress at the web crystal center as a function of distance from the solid-liquid interface. Each curve represents a different distance (LIN) of the growth front below the bottom of the susceptor lid. For the growth front level with the lid (LIN = 0) or far below it (LIN = 4 mm) the lateral stress exceeds the yield stress and a residual stress should result; for the intermediate positions, no residual stress is expected.

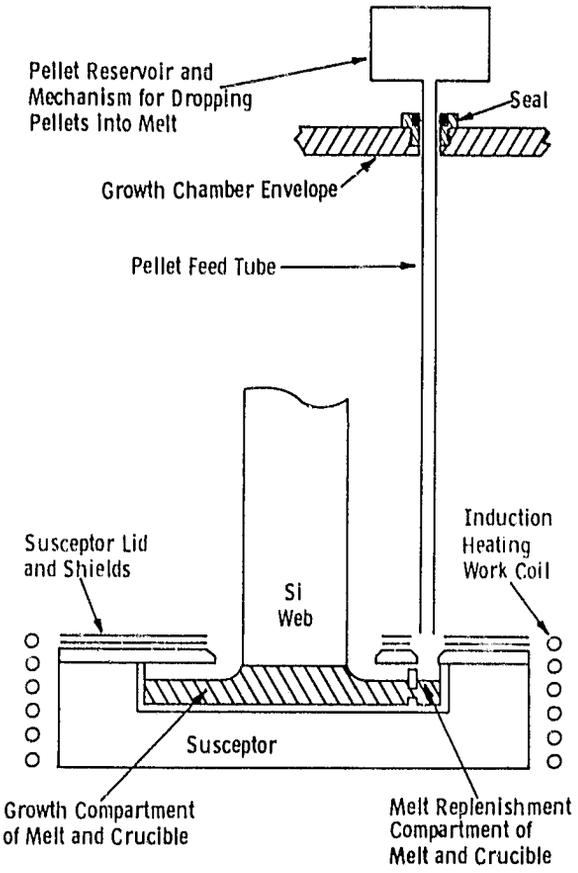

Figure 6 Schematic diagram of pelletized silicon feed system for replenished dendritic web growth.

REFERENCES

1. R. W. Aster and R. G. Chamberlain, "Interim Price Estimation Guidelines: A Precursor and an Adjunct to SAMIS III. Version I." Jet Propulsion Laboratory, 5101-33 (Sept. 1977)

2. W. H. Reed et al., "Development of a Process for High Capacity-Arc Heater Production of Silicon", Conference Record, 13th IEEE Photovoltaic Specialists Conference, IEEE, New York (1978), p. 370

3. T. Ciszik, "Maximum Growth Rates for Melt-Grown Ribbon Shaped Crystals" J. Applied Physics 47, 440 (1976)

4. J. C. Swartz, T. Surek and B. Chalmbers, "The EFG Process Applied to the Growth of Silicon Ribbons", J. Electronic Materials 4, 255 (1975).

5. R. G. Seidensticker, et al., "Computer Modeling of Dendritic Web Growth Processes and Characterization of the Material", Conference Record, 13th IEEE Photovoltaic Specialists Conference, IEEE, New York (1978) p. 358

6. R. G. Seidensticker and R. H. Hopkins, "Silicon Ribbon Growth by the Dendritic Web Process" J. Crystal Growth, In press.

7. B. A. Boley and J. H. Weiner, "Theory of Thermal Stresses", John Wiley New York (1960)

8. R. W. Gurtler, "Nature of Thermal Stresses and Potential for Reduced Thermal Buckling of Thin Silicon Ribbon Grown at High Speed", J. Crystal Growth, In press

9. R. G. Seidensticker, A. M. Stewart and R. H. Hopkins, "Solute Partitioning During Dendritic Web Growth", J. Crystal Growth 46, 51 (1979)

10. R. H. Hopkins, et al., "Crystal Growth Considerations in the Use of Solar Grade Silicon", J. Crystal Growth 42, 493 (1977)